NUREG/CR-3675
SAND81-1726
R7
Printed August 1984

In-Core Fuel Freezing and Plugging Experiments: Preliminary Results of the Sandia TRAN Series I Experiments

D. A. McArthur, N. K. Hayden, P. K. Mast

Prepared by
Sandia National Laboratories
Albuquerque, New Mexico 87185 and Livermore, California 94550
for the United States Department of Energy
under Contract DE-AC04-76DP00789

8411290576 841031
PDR NUREG
CR-3675 R PDR

Prepared for
U. S. NUCLEAR REGULATORY COMMISSION

SF2900Q (8-81)

NOTICE

This report was prepared as an account of work sponsored by an agency of the United States Government. Neither the United States Government nor any agency thereof, or any of their employees, makes any warranty, expressed or implied, or assumes any legal liability or responsibility for any third party's use, or the results of such use, of any information, apparatus product or process disclosed in this report, or represents that its use by such third party would not infringe privately owned rights.

Available from

GPO Sales Program
Division of Technical Information and Document Control
U.S. Nuclear Regulatory Commission
Washington, D.C. 20555

and

National Technical Information Service
Springfield, Virginia 22161

NUREG/CR-3675
SAND81-1726
R7

IN-CORE FUEL FREEZING AND PLUGGING EXPERIMENTS: PRELIMINARY RESULTS OF THE SANDIA TRAN SERIES I EXPERIMENTS

D. A. McArthur and N. K. Hayden
Sandia National Laboratories, Albuquerque, NM 87185

and

P. K. Mast
Science Applications, Inc., Albuquerque, NM 87102

Sandia National Laboratories
Albuquerque, New Mexico 87185
Operated by
Sandia Corporation
for the
U.S. Department of Energy

Prepared for the
Office of
U.S. Nuclear Regulatory Commission
Washington, D.C. 20555
Under Memorandum of Understanding DOE 40-550-75
NRC FIN No. A1016

ABSTRACT

The freezing and plugging behavior of molten reactor materials (UO_2 and 316 SS) is of primary importance in analyzing hypothetical accident scenarios of the Liquid Metal Fast Breeder Reactor (LMFBR). However, the reactor materials melt and vaporize at such high temperatures that it is very difficult to obtain data on the behavior of the pure materials in the laboratory. Because almost no data are available for the pure materials, several different theoretical models have been developed to predict freezing behavior. However, these models yield such a wide range of predictions that useful accident analyses are difficult to perform.

Described in this report is a new experimental apparatus (the "TRAN" apparatus) in which a pulsed nuclear reactor (the Sandia Annular Core Research Reactor) is used to melt the reactor materials rapidly. After the melt is formed, it is forced under moderate pressure into a "freezing" channel that has a geometry representative of the LMFBR fuel pin structure. The flow and freezing behavior of the pure reactor materials is then inferred from the final distribution of frozen materials, as well as from the transient behavior of the driving pressure. Theoretical models of varying complexity have been developed to relate the observed freezing behavior to the flow and heat transfer characteristics of the reactor materials.

The first series of TRAN experiments, described in this report, was intended to investigate the validity of current freezing models by applying them to a simple situation. Therefore the TRAN Series I experiments used pure UO_2 as the molten material, and a simple cylindrical freezing channel to simplify the analysis. Five experiments were performed at different initial channel temperatures. These experiments showed that a conduction-like fuel crust was formed for initial steel temperatures less than 973 K, but much of the crust thickness was composed of a frozen fuel film left behind as the molten fuel slug moved up the channel. In one instance two blockages containing molten steel formed at the leading edge of the flow. Fuel penetration distances intermediate between conduction theory and bulk-freezing theory were observed. A new model embodied in the PLUGM code was developed to describe these low-temperature results. At an initial steel temperature of 1173 K, however, rapid, massive melting of steel was observed, resulting in complex curved interfaces between the fuel and molten steel but with very little entrainment of molten steel into the fuel. In summary, generally longer penetration distances were observed compared to previous models, and the steel-entrainment assumptions of previous models were not verified at these driving pressures; also, important finite-mass effects and liquid-film-deposition effects were inferred from the results.

CONTENTS

CONTENTS (Continued)

CONTENTS (Continued)

ILLUSTRATIONS

ILLUSTRATIONS (Continued)

ILLUSTRATIONS (Continued)

TABLES

ACKNOWLEDGEMENTS

In the early stages of this work, Ray Ostensen outlined the overall concept of a series of experiments in which parameters would be varied systematically to explore regions of fuel-freezing behavior. When detailed design began he contributed further by defining the fluid flow conditions required when simulating the reactor accident conditions. Ahti Suo-Anttila performed fluid flow calculations to verify the initial design, and Ken Reil assisted in overall design and analysis of safety.

During the entire experiment series, the excellent technical assistance of Gary L. King contributed greatly to smooth-running experiments in which the initial conditions were well defined. Dale G. Pipher contributed his perspective on conservative and efficient design of in-core experiments. Sherwood Duliere, Carol Fryer, and Ellen Edge contributed their excellent microstructural analysis of the freezing channel debris, using the Sandia Hot Cell Facility. The cooperation of the operations staff of the Sandia Annular Core Research Reactor also contributed to a successful experiment series.

1. INTRODUCTION

The transition phase in the study of LMFBR core disruptive accidents has recently been identified as a high-priority research area in several general safety surveys.[1,2,3] During the transition phase of an LMFBR Hypothetical Core Disruptive Accident (HCDA), melting of individual subassemblies in the active core region leads to the gradual loss of the core geometry. If this process proceeds without significant fuel removal, the active core makes a "transition" from its original geometry to a large molten pool of reactor materials. Small perturbations of this molten pool can lead to recriticalities, further energy release into the melt, and large-scale coherent motions. Numerical modeling of whole-core behavior during such a fully-developed transition phase has shown a strong tendency for energetic termination of this transition phase, if sufficient fuel removal does not occur.[4]

Because of the unpredictable nature of the molten pool of reactor materials, this progression into the late transition phase should be avoided. Processes that remove fuel permanently from the active core region will reduce both the likelihood and severity of recriticalities that occur as a result of molten-fuel motion. A neutron-active molten pool therefore should not develop if molten core materials can pass through the surrounding blanket structure, leave the core region, and reach a coolable configuration. An assessment of such fuel removal requires a good understanding of the phenomena involved in the freezing and plugging of molten core materials (UO_2 and 316 SS) in the LMFBR blanket structure.

Described in this report are the initial results of a new experiment concept in which a specialized pulsed nuclear reactor is used to melt the reactor materials before injection into the freezing channel. This new technique permits the systematic study of freezing and plugging phenomena over a much wider range of melt composition and initial temperature, with better control of the driving pressure and void fraction of the flow. Upward injection of the flow can also be studied for the first time. The TRAN program is divided into several experiment series employing freezing channels of increasing complexity. To study basic heat transfer phenomena with high-temperature materials and to simplify the theoretical analysis, the TRAN Series I experiments employed a thick-walled cylindrical freezing channel.

This report describes previous work, the TRAN Series I experiment design in detail, the diagnostic methods used to analyze the experimental results, and the preliminary results of the five TRAN Series I experiments.

2. SURVEY OF PREVIOUS WORK

2.1 Experiments

Because fuel freezing and plugging in small-hydraulic-diameter channels is important in development of the transition phase,[5] numerous experiments have been performed to study these phenomena, either with low-temperature simulant materials,[6] or with high-temperature UO_2-containing melts.[7-9] Both simple hollow cylinders and various pin-bundle geometries have been used as freezing channels. Some experiments have involved melts with temperatures substantially above the melting point. Driving pressures ranging from 0.1 MPa to well over 5 MPa have been employed, with injection of the melt into the freezing channel either in a horizontal or downward direction. Although a few radiographic measurements of the transient fuel flow have been made,[8] most experimenters have attempted to interpret the final distribution of the frozen material in order to understand the transient freezing process.

Because of the high temperatures and pressures involved in the hypothetical accident scenarios, all experiments performed thus far require some form of extrapolation from the measurements actually made to the accident conditions of interest. The advantages and disadvantages of previous experiment concepts are briefly summarized here, with regard to the information they are expected to yield about the phenomena that actually occur under accident conditions.

The simulation experiments at low temperatures are useful for investigating certain separate effects but would not be expected to yield direct information on the dominant phenomena that occur with the real materials at prototypic temperatures. Such experiments have provided information on phenomena such as conduction-controlled freezing, and the effects on the freezing process of gas or solid particles contained in the melt. Therefore such simulant experiments are very useful for model development and validation.

The thermite experiments[7,8] are closer to the actual reactor accident conditions, because they involve real reactor materials (UO_2 and 316 SS) at high temperatures ($\approx$3500 K). In these experiments a constant sensible heat of $\approx$350 K above the melting point is provided by the thermite chemical reaction. However, it has been difficult to vary the amount of sensible heat or to control the driving pressure. The melt always involves a substantial metallic molybdenum fraction and usually a large noncondensable gas fraction (N_2), that results in a foam-like flow in the early stages of the experiment. In some experiments a separation has also been observed between the Mo and UO_2

phases. Thus, data have not been obtained from experiments with careful control of driving pressure, with variation of melt temperature and composition, with upward injection appropriate to the upper axial blanket conditions, or with a low void fraction melt. In addition, from the analytical point of view, the experiments are extremely difficult to model or interpret, or to apply directly to reactors because of the use of non-reactor materials.

The induction-heated-UO_2 experiments[9] involve pure UO_2 melts at temperatures close to the melting point, with downward melt release into a freezing channel. This heating method requires that the experiments be performed in a moderate-pressure atmosphere so that driving pressure differentials have thus far been limited to <0.2 MPa. The few published data from this experiment series do not cover a wide parameter range systematically.

2.2 Analysis

Several models have been proposed to explain the results of the thermite experiments: conduction freezing,[10] bulk freezing,[7,11] ablation freezing,[12] and thin film.[13] In each of these models, significantly different phenomena are assumed to control the freezing and plugging process, leading to unique final fuel distributions and penetration distances. The penetration distances predicted by the conduction model and the ablation-freezing model, for example, differ by more than an order of magnitude. These existing models assume an infinite reservoir of fuel.

A capsule description will be given here of the main features of the four models in current use to analyze fuel freezing situations. Figure 1 illustrates the final fuel distributions corresponding to each model.

Conduction Freezing Model: The conduction freezing model assumes that a stable UO_2 crust freezes on the channel wall, and grows proportionally to a growth constant λ. The channel plugs when the crust thickness is equal to the channel radius, thereby pinching off the flow from upstream. The final fuel distribution appears as in Figure 1a.

By making simplifying assumptions about pressure drops and the axial crust distribution, and by ignoring fuel superheat, simple analytic solutions for the penetration distance and mass penetration have been derived for the conduction-freezing model:[12]

$$\frac{x_p}{D} = 0.206 \left\{\frac{\nu}{\lambda^2 \alpha_s}\right\}^{7/11} \left\{\frac{\Delta P D^2}{\rho_l \nu^2}\right\}^{4/11} \qquad (1)$$

$$\frac{m_p}{\rho_l L C_p D} = 0.0133 \left\{\frac{D\nu}{\lambda^2 \alpha_s L}\right\} \left\{\frac{\Delta P D^3}{\rho_l \nu^2 L}\right\}^{4/7} - 0.159 \qquad (2)$$

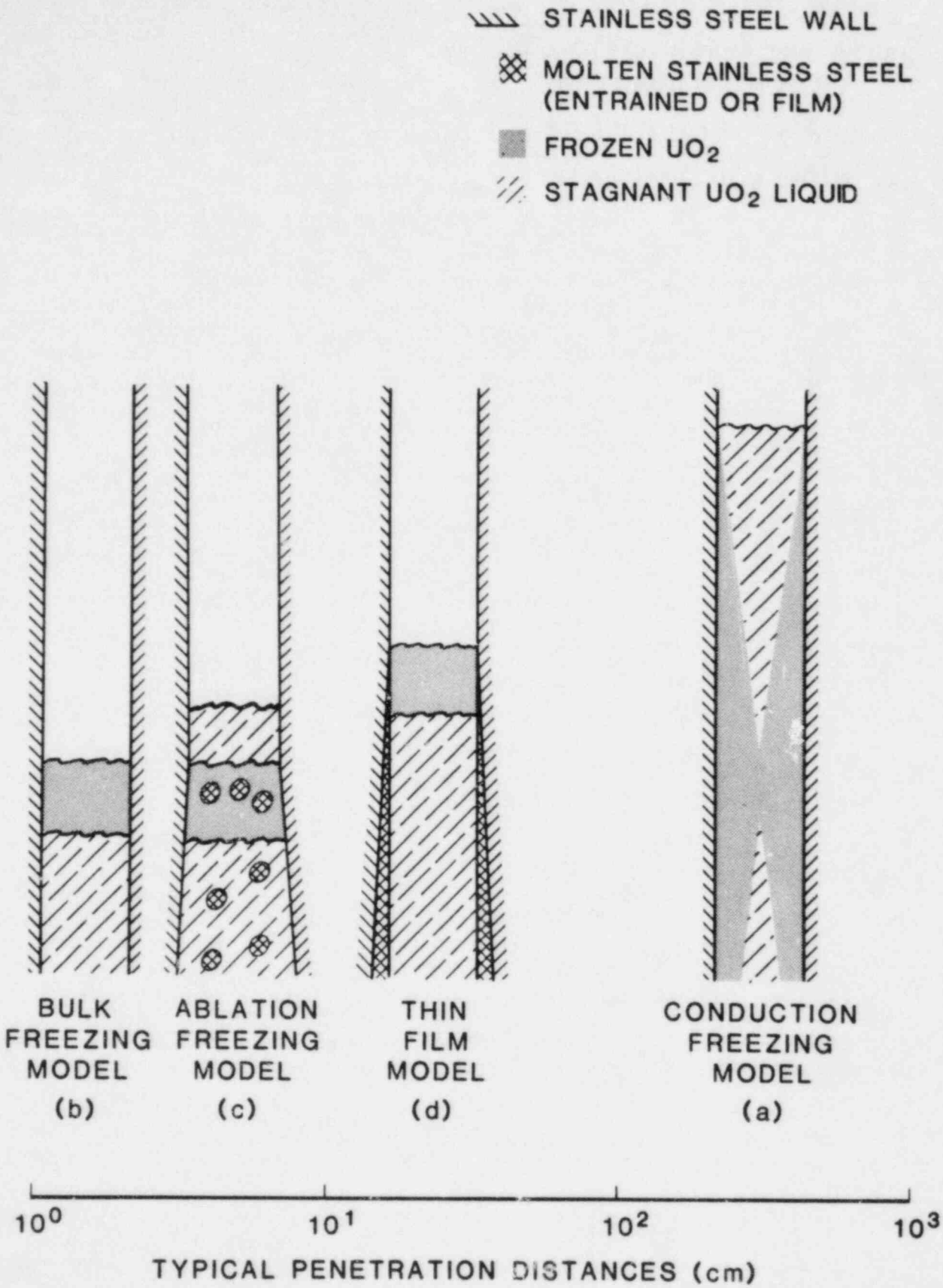

Figure 1 Final fuel distributions predicted by various models.

Eq. 1 gives the penetration distance, x_p, in a tube of diameter D with driving pressure ΔP. Eq. 2 gives the mass penetration out the exit of the tube of finite length L. The quantities ρ_l, C_p, and ν represent the density, specific heat, and kinematic viscosity of the bulk melt, and α_s is the thermal diffusivity of the steel wall.

The quantity λ is the growth constant for the fuel crust, where the time-dependent crust thickness is given by:

$$\delta = 2\lambda \sqrt{\alpha_s t} \qquad (3)$$

This equation is valid for the case where the fuel is not superheated. For the UO_2/steel system, the value of λ is ≈ 0.8.[14]

Eqs. 1 - 3 are very simple representations of the conduction model. For instance, in Eqs. 1 and 2 a simple crust profile is assumed over the tube length. Also, the equations do not account for superheat or pressure losses such as entrance effects. If superheat is accounted for, the plug will occur downstream of the channel entrance (Figure 1a), and the penetration distance, x_p, will be greater. In general, Eq. 1 predicts penetration distances on the order of 10^2 to 10^3 cm for conditions of interest in the transition phase. More accurate numerical solutions to the conduction model equations generally predict shorter penetrations, on the order of 10^2 cm.

The predicted penetration distances of the conduction model generally agree quite well with the results of low-temperature simulant experiments.[6] However, Eqs. 1 and 2 overpredict the penetration in thermite experiments by an order of magnitude. Also, the final fuel distributions in the thermite experiments did not appear as in Figure 1a. Some workers, notably Ostensen and Jackson, proposed the bulk-freezing model to explain the thermite results.

Bulk-Freezing Model: The bulk-freezing model assumes that a stable UO_2 crust cannot form and adhere to the wall. This may be due to either the wall being molten or to turbulent shear stresses in the flow that strip the crust from the wall as soon as it forms. Thus, bulk cooling of the molten UO_2 occurs via convective heat transfer from the fluid to the wall surface. Plugging occurs at the leading edge when it reaches the solidus temperature, after losing the heat of fusion. The final fuel distribution is shown in Figure 1b.

A penetration distance is obtained by integrating an energy balance equation for the leading edge of the flow; the lower limit of integration being the initial fuel temperature and the upper limit being the solidus temperature of the fuel. The velocity of the fuel and the

wall temperature are both assumed to be constant. The resulting equation for the penetration distance is†:

$$x_p = \frac{D^{6/5} C_p \rho_l \nu^{0.2} \nu^{0.8}}{0.092 k_l P_r^{1/3}} \ln \frac{T_o^* - T_w}{T_{f,mp} - T_w} \qquad (4)$$

Eq. 4 typically predicts penetration distances on the order of 10^0 - 10^1 cm for UO_2/steel systems.

Ablation-Freezing Model: The ablation-freezing model is closely related to the bulk-freezing model. It is assumed that in addition to frozen UO_2, molten steel is entrained into the bulk flow. The steel entrainment occurs at the entrance to the channel after some finite amount of time, during which the steel is heated and a molten steel layer grows. A mixed "clinker" of frozen UO_2, molten UO_2, and molten steel is then formed. As in the bulk-freezing model, plugging is assumed to occur near the leading edge when all superheat and latent heat of fusion has been removed from the UO_2, and the bulk temperature of the UO_2 is at the solidus. The final fuel distribution is shown in Figure 1c.

The penetration distance of the fuel front in the ablation-freezing model is predicted by:

$$x_p = x_a + x_c \qquad (5)$$

In Eq. 5, x_a is the distance travelled by the fuel front when steel ablation begins, forming the "mixed clinker", and x_c is the distance travelled by the mixed clinker before freezing. The distances x_a and x_c are given as:

$$x_a = U t_a \qquad (6)$$

and

$$x_c = x_{p,bf} \left\{ 1 + \frac{T_{f,mp} - T_{s,mp}}{h_s / C_{p,s} + T_{s,mp} - T_{s,o}} \right\}^{-1} \qquad (7)$$

---

†In Reference 11, Pr ~1 was used in deriving the constants which appear in the equation for x_p. Here, the properties have been left as variables for clarity.

In Eq. 6, t_a is the time at which ablation begins and is given by:

$$t_a = \frac{16\lambda^2\alpha_f}{(fU)^2}\left\{\frac{T_{f,mp} - T_{s,o}}{T_{f,o} - T_{f,mp}}\right\}^2 + t_L \qquad (8)$$

The first term in Eq. 8 is the UO_2 crust lifetime, and the second term, t_L, is the time required for the molten steel layer to equal the laminar boundary thickness. The term t_L is insignificant in most cases (on the order of 10^{-4} s), and can often be ignored. Solving Eqs. 5 through 8 usually predicts penetration distances of UO_2 in steel on the order of 10^0 - 10^1 cm.

Thin-Film Model: A fourth phenomenological model of fuel freezing and plugging in the transition phase is the thin film model. In this model, it is also assumed that no stable crust forms, i.e., frozen UO_2 is entrained in the liquid UO_2 flow. The steel wall is also assumed to melt; however, it is not entrained. The heat transfer, then, is very similar to that in the bulk-freezing model, except that the effect of an axially moving liquid substrate is taken into account. The effect of the liquid steel film is reportedly a reduced effective heat transfer coefficient from the bulk melt to the wall surface. The penetration distance is given by:

$$x_p = (h_e/h_c)^{-1}\, x_{p,bf} \qquad (9)$$

where h_e/h_c is the ratio of the effective heat transfer coefficient to the standard turbulent heat transfer coefficient. Typical values for the ratio are h_e/h_c = 0.2 - 0.4 for UO_2/steel systems.[13] The final fuel distribution should appear as in Figure 1d. Note that the distinction between Figures 1b and 1d is the evidence of molten steel wave patterns.

The four freezing models assume certain criteria for crust stability (both mechanical and thermal), and onset of steel melting and entrainment. In particular, the initial temperatures above which instantaneous steel melting has traditionally been assumed are taken from Reference 12. That analysis used constant room temperature properties for the steel, however. The analysis has been redone and suggests that the range of conditions for which steel will melt is narrower than previously indicated. These interfacial temperature calculations are discussed in Reference 15.

2.3 Summary of Previous Modeling Work

In summary, four distinct phenomenological models have been previously developed for predicting penetration distances and final fuel distributions for UO_2 freezing in steel channels. In the thermite tests, the ablation-freezing model most closely portrays the final fuel

distributions, but the actual penetration distances and the typical location of the steel plugs disagree significantly. Although the conduction model represents low-temperature simulant experiments very well, the high-temperature thermite experiments did not display conduction-type crusts or plugs.

A primary purpose of the TRAN experiments is to provide reliable data on freezing and plugging phenomena that can be incorporated into a qualitatively- (and hopefully also quantitatively-) accurate model. As will be shown later none of these simple analytical models by themselves predict or explain the results of the TRAN experiments. The phenomena observed in the TRAN experiments have led to modeling that combines some previous concepts, as well as introducing new effects. The analytic interpretation of the TRAN Series I results, companion model development, and phenomenological conclusions are discussed in Section 5 of this report.

3. IN-CORE EXPERIMENT CONCEPT

3.1 Unique Features of In-Core Experiments

In performing an in-core experiment on freezing and plugging of reactor material melts, the reactor is used to melt the material rapidly and heat the melt to a desired temperature. The Annular Core Research Reactor (ACRR)[16] at Sandia National Laboratories is able to melt small-diameter UO_2 samples ($d \approx 1$ cm), and heat them relatively uniformly to temperatures of about 4300 K within 30 ms. The resulting melt (either pure UO_2 or variable UO_2/steel mixtures) is then available for injection either upward or downward into a freezing channel, at an arbitrary pressure of up to 10 MPa (for existing ACRR safety constraints).

Compared to other high-temperature experiments using reactor material simulants[7,8] or real reactor materials,[9] in-core experiments offer significant advantages: (1) the ability to vary the sensible heat above melt over a wide range, (2) the decoupling of the melt temperature from the driving pressure, (3) the ability to study pure UO_2 melts at high sensible heat and variable driving pressure, (4) the ability to study upward melt injection for the first time, (5) the reduction or elimination of the large noncondensable gas fraction present in the thermite melts, and (6) the ability to study a range of UO_2/steel melt combinations at arbitrary temperatures and driving pressures (including the pure UO_2 case). The principal disadvantages of in-core experiments appear to be the relatively small amount of fuel which can be melted (at most, a few kg), and the difficulties of posttest examination of an irradiated experiment.

A series of in-core experiments with freezing channel geometries of increasing complexity is planned, in an effort to understand the separate effects involved in the actual pin bundle geometry. In addition, as experience with the safety aspects of the TRAN apparatus is gained, experiments corresponding to perhaps seven pin bundles might eventually be performed. Finally, the Hot Cell Facility (HCF) at Sandia National Laboratories is able to perform a wide variety of posttest examination operations on irradiated experiments.[17]

3.2 General Description of the TRAN Experiments

The general concept of the TRAN fuel freezing experiment is shown in Figure 2. A 44 g, 10-cm-long column of UO_2 is melted rapidly by an intense neutron pulse from the ACRR, and is propelled upwards into the preheated freezing channel by helium gas applied to the base of the

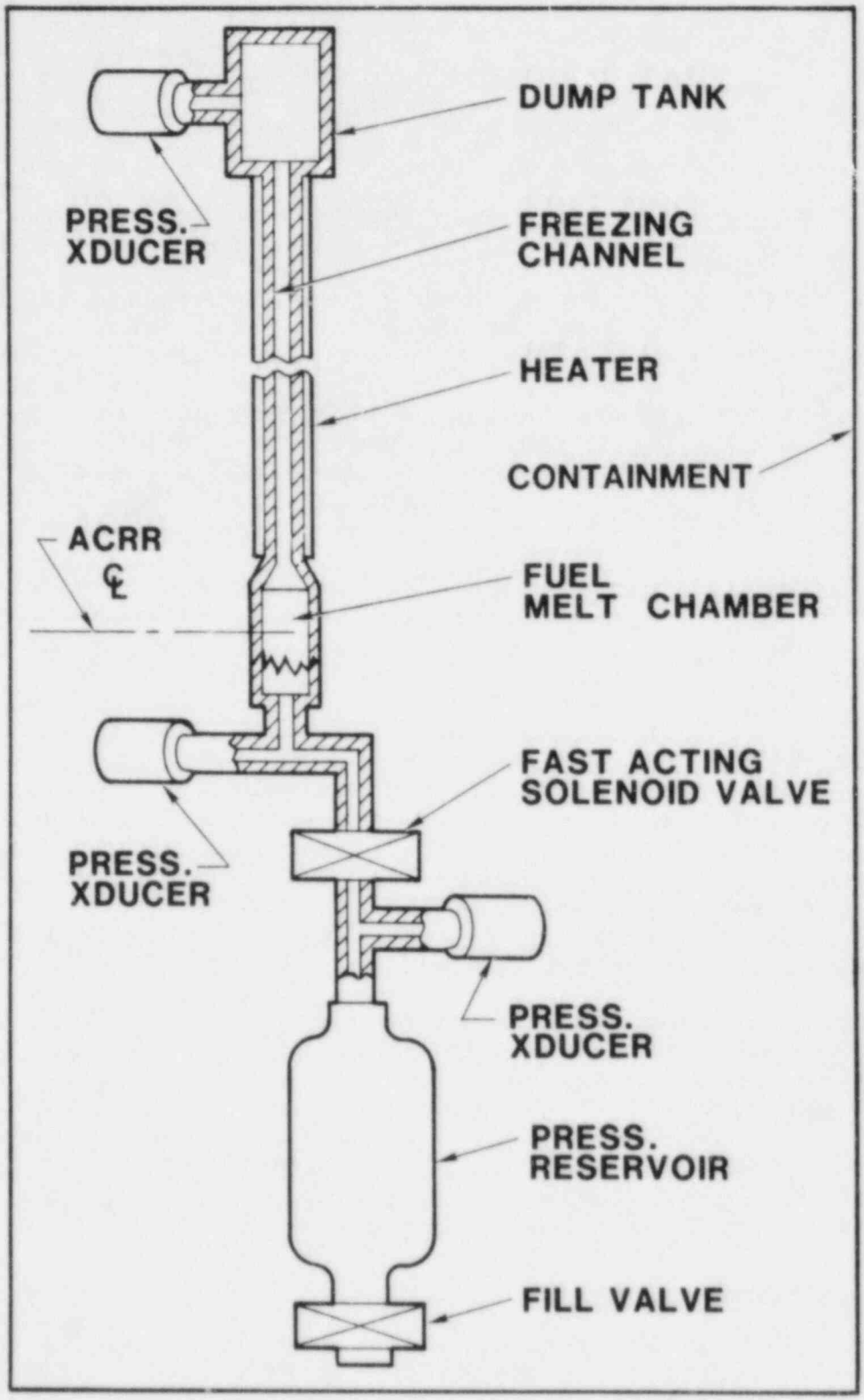

Figure 2 Schematic diagram of the TRAN series I experiment.

molten fuel column. A pressure system assembled primarily from commercial components provides a fast-risetime (10% to 90% pulse risetime ≈5 ms) helium gas pressure pulse (see Figure 3). The delay between the valve trigger pulse (at t=0 in Figure 3) and the initial peak of the pressure pulse is roughly constant at about 40 ms for all valves used.

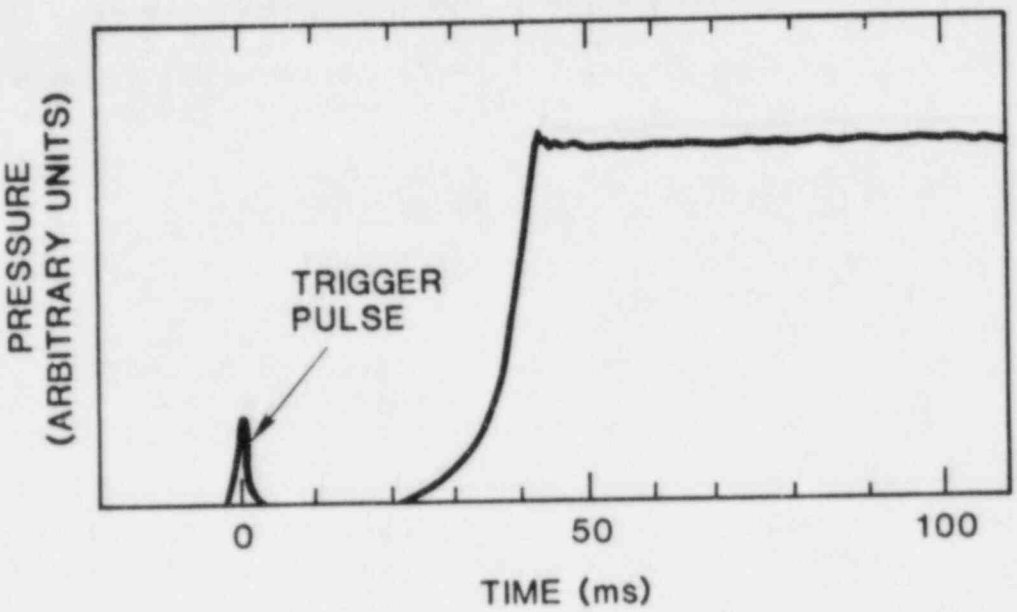

Figure 3 Representative shape of the applied pressure pulse.

The ≈300 cm^3 volume of the pressure system is large compared to the ≈15 cm^3 volume occupied by the fuel column and the freezing channel, so that the molten fuel flows into the freezing channel under a nearly constant driving pressure. A large-volume (≈100 cm^3) dump tank is also provided at the top of the apparatus, so that any noncondensable gas that escapes from the fuel, or any gas that leaks past the fuel column before melting, will produce a negligible backpressure at the end of the freezing channel. Eddy-current pressure transducers are located in the pressure system, just below the fuel column, and in the dump tank. These transducers permit the monitoring of the applied pressure and the gas flow out of the reservoir and into the dump tank. Thermocouples are located at eleven selected points, to regulate and monitor the temperature of the freezing channel, to monitor critical temperatures such as the solenoid valve temperature, and to detect any temperature increases caused by the freezing of fuel in the freezing channel. The TRAN-2, -3, and -4 experiments also incorporated five platinum self-powered detectors in an attempt to measure the time-dependent fuel motion out of the fuel melting chamber and through the freezing channel.

4. RESULTS OF TRAN SERIES I EXPERIMENTS

These experiments are the first to use pure reactor materials at conditions expected in transition phase scenarios, including high melt temperatures, low driving pressures, and upward melt injection. Because the objective of these Series I experiments was to investigate the high-temperature interaction phenomena of the real reactor materials, a simple cylindrical-flow-channel geometry was chosen to simplify the theoretical analysis.

4.1 General Characteristics of the Experiment Results

Figure 4 shows a schematic drawing of the final fuel distribution that was characteristic of most TRAN Series I experiments. Typically, the freezing channel was not blocked completely, but was lined with a frozen fuel layer which extended from 40 to 90 cm beyond the entrance to the freezing channel (however, very solid blockages were observed in one experiment). A small amount of fuel or fuel/steel debris was usually observed beyond the freezing channel exit. Much of the initial fuel load was found in the fuel melting chamber and below, indicating that gravity effects or fuel dispersal by entrained gas pressurization were important at some time during the experiment while the fuel was still molten.

The preliminary results of the TRAN Series I experiment program are summarized briefly in Table 1. In Table 1, T_S is the initial temperature of the steel freezing channnel, T_F is the temperature of the molten fuel, P_D is the driving pressure differential across the column of molten fuel, L_C is the length over which frozen fuel is observed in the freezing channel, and FF_C is the fraction of the total fuel load which is frozen in the freezing channel or higher at the end of the experiment. Table 1 is subdivided into two main ranges of T_S, corresponding to how rapidly steel melts upon contact with molten UO_2. For T_S <973 K, an infinitely-thick steel wall is not expected to melt upon initial contact, while for T_S >1173 K, the steel is expected to melt instantaneously. Qualitatively different fuel-steel interaction phenomena were observed in these two ranges.

Virtually no gas flowed past the molten fuel columns in the early stages of fuel flow. However, in all experiments except TRAN-2 a somewhat restricted gas flow through the freezing channel began after about 20-60 ms of fuel flow, with pressure equilibration being reached after 1-2 s. It is not clear whether the gas flow restrictions observed were caused by porous blockages in the channel, or by the combination of gas heating with narrowing of the channel diameter by the fuel crust. Because some debris was observed beyond the freezing channel in several cases, it is conceivable that porous blockages may

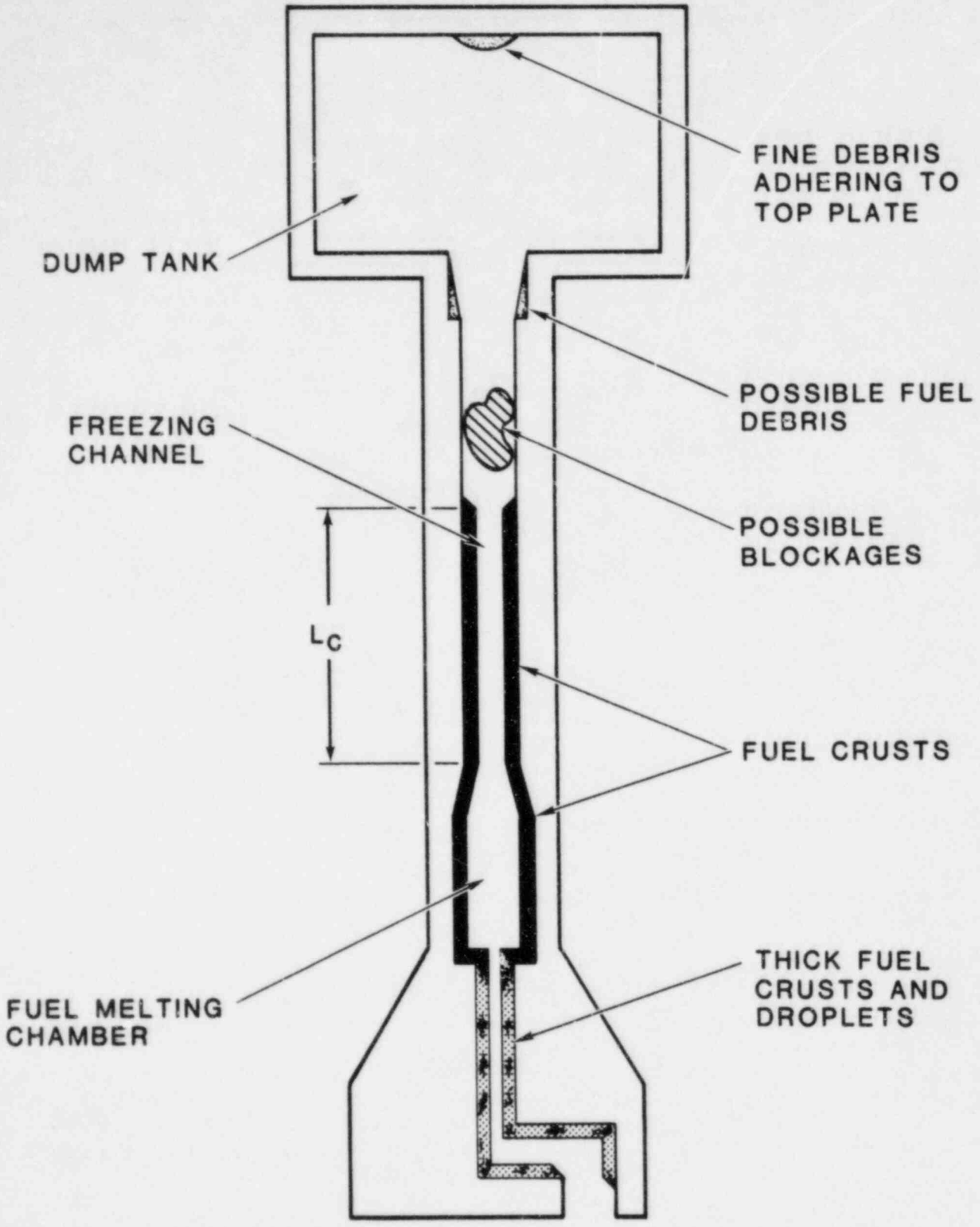

Figure 4 Schematic drawing of typical final fuel crust distribution in the TRAN series I experiment.

Table 1 Preliminary Results of the TRAN Series I Experiments

	T_S(K)	T_F(K)	P_D(MPa)	L_c(cm)	Blckgs?	Steel Removal	FF_c(%)
TRAN-1	673	3170	1.6	70±10	c	none	>32
TRAN-2	873	3720	1.0	87	two	slight	51[b]
TRAN-3	943	3770	1.0	67	none	slight if any	42
TRAN-4	1173	3750	1.0	48	none	much near channel entrance	42
TRAN-5	1173	3590	0.3[a]	≈45	c	some near channel entrance	27

[a] P_D is the initial driving pressure difference; TRAN-5 had a back-pressure of 0.2 MPa in the channel and a pressure applied below the fuel of 0.5 MPa.

[b] The mass of fuel in the two blockages is about 0.9 g.

[c] Significant restriction in gas flow observed.

have been present for a short time after fuel freezing, but these may have broken up and dispersed as the fuel cooled.

The three experiments conducted in the lower initial steel temperature range all exhibited substantial fuel penetration, even in the case of TRAN-2 where a blockage occurred. In TRAN-1, which had an initial steel temperature of 673 K, no evidence of steel melting was observed from either the radiographs of the test section or from the posttest destructive examination of the freezing channel. The radiographs for both TRAN-2 and TRAN-3 (initial steel temperature of ≈900 K), however, suggested that some steel melting may have occurred near the entrance to the freezing channel. For the case of TRAN-2, this was confirmed by the posttest destructive examination which showed that steel melting and entrainment did occur. In fact the high steel content (≈20%) and the microstructure of the TRAN-2 blockages suggest that the entrained steel may have caused the blockages in that experiment.

In the higher steel temperature range, where substantial mixing and interaction of fuel and steel might be expected (but was not observed), significantly shorter fuel penetration lengths were observed. No thick, axially-confined blockages analogous to those of TRAN-2 were observed, although partial blockages might be inferred from the radiographs at some axial locations. Both TRAN-4 and TRAN-5 showed evidence of fuel slumping or draining out of the freezing channel into the upper part of the fuel melting chamber. However, the mass of fuel frozen in the freezing channel and beyond differed significantly between TRAN-4 and TRAN-5.

TRAN-5 not only employed the lowest driving pressure difference, but was also the first experiment in which a significant backpressure (≈0.2 MPa) was present in the freezing channel. It was therefore interesting that a large, short-duration, positive pressure pulse was observed in the dump tank as fuel first began to flow up the channel. Evidence from previous experiments without backpressure suggests that this pressure pulse was caused by heating of the dump tank gas by finely-divided debris near the front of the fuel flow. This pressure pulse also suggests that the lower P_D and the backpressure resulted in less fuel frozen above the fuel melting chamber.

4.2 Conclusions on Fuel Freezing Behavior

The following conclusions can be drawn from the five experiments of the TRAN Series I program:

(1) Fuel penetration lengths (L_c in Table 1) have generally been considerably longer than those predicted by the common models used to analyze reactor accident scenarios. For example, the bulk-freezing and ablation-freezing models predict much shorter penetration lengths (5 to 20 cm) than observed in these experiments, under conditions in which these models are expected to apply (the bulk-freezing model applies in all experiments, and the ablation-freezing model also applies for experiments with steel wall initial temperatures of 1173 K or greater). The penetration length appears to decrease with increasing steel temperature, though perhaps not in a simple fashion. Simple conduction models predict very long penetration lengths, and the more sophisticated conduction models that predict shorter penetration lengths do not give the correct form of the crust thickness. The finite mass in the fuel slug was also an important factor in determining the fuel penetration distance, and a new model accounting for this effect was developed as part of the TRAN program. The long penetration distances observed in these experiments indicate the possibility of greater fuel removal than assumed in many models of LMFBR accident scenarios.

(2) The presence of a stable fuel crust (or frozen fuel layer) was an important feature of the experimental results. The detailed character of this frozen fuel layer varied strongly with initial steel temperature. The layer was very uniform in thickness and in grain structure at initial steel temperatures <973 K, but variable in thickness and "foamy" in structure at initial steel

temperatures >1173 K. The fuel layer limited the heat transfer from the bulk fuel flow to the steel wall, resulting in fuel penetration distances that were longer than the predicted distances.

In the lower-temperature experiments the final frozen fuel layer probably consisted of a frozen crust formed during fuel flow, with an overlying fuel layer which was originally deposited as a liquid film (analogous to the liquid sodium film left behind during sodium voiding).

In those experiments in which steel melting occurred, the fuel layer was sufficiently fluid to participate in fluid instabilities with the underlying molten steel layer, as well as form complex fuel/steel/fuel layers at one or more axial locations. However, at the driving pressures used in these experiments (between 0.3 MPa and 1.6 MPa), the fuel layer was sufficiently stable that fine-scale mixing of fuel and steel did not occur on a widespread basis. The observed mixing of fuel and steel occurred primarily through formation of small globules of fuel/steel eutectic that were surrounded by fuel crust.

Thus, these experimental results disagree strongly with the ablation-freezing model, which asssumes immediate entrainment of molten steel into the fuel flow, with fine-scale mixing.

(3) The threshold for rapid melting of an infinitely-thick steel wall occurs for initial steel temperatures between 973 K and 1173 K, in contrast to earlier models which predicted steel melting for temperatures as low as 673 K. This discrepancy was removed by improved heat transfer calculations in which the temperature dependence of steel properties was included. These calculations predicted the instantaneous melting of a thick steel wall at about 1073 K or greater.

(4) A consistent feature of the results appears to be the presence of a finely-divided debris flow which precedes the main fuel flow. This debris flow does not appear to contain appreciable gas because pressure transducers do not show an accompanying pressure rise. The debris flow appears to be independent of the presence of a background pressure in the freezing channel, based on the pressure transducer record and the gamma scans of TRAN-5. The debris has sufficient kinetic energy to penetrate all the way through the 130-cm-long freezing channel and lodge at the top of the dump tank. The character of the debris depends on the initial steel temperature: at low initial steel temperatures the debris appears to be fine fuel particles, but at high initial steel temperatures the debris consists of fine, well-mixed fuel and steel particles. It is not clear to what extent this effect is characteristic of reactor accidents. If it is characteristic then depending on the free volume available beyond the blanket structure of an LMFBR, these particles could be important in the heating of vapor or sodium beyond the blanket structure during an accident sequence.

4.3 Preliminary Implications for LMFBR Safety

The TRAN Series I results are of considerable importance for understanding fuel/steel heat transfer phenomena, especially for thick channel walls. The experimental results are discussed in relation to three questions of importance to reactor safety:

(1) How much fuel freezes and remains in the region above the active core (analogous to FF_c in these experiments)?

(2) Are tight blockages formed which would prevent the escape of gas or molten material from the active core region?

(3) Are the detailed phenomena of fuel freezing sufficiently well understood to permit the extrapolation from laboratory experiments to the accident scenarios of importance?

The observed fuel penetration distances are much longer than those predicted by the bulk-freezing model (which should apply even in the absence of steel melting). An initial interpretation of the low-temperature TRAN Series I results implies that for a driving pressure of ≈1 Mpa and a structure temperature <973 K, more fuel will be relocated into the axial blanket structure than indicated by the thermite experiments. The frozen mass of fuel, FF_c, ranged between 30 and 50 percent of the initial fuel load. This amount of frozen fuel per flow subchannel in the axial blanket structure would represent a substantial fuel removal from the active core of an LMFBR. Based on these preliminary results it appears that the fuel penetration distance will decrease with increasing steel temperature, and the amount of fuel removed will decrease with decreasing driving pressure. However, these Series I experiments do not yet include the effects of the complex fuel pin structure, or the various mechanisms which might permit frozen fuel to melt the structure on which it has frozen and drop back into the active core region. Because the TRAN Series I experiments do not include the effects of fuel/steel mixtures, the low heat capacity of cladding, and the potential for crust instability on the outside of cladding, TRAN Series II experiments have been designed to investigate these phenomena in greater detail.

5. ANALYSIS OF THE TRAN SERIES I EXPERIMENTS

Detailed posttest destructive examinations have been performed for the TRAN-1, -2, and -4 experiments (see appendices C, D, and F, respectively). The results of these examinations show that a significant variation in final fuel distributions was obtained for these three experiments. The TRAN-1 experiment, with a low initial steel temperature of 673 K, was characterized by the absence of a fuel blockage formation and a fairly long (80 cm) fuel penetration distance. The channel surface was covered by a nearly uniform thickness of fuel crust for the entire length of the penetration distance. The TRAN-2 experiment, with a somewhat higher initial steel temperature of 873 K, also exhibited a long penetration distance with a fuel crust over the length of the penetration. For this experiment, however, there was a small amount of steel melting near the channel entrance and a blockage at the leading edge of the fuel flow. The TRAN-4 experiment, with the high initial steel temperature of 1173 K, resulted in a substantially shorter penetration distance (50 cm), significant steel melting, and complex steel entrainment and fuel/steel mixing. A tight blockage (impervious to gas flow for a significant fraction of a second) such as occurred in TRAN-2 was not observed.

A safety analysis of the transition phase of an LMFBR accident requires that one be able to predict the fuel removal characteristics through the various potential escape paths such as the upper axial blanket region and the intersubassembly gaps. Thus one needs to be able to predict the fuel removal in such experiments as TRAN Series I, as well as under more complex conditions (different driving pressure, fuel/steel mixtures, different geometries, etc.).

Four simple analytic models of fuel plugging and freezing were described in Section 2. A comparison of the qualitative final fuel distributions for these models (Figure 1) with the final fuel distributions seen in the posttest destructive examination of TRAN-1, -3, and -4 clearly shows a major inconsistency. In TRAN-1 and TRAN-4, no blockage was formed and the channel was not filled with fuel. Even in TRAN-2, however, where a blockage was observed, most of the channel was void of fuel. This was inconsistent with all of the models, which show most of the channel filled with fuel. Thus, one obvious inconsistency between the TRAN results and the four simple models was the assumption of infinite fuel availability in the models; only a finite amount of fuel was available in the experiments.

The results of the four analytic models as applied to the TRAN Series I experiments, (ignoring finite-mass effects) are shown in Tables 2 and 3. The predicted penetration distances for the conduction model are several meters for each experiment. Thus, this simple model is

Table 2

Penetration Distance in the TRAN Series I Experiments as Predicted by Four Analytic Models

Exp.	Penetration Distance (m)			
	Conduction[a]	Bulk	Thin Film[b]	Ablation
TRAN-1	5.1	0.07[c]	n.a.	n.a.
TRAN-2	4.3	0.10[d]	0.34	0.47
TRAN-3	4.3	0.11[d]	0.36	0.33
TRAN-4	4.3	0.11[d]	0.36	0.28
TRAN-5	2.8	0.09[e]	0.30	0.56

[a] Using $\lambda = 0.8$
[b] Assuming $h_e/h_c = 0.3$
[c] Assuming velocity = 13 m/s
[d] Assuming velocity = 10 m/s
[e] Assuming velocity = 7 m/s

Table 3

Location of Blockage in the TRAN Series I Experiments as Predicted by Four Analytic Models

Exp.	Location of Blockage (m)			
	Conduction[a]	Bulk	Thin Film[b]	Ablation
TRAN-1	0.0	0.07[c]	n.a.	n.a.
TRAN-2	0.0	0.10[d]	0.34	0.05
TRAN-3	0.0	0.11[d]	0.36	0.05
TRAN-4	0.0	0.11[d]	0.36	0.04
TRAN-5	0.0	0.09[e]	0.30	0.03

[a] Using $\lambda = 0.8$
[b] Assuming $h_e/h_c = 0.3$
[c] Assuming velocity = 13 m/s
[d] Assuming velocity = 10 m/s
[e] Assuming velocity = 7 m/s

inappropriate because of the limited fuel available in the experiments. Further, the model is obviously in error for TRAN-2 because a blockage actually did form with a penetration distance much less than 4.3 m. Both the bulk freezing and thin-film models predict penetration distances shorter than the observed penetration in the experiments. Also, only TRAN-2 exhibited the type of leading edge blockage that these models predict. The ablation freezing model predicts a penetration distance for TRAN-5 that is reasonably close to that observed in the experiment. However, the model also predicts the blockage forming near the channel entrance and that the channel extending from the blockage to the leading-edge of the flow would be filled with UO_2. This predicted final fuel distribution is not consistent with the observed final distribution.

Thus, it is clear that the actual behavior seen in these TRAN Series I experiments is more complex than the behavior assumed in the existing simple fuel-freezing models. Simple models, such as those previously described, are desirable, because they can presumably be readily incorporated into larger accident analysis codes. However, before such a simplified model can be developed and verified, a better understanding of the fuel freezing and steel melting and entrainment problem is required. It has been the goal of the TRAN analysis effort to try to provide this improved understanding.

There are clearly several important phenomena that are not correctly treated by the existing models. A key phenomenon for these experiments is the finite amount of molten fuel that is injected into the freezing channel. The effect of such finite-mass is not accounted for by existing models. To determine the importance of finite-mass effects, a new analytic model has been developed that accounts for finite-mass effects in the context of conduction-limited freezing.[14] The key features of this model are illustrated in Figure 5. A finite mass of fuel is accelerated through the freezing channel by the applied driving pressure. While the slug is adjacent to the channel wall, crust growth occurs by standard conduction-limited behavior. At the trailing edge of the moving fuel slug, a film of liquid fuel is deposited over the crust that has formed. Thus, depletion of the liquid fuel in the slug occurs by a combination of crust growth and film deposition so that the slug length, L_s, decreases with time.

A key parameter in such a model is the amount of liquid fuel deposited as a film at the trailing edge of the fuel slug. Experiments that have been done to investigate sodium expulsion from LMFBR subassemblies and the size of sodium films left behind indicate that for turbulent flow in a cylindrical flow channel, the liquid films can be characterized by an areal fraction (fraction of available flow channel) of about 0.15.[18] This result is reasonably independent of velocity and material properties (various simulant fluids were used). This film thickness criterion has been applied for the TRAN analysis.

This finite-mass conduction-freezing/film-deposition model was applied to the analysis of TRAN-1, -2, and -3. The calculations were performed for an initial fuel mass that was set equal to the final mass of fuel measured to be in the freezing channel (see discussion that

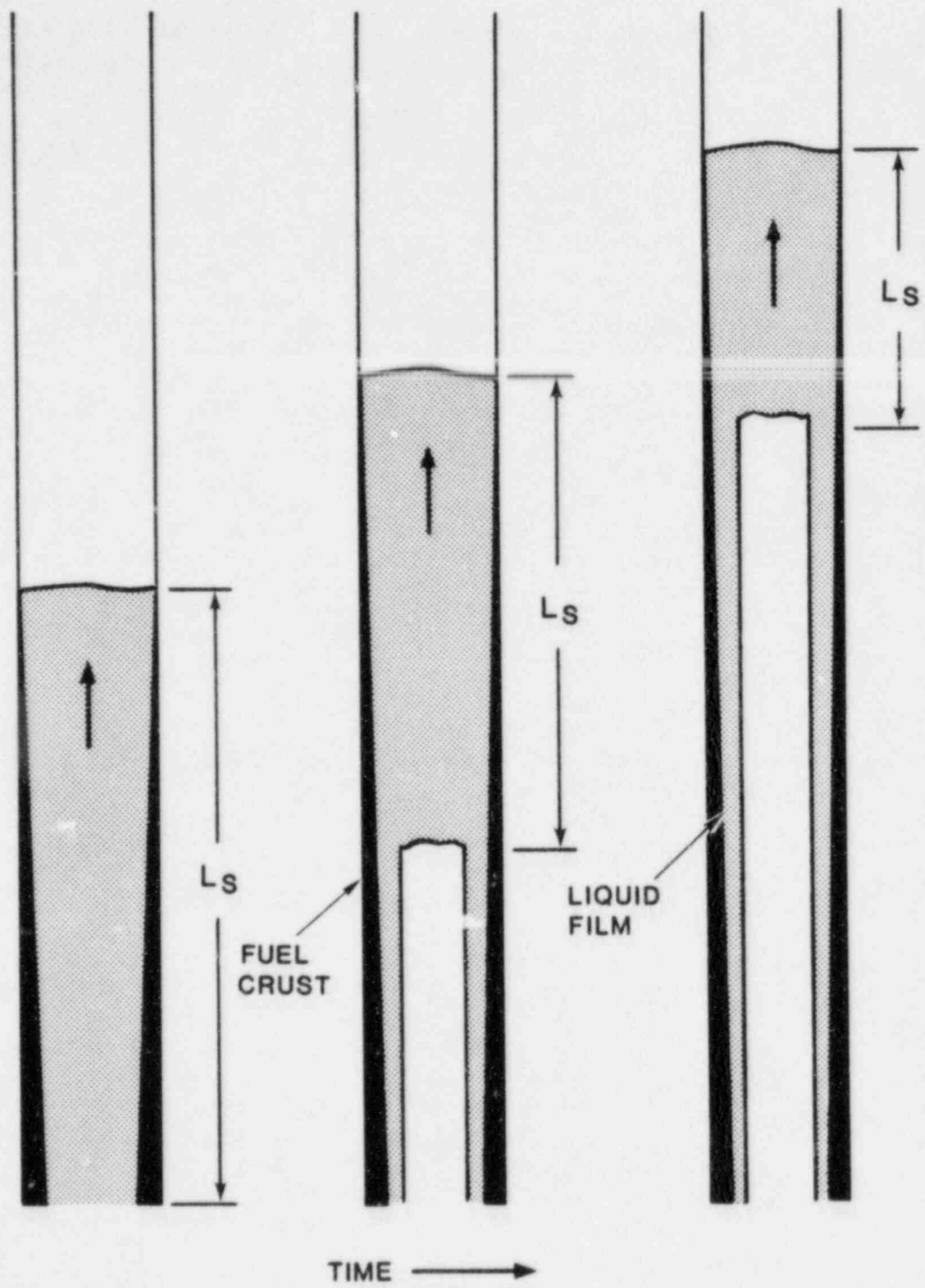

Figure 5 Features of the finite-mass conduction freezing model.

follows). In this manner, the analytic model gave good qualitative agreement with the penetration distances and crust thickness measured in the experiments. Thus, it was concluded that the phenomenon of mass depletion by crust growth and film deposition is very important for the understanding of the TRAN results.

While the above analytic model demonstrated the importance of finite-mass effects, it could not be readily extended to incorporate other important effects. For this reason, the PLUGM code[19] was developed to more accurately predict the TRAN experiment results. The main features of the code that apply to the analysis of the TRAN Series I experiments include:

- Detailed calculation of crust growth and wall heatup accounting for possible wall melting
- Calculation of convective heat transfer from the bulk melt to the crust surface based on local bulk-melt Reynolds number
- Hydrodynamic analysis of the pressure-driven molten-fuel slug accounting for inertial effects, area-change pressure drops, and friction losses
- Calculation of molten fuel depletion by crust growth and liquid-film deposition at the trailing edge of the fuel flow
- Calculation of enhanced film deposition by Rayleigh-Taylor instabilities caused by slug acceleration effects.

It is important to note that currently the PLUGM code does not have the capability to model the entrainment of fragmented crust or molten wall into the flowing bulk melt material. Thus, stable crusts are assumed, even in the presence of an underlying molten wall layer. The steel entrainment seen in TRAN-2 and TRAN-4 (and presumably in TRAN-3 and TRAN-5) is not accounted for in any of the current analyses. Thus, the blockage formation seen in TRAN-2, which appears to be caused by the presence of entrained steel, cannot currently be analyzed.

An important parameter in the PLUGM analyses of these TRAN Series I experiments is the initial mass of molten fuel assumed to flow into the freezing channel. In all cases, the initial fuel load in the melting chamber was about 44 g. However, as was shown in Table 1, typically less than half of the initial fuel load ended up in the fuel freezing channel. Some of the remaining fuel was deposited on the melt chamber walls in the form of crust or a liquid film or both. However, crust growth and film deposition in the melt chamber could not account for all of the remaining fuel. A substantial amount of the fuel actually drained (or was dispersed) below the melt chamber. The mechanism for this downward displacement is currently unknown. However, one possible explanation might be the presence of trapped gas in the original fuel sample, which upon fuel melting was heated and compressed, thereby leading to internal pressurization of the molten fuel. If the internal gas content was high enough, the gas pressure internal to the molten fuel could initially exceed the applied driving

pressure and result in downward dispersal (below the melt chamber) of some of the molten fuel. The PLUGM code cannot model such internal pressurization and downward dispersal. Thus, it was neccessary to perform the PLUGM calculations with less than the actual 44-g-initial fuel load. The initial mass used in the calculations was then simply determined from the final mass of fuel that ended up in the fuel crust along the length of the freezing channel (as determined from the posttest examination of the experiments). These amounts (shown in Table 4) differ slightly from the values given in Table 1, because they do not include the fuel in the blockage (TRAN-2) or in the dump tank.

The PLUGM code was applied to the analysis of all five of the TRAN Series I experiments. The important parameters used in these calculations are summarized in Table 4. It is expected that the calculation for TRAN-1 is the most accurate, because there is no steel melting or entrainment in this experiment. The steel melting that was observed in TRAN-2 and TRAN-4 (and is thought to have occurred in TRAN-3 and TRAN-5) is also modeled. However, the entrainment of steel and the possible effect this has on the fuel flow (possible blockage formation) is not modeled. Thus, the current PLUGM calculations, especially for TRAN-4 and TRAN-5, are not intended as best estimate analyses. They are nonetheless useful for interpretation of the experiment results.

Table 4

Summary of Key Parameters Used in the PLUGM Analysis of the TRAN Series I Experiments

Exp.	Mass of Fuel in Crust (g)	Initial Fuel Temperature (K)	Initial Steel Temperature (K)	Driving Pressure (MPa)
1	15.3	3170	673	1.6
2	21.1	3720	873	1.0
3	14.9	3770	943	1.0
4	14.7	3750	1173	1.0
5	11.3	3590	1173	0.3*

*Variable in time due to dump tank pressurization

In Table 5 a summary of the PLUGM results is presented showing the measured and PLUGM-calculated values for the penetration distance, the crust thickness at the entrance to the channel, the axial extent of wall melting, and the wall melt thickness at the entrance to the freezing channel. Only selected measured values are available for comparison with the calculations.

Table 5

PLUGM Predictions of the Fuel Crust Distributions in the TRAN Series I Experiments

	Axial Crust Length (m)		Crust Thickness at Inlet (mm)	
Exp.	meas.	pred.	meas.	pred.
1	0.70	0.70	0.25 - 0.31	0.26
2	0.87	0.98	0.23 - 0.52	0.18
3	0.67	0.77	---	0.17
4	0.48	0.77	0.13 - 0.46	0.17
5	0.45	0.53	---	0.21

As can be seen from Table 5, for the assumed mass of fuel in the freezing channel, the predicted and measured crust lengths match extremely well for the TRAN-1 experiment. Shown in Figure 6 are the measured and predicted axial crust thickness distributions for this same experiment. Additional details of the PLUGM calculation for TRAN-1 are shown in Figures 7 and 8. Figure 7 shows the position of the liquid fuel slug in the channel as a function of time. Depletion of the molten fuel can be seen as the slug moves up the channel. As a result of this mass depletion the slug mass and length decrease thereby resulting in an acceleration of the fuel. This is shown in Figure 8. This behavior is typical for all the TRAN calculations.

The results for experiments TRAN-2 through TRAN-5 as shown in Table 5 indicate a somewhat ($\simeq$10%) longer predicted crust length than was actually observed in the experiments. In TRAN-2 a blockage was formed so that the PLUGM modeling assumption of complete mass depletion by crust growth and film deposition would not be valid. Thus, at the time the leading-edge blockage formed, there may have been a small molten-fuel slug behind the blockage, which subsequently drained back down the freezing channel. This would lead to a higher linear density of fuel in the freezing channel than predicted by PLUGM. In TRAN-4 and TRAN-5, there is evidence of complex molten steel entrainment, which led to enhanced bulk-fuel cooldown and obviously affected the

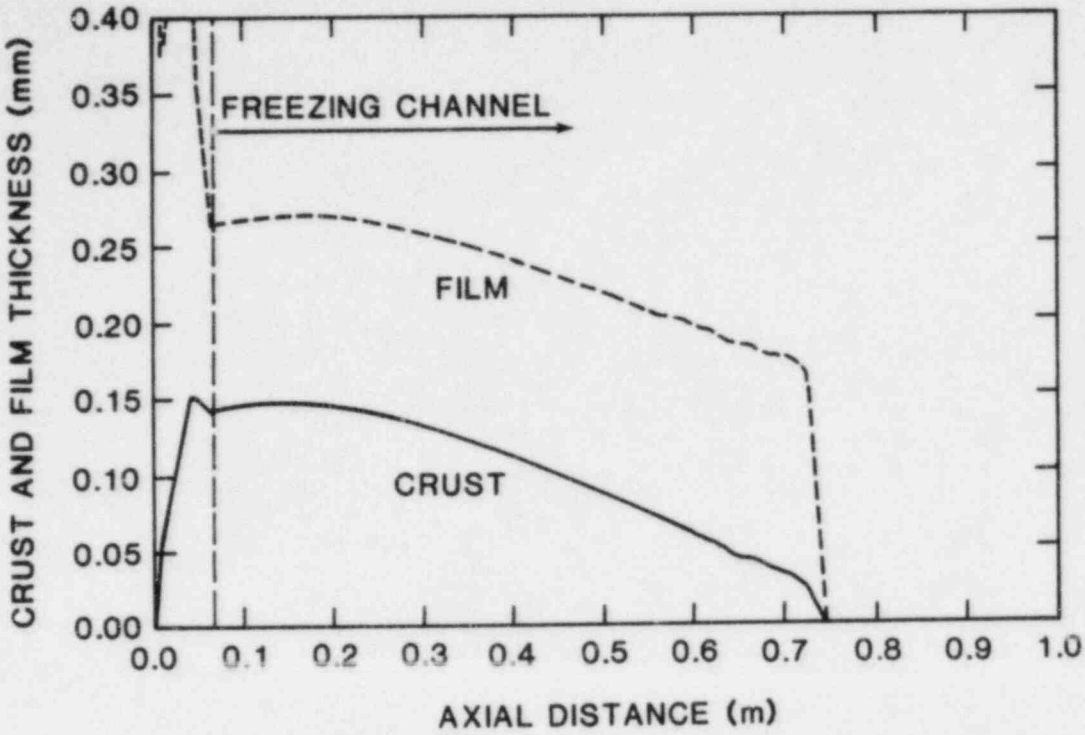

Figure 6 Predicted TRAN-1 axial crust thickness distribution.

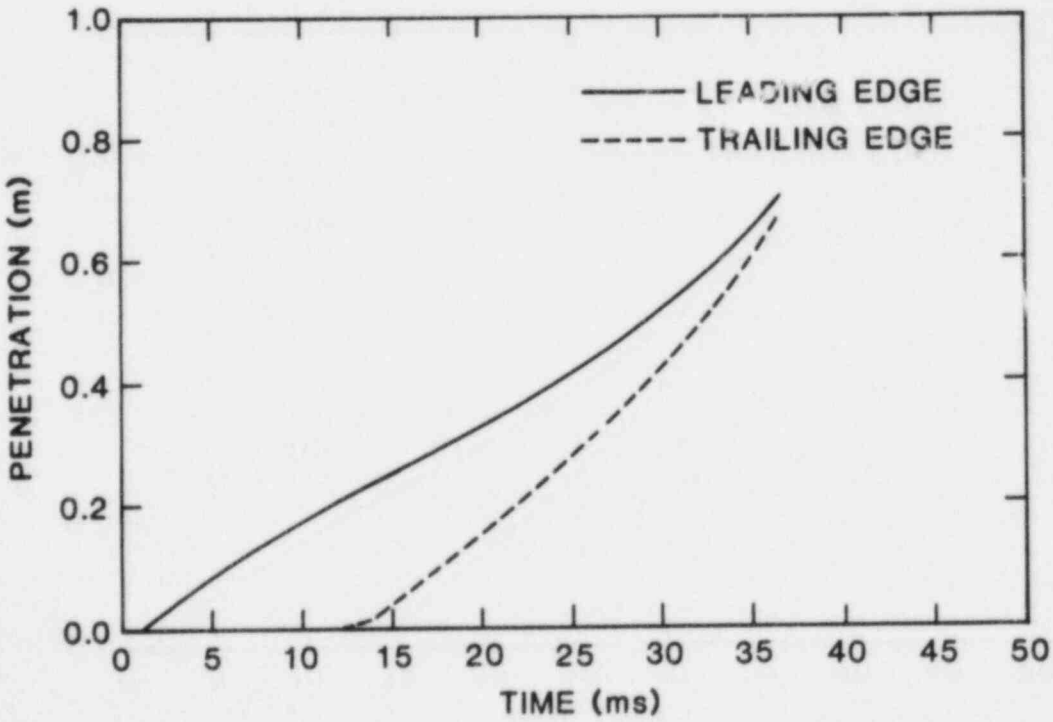

Figure 7 Predicted fuel slug position history for the TRAN-1 experiment.

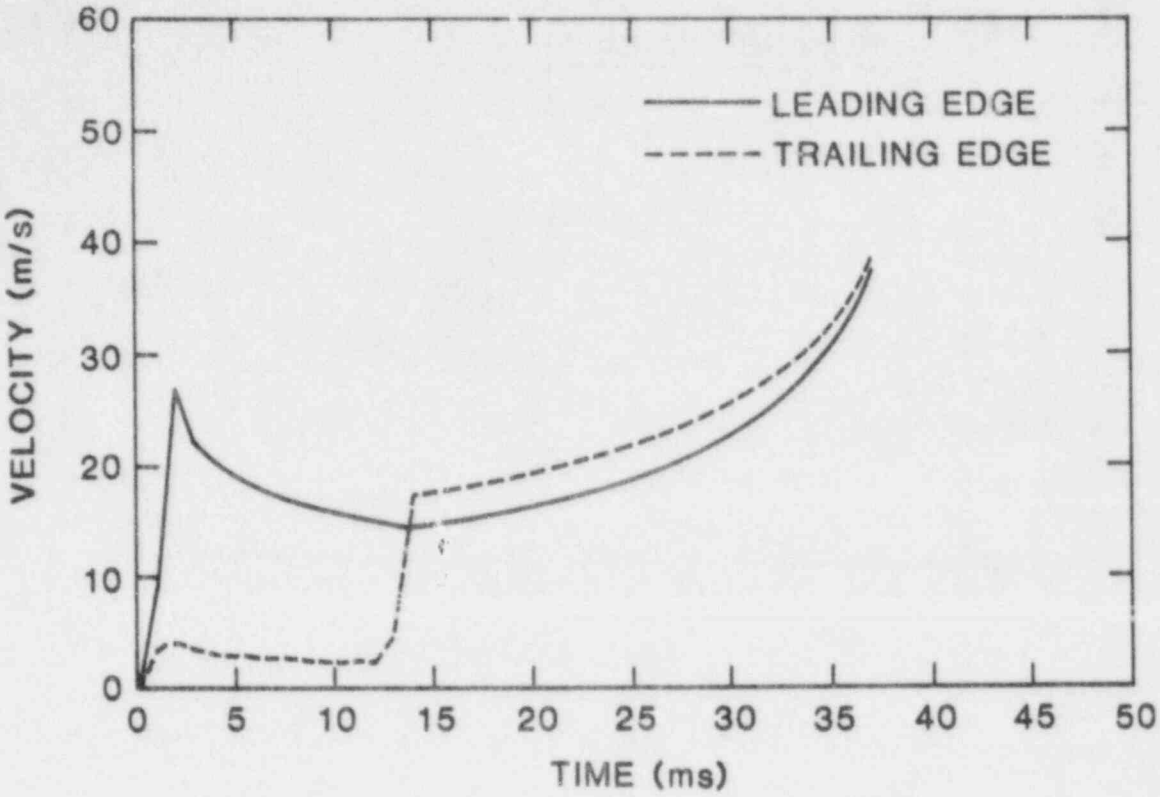

Figure 8 Predicted fuel slug velocity history for the TRAN-1 experiment.

hydrodynamics of the fuel flow. These phenomena are also not accounted for in PLUGM, and thus the disagreement between measured and calculated penetration is not surprising. The cause of the discrepancy for TRAN-3 is not known. There was no evidence for a complete blockage as in TRAN-2. However, it is predicted that there was more steel melting than in TRAN-2, and this steel melting and possible entrainment may be responsible for altering the hydrodynamics of the fuel flow.

The wall melting results are shown in Table 6. As can be seen, wall melting was restricted to the first 10 to 20 cm of the freezing channel in TRAN-2 and TRAN-3. More melting was expected in TRAN-3 than in TRAN-2 because both the steel and fuel initial temperatures were higher. In TRAN-4 and TRAN-5, wall melting was predicted to extend over the entire length of the freezing channel that contained fuel crust. However, the thickness of the molten layer was larger near the channel inlet than at the top of the fuel penetration. This is seen in Figure 9, which shows the final axial distribution of the molten steel layer in TRAN-4. Figure 10 shows the development in time of the molten steel layer at the channel entrance in TRAN-4. It should be noted that the calculation of crust growth and wall melting terminates when the trailing edge of the slug passes a given position. Thus, freezing of the liquid film layer and possible further wall melting are not explicitly calculated. It can be seen in Figure 8 that the molten steel layer is still growing when the trailing edge of the slug

passes the channel entrance. Thus, the cooldown of the liquid film probably resulted in some additional wall melting.

Table 6
PLUGM Predictions of Wall Melting in
the TRAN Series I Experiments

	Axial Extent of Melting (m)		Melt Thickness at Inlet (μm)	
Exp.	meas.	pred.	meas.	pred.
1	none	none	none	none
2	0.09 - 0.12	0.1	500	75
3	*	0.18	*	70
4	0.24	entire length	55 - 500	120
5	*	entire length	*	90

*not measured

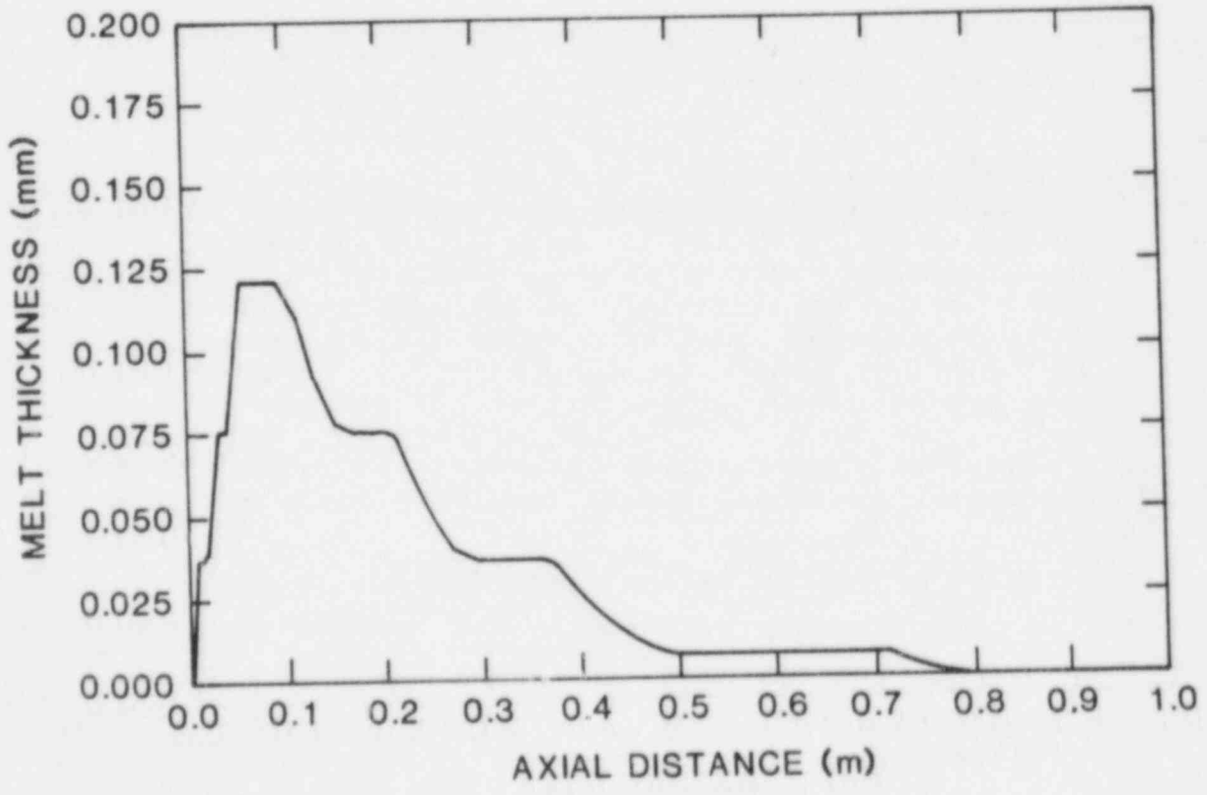

Figure 9 Predicted wall melt distribution in the TRAN-4 experiment.

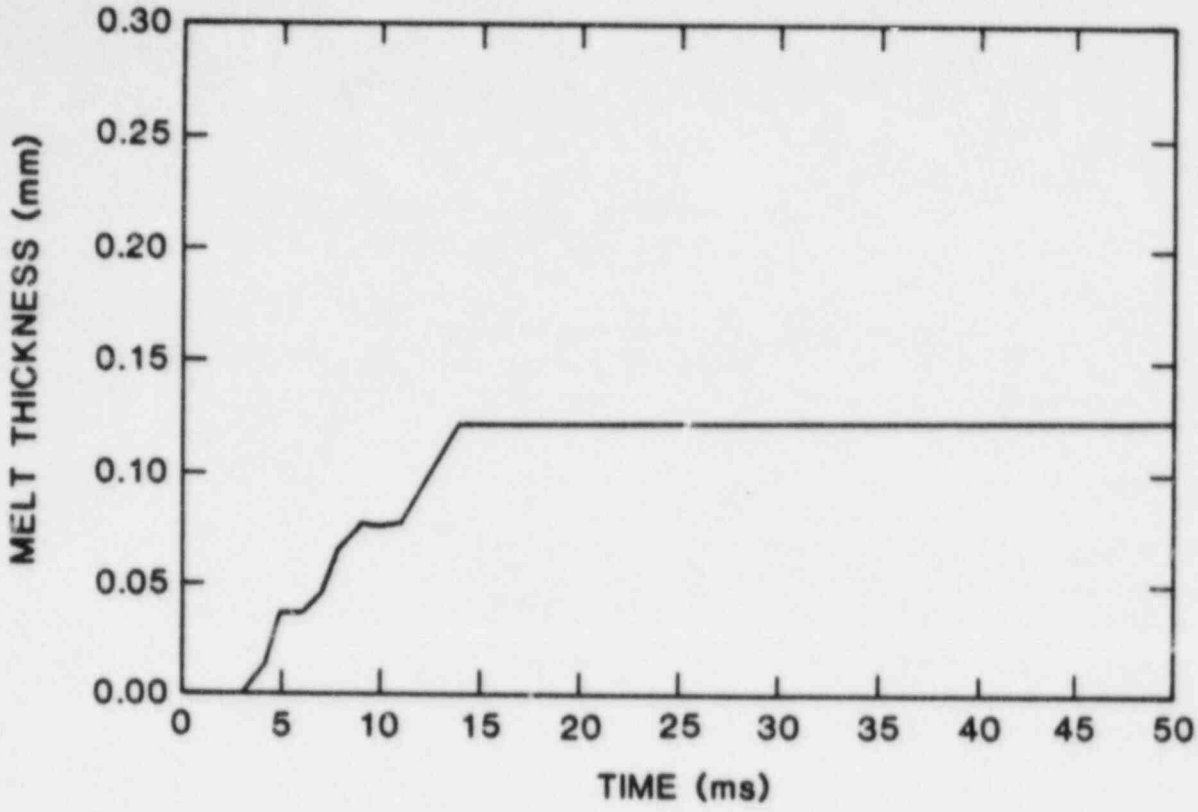

Figure 10 Predicted wall melt history at the freezing channel inlet in the TRAN-4 experiment.

The excellent agreement between the PLUGM predictions and the measured values for TRAN-1 indicate that the relevant phenomena are being adequately modeled by PLUGM for the case of no wall melting. In this case the fuel freezing behavior is well described by a conduction-freezing model if the acceleration and film-deposition effects are accounted for. This same model also forms a good basis for the description of the higher temperature experiments. Thus, the model qualitatively predicts such parameters as the extent of wall melting.

However, it is clear that additional modeling is required for a complete desciption of these experiment results. These models must describe:

- the timing of molten wall entrainment
- the amount of molten wall entrainment as a function of time
- the characteristic size of the entrained material
- the bulk internal heat transfer between entrained wall material and molten fuel
- the effect of bulk melt cooldown and wall material entrainment on the hydrodynamics of the flow (film deposition)

Further development work on PLUGM to model these phenomena is continuing.

APPENDIX A

TRAN EXPERIMENT PACKAGE DESIGN

1. OVERALL DESIGN

Figure 11 shows an approximate scale cutaway drawing of the apparatus. The pressure system components consisted of Whitey and Nupro valves, a Whitey pressure cylinder, and Cajon precision pipe fittings. The pressure system components were sealed together with Teflon tape. The maximum fill pressure of the system was limited to 1850 psi by a safety rupture disk on the pressure reservoir valve. The solenoid valve was a Circle Seal SV30S32P4PE, requiring a 24-volt actuating pulse which was controlled by a special noise-insensitive trigger circuit.* A delay of about 45 ms between the valve actuating pulse and the peak of the applied pressure pulse was measured for all valves. During the actual experiment, the solenoid valve was left open for ten seconds (to allow complete freezing) and then closed again to reduce possible contamination of the pressure system. Kaman Sciences KP-1911 absolute pressure transducers were used, with a typical pressure range of 0-2000 psi to cover the entire range of interest. These were sealed into the apparatus with Pressure Science C-seals which were coated with either silver (for $T_s < 873$ K) or gold ($T_s > 873$ K). Care was taken to reduce incidental heating of the Kaman "hard" cables as they passed by the freezing channel, to reduce zero shifts in the pressure readings as the apparatus was heated.

Much useful information can be obtained by analyzing the flow of gas and molten fuel through the melt chamber and freezing channel. For this reason, Table 7 gives the volumes of the gas reservoir and associated pressure transducer (V_{gr}), the free volume between the solenoid valve and the base of the fuel (V_{vf}), the volume of the freezing channel (V_{fc}), the volume of the dump tank and connecting channels (V_{dt}), and the length of the freezing channel (L_{fc}). In Table 7, the volumes, V, are given in cm^3 and the length, L, in cm.

In TRAN-1, -2, and -3, Samox-insulated high temperature heater tapes were applied directly to the 316 SS freezing channel. Because the heater tapes degraded and shorted out to the metallic freezing channel at sustained temperatures above 973 K, Watlow biaxial heaters were wound onto the freezing channel for TRAN-4 and TRAN-5. Johns-Manville Q-Fiber felt insulation was used to insulate the preheated freezing

---

*Designed and fabricated by G. L. King, Sandia National Laboratories, Albuquerque, NM 87185

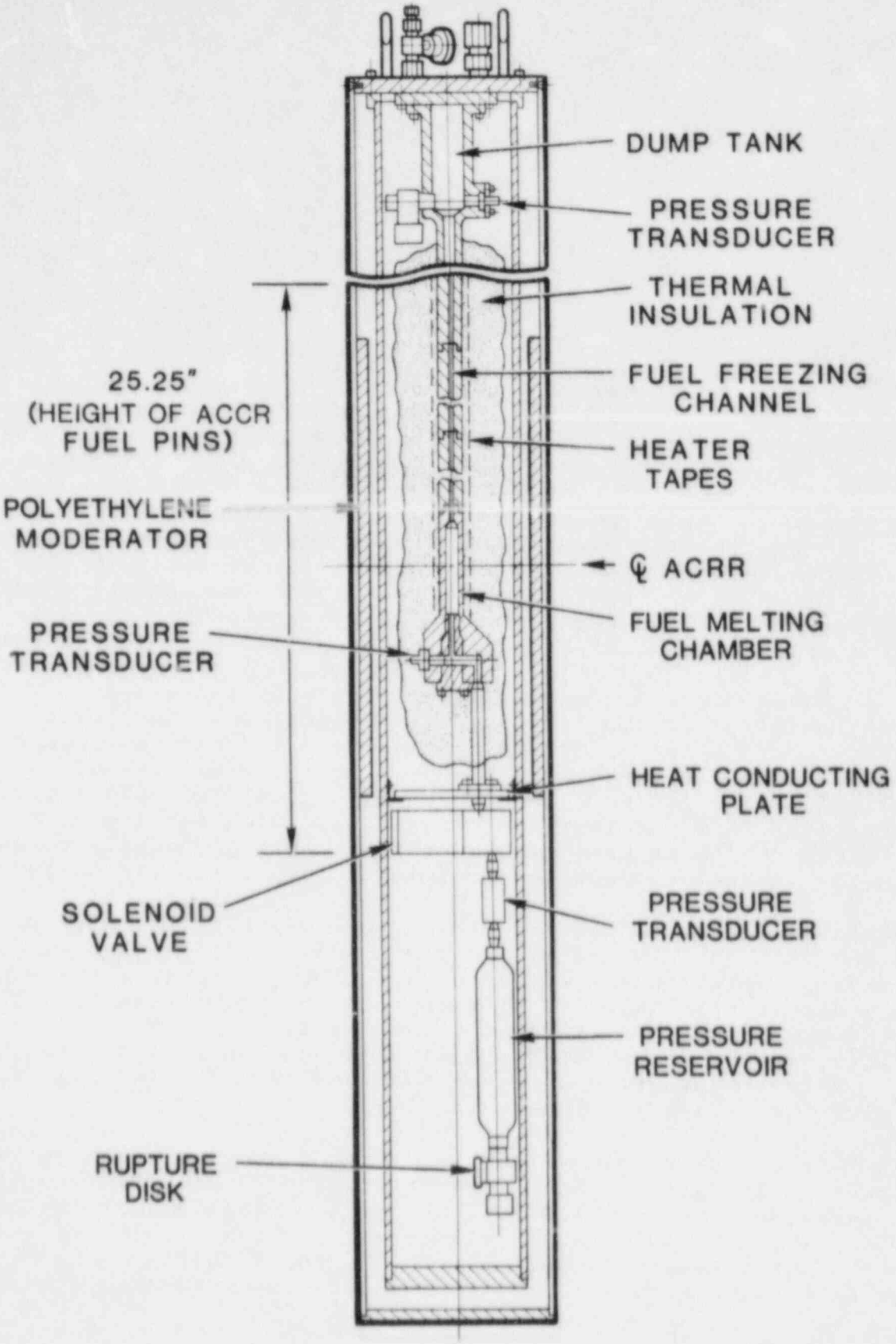

Figure 11 Approximate scale drawing of the TRAN series I apparatus.

Table 7. TRAN Series I Package Design Parameters

V_{gr}	V_{vf}	V_{fc}	V_{dt}	L_{fc}
315	37	10.2	135	130

channel from the containment canister. The containment canister was backfilled with 0.05 MPa of helium for thermal coupling to the cooling air flow outside the containment canister. The temperature-controlling thermocouples were wired to the surface of the 316 SS freezing channel, underneath the heaters.

A heat-conducting plate was placed just above the solenoid valve, to conduct leakage heat from the pressure inlet pipe to the containment canister wall. With this arrangement, the solenoid valve temperature never exceeded 308 K, well below its maximum operating temperature of 343 K.

2. FUEL LOAD AND FUEL MELTING CHAMBER DESIGN

Special UO_2 pellets of 80 percent theoretical density and enrichments ranging between 9.5 and 11.1 percent were fabricated by Los Alamos National Laboratory. The pellets were 5.08-cm long with a 0.80-cm-outside diameter. Two fuel pellets were placed in the fuel melting chamber, which had a 0.820-cm-inside diameter and a length of approximately 11 cm. The average density of 80 percent was chosen to minimize spurting of the molten fuel when it underwent expansion upon melting. The radial gap of 0.01 cm was chosen to be small enough that the gap was sealed by radial expansion well before fuel melting occurred (2.5 percent expansion required), but large enough to minimize solid-state single-phase pressures against the melting chamber wall, which might occur before fuel melting. A cone-shaped transition was used between the end of the fuel melting chamber and the freezing channel to provide smooth flow from the melting chamber into the freezing channel (Figure 12). A total fuel mass of 44 g of UO_2 was chosen as being representative of the mass of fuel in the active core of an LMFBR per flow subchannel.

The diameter of the fuel pellets, the thickness of the melting chamber wall, and the enrichment of the fuel pellets represented a compromise between several competing factors. On the one hand, large-diameter fuel pellets of high enrichment would permit the maximum amount of fuel to be used in experiments and allow the highest possible sensible heat above melt. On the other hand, maximum uniformity of the fuel temperature was desired. Also, in the event of rapid plugging, much of the fuel would not leave the melting chamber and its heat content must be absorbed by the melting chamber wall without seriously weakening it (if seriously weakened it might burst under the application of

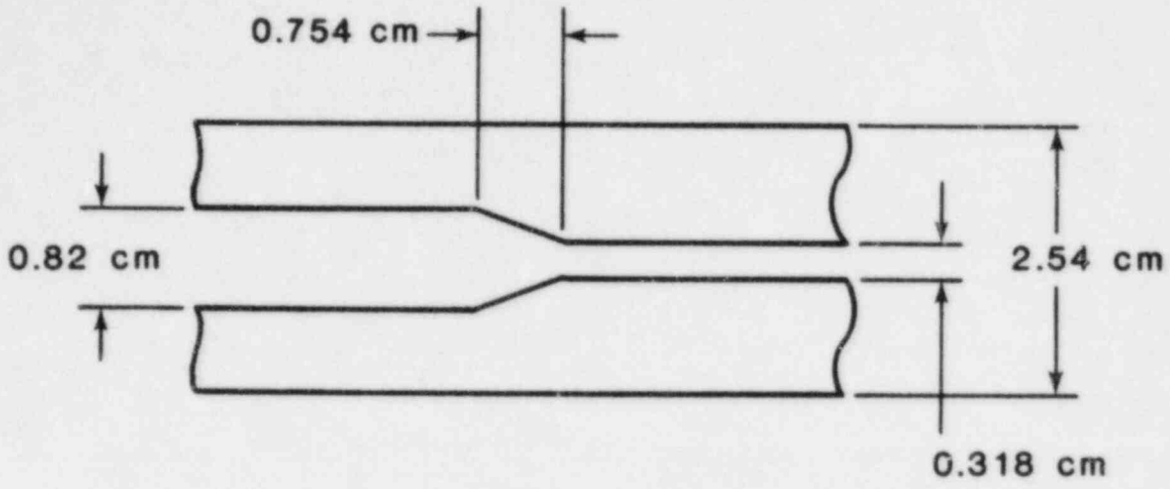

Figure 12 Transition region between the fuel melting chamber and the freezing channel.

constant driving pressures up to 10 MPa). These requirements result in a low fuel enrichment, a small fuel pellet diameter, and a thick melting chamber wall. To achieve an optimum design, transient calculations of heat transfer from the molten fuel to the melting chamber wall were performed with TAC2D,[20] and detailed neutron transport calculations of the axial and radial energy deposition in the fuel were performed with TWOTRAN.[21]

For an initial steel temperature of 1073 K and a peak fuel temperature of 4273 K, Figure 13 shows calculated temperature profiles in the melting chamber wall, shortly after the reactor pulse (t=0.3 s), at t=6.5 s, and at the peak temperature reached by the outside surface of the wall (t=26.5 s). Although higher temperatures are reached at the earlier time, the bulk of the wall is still near its initial temperature. Therefore the late-time condition of a somewhat lower but nearly uniform wall temperature was chosen as the limiting safety condition. The optimum wall thickness of 0.87 cm was chosen to permit operation up to a fuel temperature of 3970 K, initial steel temperature of 1070 K, and a driving pressure of 10 MPa, without exceeding a peak outside wall temperature of 1370 K (above which the steel weakens drastically).

At the optimum wall thickness a fuel enrichment of 11 percent yields the required range of fuel energy depositions, and results in a peak-to-average ratio of 1.15 for the radial energy deposition. Some fuel pellets with two radial zones of 11.1 and 9.5 percent enrichment were also fabricated, which lowers the peak-to-average ratio to 1.10. However, all experiments thus far have been performed with fuel pellets of a single enrichment of 11.1 percent.

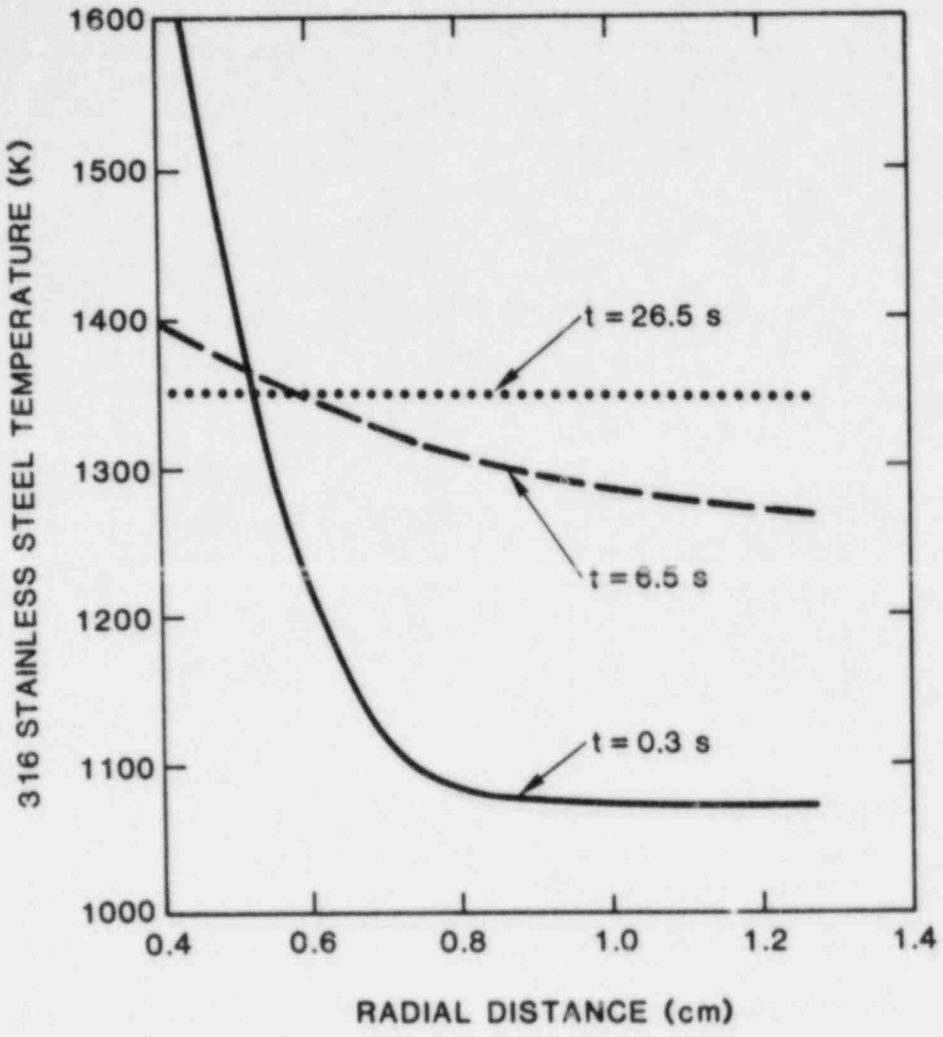

Figure 13 Temperature profiles in the melting chamber wall.

3. FREEZING CHANNEL DESIGN

The TRAN program has been subdivided into several experiment series, with freezing channels of increasing complexity and prototypicality. Series I is primarily concerned with proving feasibility of the experimental concept and investigating freezing in a simple geometry which allows detailed theoretical analysis. For this reason a thick-walled cylindrical freezing channel was chosen with an inside diameter corresponding to available gun drill sizes and to a representative hydraulic diameter of a CRBR coolant subchannel. In a thick-walled cylindrical freezing channel the parameter range over which instantaneous steel melting occurs can be investigated, as well as such fundamental crust properties as thermal and mechanical instability. The well-controlled driving pressure and much wider range of fuel temperatures available with the TRAN concept should yield much useful new data.

The TRAN Series I freezing channel had an inside diameter of 0.32 cm, a wall thickness of 1.11 cm, and a heated constant-diameter length of 130 cm. It was fabricated by gun-drilling sections of 316 SS bar, each 41-cm long, welding these sections together, and reaming out the channel to remove any slight diameter changes caused by welding. The resulting pressure vessel was proof-tested hydrostatically to about 41 MPa.

APPENDIX B

POSTTEST ANALYSIS PROCEDURES

The most important result desired from the TRAN experiments is a good understanding of the phenomena involved during penetration and freezing of pure reactor materials in LMFBR pin-bundle geometries. However, TRAN Series I uses a thick-walled cylindrical freezing channel to simplify theoretical analysis of the phenomena in terms of current fuel-freezing models. Therefore, the results of each TRAN experiment will be compared to the predictions of new or existing models to ascertain which models best describe fuel freezing over a given parameter range.

Thus, the final distribution of the frozen fuel and the mass of fuel which penetrates into the freezing channel or beyond are important results, as well as the time-dependence of the freezing process and the porosity of any blockages or flow restrictions which might form. Several on-line diagnostic methods have been used to infer this information. In this section the characteristics of pressure and fuel-motion-measuring instrumentation are discussed, as well as the measurements made to analyze the final fuel distribution and the interaction of the molten fuel with the steel walls of the channel. These items will be discussed roughly in the order in which information was obtained after each experiment.

1. PRESSURE TRANSDUCER DATA

1.1 Characteristics of Pressure Transducers

The Kaman eddy-current pressure transducers used in these experiments respond to absolute pressure, produce readings which are independent of the particular fluid, respond very rapidly in the pressure ranges used here, and are relatively insensitive to radiation background and slow temperature changes. However, the individual transducers are quite expensive, and a change in pressure range requires the purchase of a new transducer.

The Kaman transducers originally ordered for the TRAN experiments were chosen to cover a very wide pressure range, but all TRAN experiments performed thus far have been at low pressures (which correspond to the most important accident scenarios for CRBR, and where almost no experiments have been performed). For this reason, the transducers have been used only in the lowest ten percent of their pressure range. As a result, the pressure signals have been smaller than normal compared to such noise components as transducer non-linearity, electrical noise,

radiation noise, and drifts associated with heating of the transducer cables. In spite of being operated in the lowest ten percent of their range, results have generally been quite good, but certain corrections had to be made to the raw data.

The most important pressure transducer correction was for the slow drift in the absolute pressure reading caused by heating of the transducer cables that occurred during the heating of the freezing channel to the desired initial steel temperature. This drift was large compared to the low initial pressure chosen, and as a result the transducers were reset to the known initial pressure readings when the apparatus was at the desired initial temperature. Although this drift made it impossible to follow slow pressure changes (such as might be caused by heating of chambers containing gas), such effects were expected to be small except in the case of TRAN-5, where the preheated freezing chamber was prefilled with helium gas.

There was no measurable heating effect on the sensitivity of the transducers in responding to pressure changes. This was confirmed by noting that the initial pressure pulse below the fuel load agreed with the expected value in TRAN-4, where the pressure pulse was applied well before either fuel melting or radiation noise pulses occurred.

In the extremely intense radiation fields of the ACRR a radiation-induced signal was present. This interfered with observation of any pressure changes occurring during the ACRR pulse. This radiation noise pulse consists of a negative signal (typically ~1.5 MPa) which roughly follows the intense portion of the ACRR pulse, followed by a slowly-decaying signal shift of about 0.15 MPa. The slow radiation noise component forces the experimenter to be suspicious of pressure changes as small as 0.15 MPa for about 100 - 400 ms after the onset of the ACRR pulse. The radiation noise pulses are not proportional to ACRR power, so it is difficult to correct for them.

Spurious negative pressure readings can also be caused by rapid heating of only the front surface of the transducer, because this rapid heating produces a distortion of the pressure-measuring membrane. Such heat-induced signals were caused in the TRAN experiments by direct contact of molten fuel or fine fuel particles (perhaps condensed fuel vapor) with the surface of the transducer. The heat-induced signals were complex and long-lasting, and usually indicated that all subsequent data from that particular transducer were invalid until it was re-calibrated. In a few cases, very small heat-induced signals were observed, and a correction was applied to the data. Such corrections are not very quantitative (being based on graphical extrapolation), and should be regarded as estimates only.

To summarize: When interpreting pressure transducer data, the initial signal level was forced to match the known initial pressure, by adding a constant to the signal. Pressure changes from this initial level were then calculated using the calibrated linear sensitivity of the particular transducer. For the He-Reservoir and Above-Solenoid-Valve transducers, the pressure trace was ignored for about 100 ms around

the ACRR pulse because of radiation noise. Pressures at late times (when pressures should have equilibrated) were not expected to agree to better than about 0.14 MPa based on the measured deviation from linearity of the transducers. Finally, if a transducer showed evidence of a large negative pressure pulse caused by heating, the data from that transducer was ignored following that heating pulse.

1.2 General Results of Pressure Transducer Data

Pressure transducers were placed at the exit of the pressure reservoir, between the solenoid valve and the initial fuel load, and in the dump tank at the top of the freezing channel. The volume of the pressure reservoir is large compared to the empty volume between the solenoid valve and the base of the fuel load. Therefore the pressure drops between 8.5 and 10.9 percent while filling the piping below the fuel load. The pressure-reservoir transducer was usually protected from hot fuel by a right-angle bend in the gas piping and by the solenoid valve itself. This transducer thus yielded a good measurement of gas flow out of the reservoir during each experiment.

The pressure transducer between the solenoid valve and the fuel load was intended to measure the pressure applied to the column of molten fuel. This transducer was used mainly to verify the opening of the solenoid valve. Data subsequent to the reactor pulse were difficult to interpret because the transducer was subjected to the most intense radiation field and was also heated by molten fuel in several instances. These phenomena resulted in complex and physically unlikely signals.

The third pressure transducer was located at the top of the freezing channel, in the side of the dump tank. The purpose of this transducer was to sense any gas flow produced by melting of the fuel, or gas leakage past the fuel at early times, and to measure the porosity of any blockage or gas flow restrictions that formed as a result of fuel freezing. The radiation background was much lower at this transducer (which was located 2 m above the ACRR core centerline), but in several experiments a small negative pressure signal was observed just before the main gas flow began at the dump tank. These negative pressure signals were presumably caused by small amounts of volatile, hot material that streamed up the evacuated freezing channel and were deposited on the transducer face. A shadow shield over the face of the transducer has reduced but not completely eliminated this problem.

To measure the approximate time of fuel freezing and the permeability of any blockages which occurred, the signals from the pressure reservoir and dump tank transducers were used. In a typical TRAN experiment, the time dependence of pressure equilibration between these two chambers was compared with the pressure equilibration rate observed when the freezing channel and fuel melting chamber were empty of fuel. A representative empty-channel equilibration experiment at P_D = 1 Mpa and a channel temperature of 1073 K is shown in Figures 14-16. Initial pressure equilibration for an empty channel occurs in 90 ms followed by a further slow pressure increase of about 20 percent in the dump tank, which apparently is associated with gas heating as it interacts

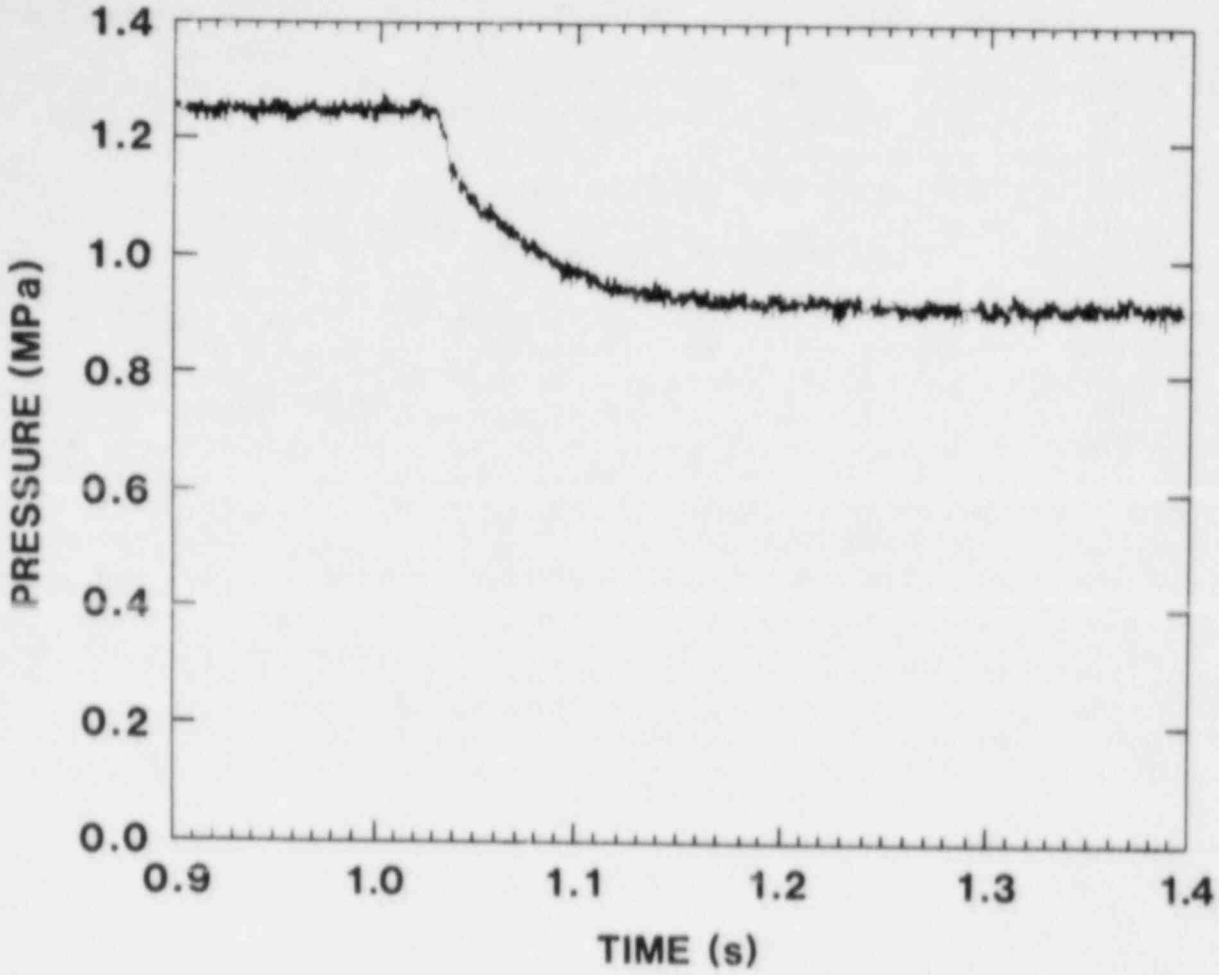

Figure 14 Helium reservoir pressure during the heated flow test.

with the hot channel wall. To analyze flow restrictions more quantitatively, the rate of increase of the dump tank pressure as a function of pressure drop between the ends of the freezing channel was plotted for a given TRAN experiment, and compared to the empty-flow-channel case.

2. FUEL MOTION DETECTOR DATA

Direct mesurements of the fuel location in a TRAN experiment are difficult because of the high pressures and temperatures involved. One possible method of sensing fuel location is by use of an array of rugged high-temperature detectors sensitive to the fission gamma-ray emission from the molten fuel. Such detectors have been tested at Sandia National Laboratories as in-core diagnostics for large-bundle LMFBR safety experiments, and the associated computer programs for unfolding the fuel distribution from the gamma-ray signal data have been developed and tested for certain geometries.[22]

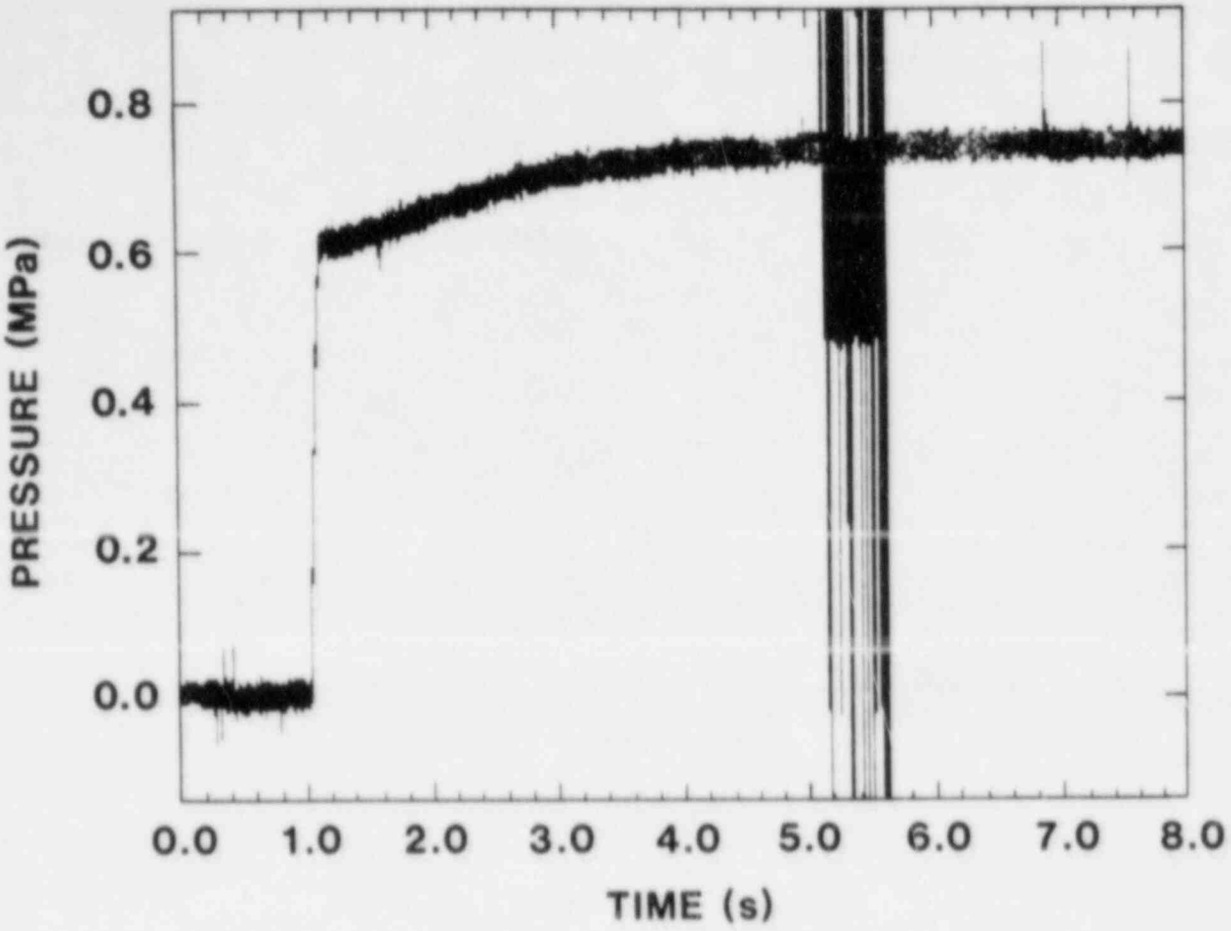

Figure 15 Long-term dump tank pressure during the heated flow test.

In experiments TRAN-2, TRAN-3, and TRAN-4, platinum self-powered detectors 0.159 cm in diameter with an emitter length of 50.8 cm were used.[23] Four detectors were wound directly onto the outside of the 2.54-cm-diameter pressure vessel containing the fuel melting chamber and the freezing channel (Figure 17). These detectors were located at the base of the initial fuel load (G_1), at the top of the initial fuel load (G_2), at 11.5 cm above the entrance to the freezing channel (G_3), and at 14.5 cm above the exit of the freezing channel (G_4). A fifth detector was wound on the outside of the 16.8-cm-diameter containment canister, at the axial midplane of the initial fuel load (to provide a measurement of the general gamma-ray background near the center of the ACRR). This detector arrangement was chosen to provide signals corresponding to the movement of the fuel out of the fuel melting chamber, and then into and through the freezing channel. Based on this geometry, signal changes of ≈3 percent were expected when the fuel moved completely out of the fuel melting chamber.*

*P. J. McDaniel, Sandia National Laboratories, Albuquerque, NM 87185, private communication.

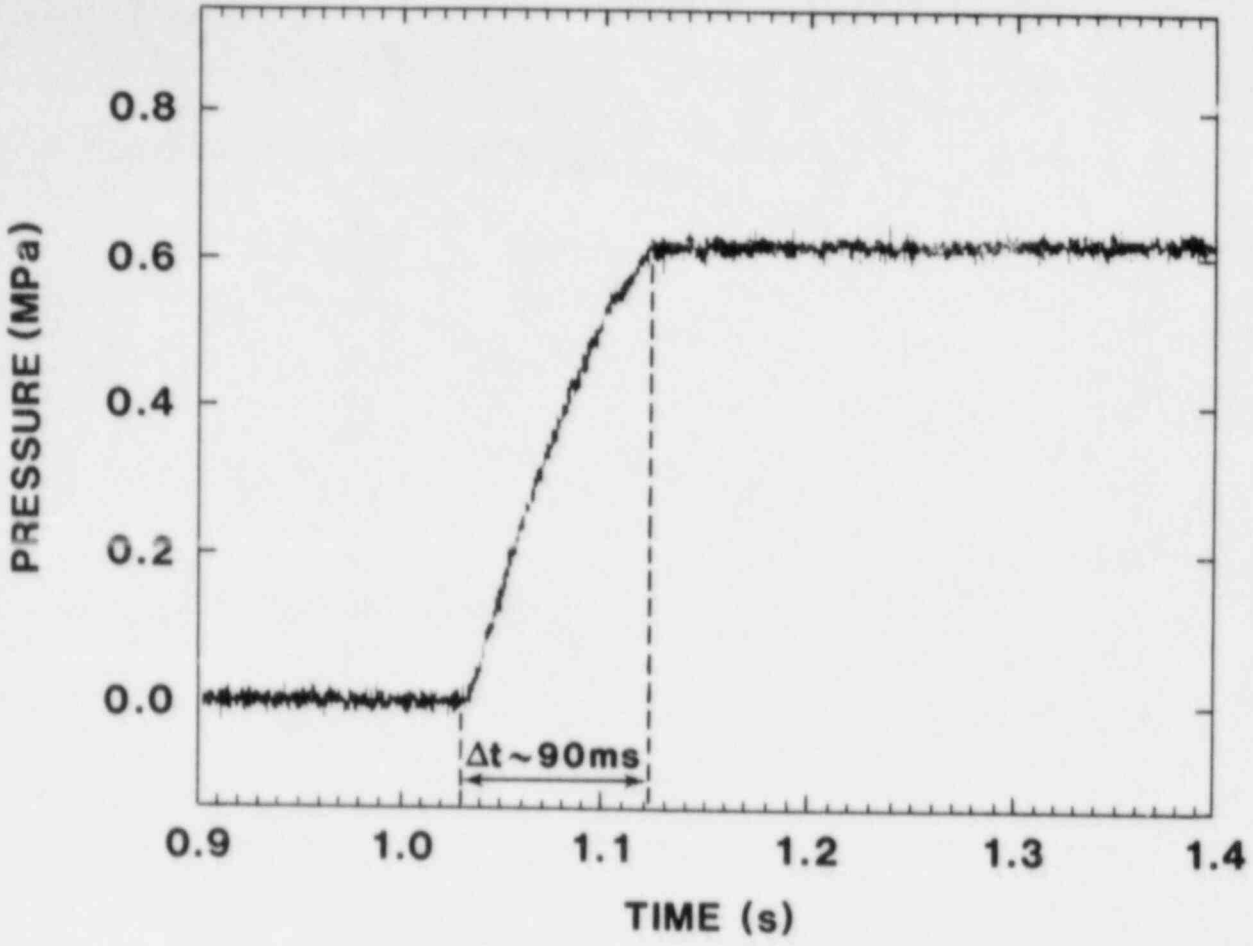

Figure 16 Early dump tank pressure during the heated flow test.

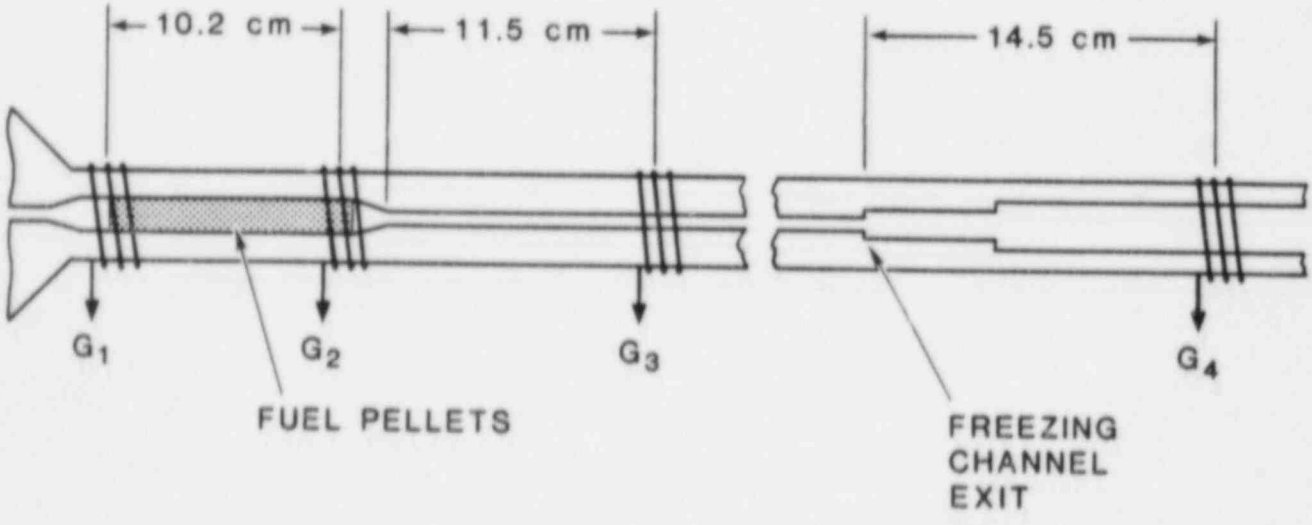

Figure 17 Locations of the self-powered gamma ray detectors.

Several preliminary experiments were performed in the ACRR to calibrate the expected signal levels for each detector. The detector at the exit of the freezing channel showed a peak signal about one percent as large as the signals from the detectors near the center of the ACRR. The time dependence of this signal was also slightly different.

Otherwise, the signal shapes from all detectors closely resembled the measured ACRR power pulse, and the observed noise levels should permit observation of 1% signal differences.

Two experiments were performed at high ACRR power levels for the TRAN-2 conditions. The first experiment involved very little fuel motion, but the second experiment (at a slightly higher power level) resulted in fuel flow out of the melting chamber and into the freezing channel. Comparison of the signals from these two experiments (TRAN-2/AE and TRAN-2/R, respectively) should have given a good calibration of the fuel motion sensitivity of this detector arrangement. Small relative differences in signals were indeed observed among the various detectors. A fairly exact computer model of the experiment geometry appears to be required to determine whether the observed signal changes were caused by fuel motion rather than by spatial differences in neutron flux, or other possible causes. Results for each experiment will be described below.

3. THERMOCOUPLE DATA

Thermocouples were used to regulate the initial temperature of the fuel melting chamber and the freezing channel, and to monitor safety-related temperature excursions. These temperatures were recorded on stripchart recorders or magnetic tape. The thermocouples were wired to the outside surface of the 2.54-cm-diameter freezing channel, and were surrounded by heater tapes (or biaxial heaters) and Q-Fiber felt insulation. Because the thermocouples were separated from the freezing channel by the 1.11-cm-thick freezing channel wall, their response to temperature changes in the freezing channel was slow (requiring 20-30 s). Therefore these thermocouples were used primarily to sense the maximum temperature of the freezing channel wall shortly after the ACRR pulse, as an indication of heat transfer from the molten fuel to the channel wall. In estimating the amount of heat transferred to the channel wall, corrections must be made for the rapid steel temperature jump caused by gamma heating (a function of axial position), and for slow heat losses through the felt insulation surrounding the pressure vessel. The temperature rises were usually consistent with deposition of a frozen UO_2 film on the inside of the freezing channel, or with an empty freezing channel heated only by gamma heating.

4. X-RADIOGRAPHY

Each TRAN package was radiographed within one to two weeks after exposure in the ACRR, using a 2.5 MeV electron Van de Graaff accelerator, with a source-to-package-centerline distance of ≈5 m and a package-centerline-to-film distance of ≈10 cm. Measured enlargement of the radiographic image was ≈2 percent. The packages were handled

carefully after exposure in the ACRR to minimize redistribution of the fuel debris. After TRAN-1, all cables, thermocouple leads, etc., were gathered into a single bundle that was located well away from the freezing channel to minimize extraneous background in the radiographs. Before radiography of TRAN-2 through TRAN-5, the heaters, thermocouples, and insulation were also gently stripped off the freezing channel by hand.

Blockages and UO_2 crusts ≈ 0.2 mm thick were clearly observed inside the freezing channel and fuel melting chamber. Thicker crusts were also observed even in regions with steel walls up to ≈ 4 cm thick. The radiographs thus yielded very valuable information about the details of the final melt distribution. However, it was sometimes difficult to see steel accumulations in the channel, and it was difficult to distinguish between fuel and steel.

The radiographic detail allows one to distinguish fairly well between finely-divided fuel powder, loose flakes, crusts, and compact blockages. The thickness of the frozen fuel layer can also be estimated by measuring the optical density variation across the image of the channel diameter with a microdensitometer. However, because of azimuthal crust thickness variations and possible crust density variations, it was difficult to obtain precise fuel masses from the radiographs.

Because no mixing of fuel and steel was observed in TRAN-1 (see Appendix C), the dense areas observed in TRAN-2 and TRAN-3 radiographs were interpreted as pure fuel accumulations. On this basis the maximum length (L_c) of the frozen fuel layer observed on the freezing channel wall was taken as the fuel penetration distance. Fuel debris and blockages have also been observed beyond L_c in TRAN-1 and TRAN-2, but much of this material probably was originally deposited near L_c, and was moved upward beyond L_c by gas flow after freezing had occurred.

5. AXIAL SCANS OF GAMMA RAY INTENSITY

Presumably the most accurate final distribution of fuel would be obtained by direct measurement of fuel masses following total dismantling of a TRAN experiment. However, such detailed analysis involves some delay as well as additional cost. Therefore gamma scanning of the TRAN experiment packages was developed, to infer the final fuel distribution from the distribiution of suitably-chosen fission products. Compared to dismantling and chemical analysis in the Sandia National Laboratories' Hot Cell Facility (HCF), gamma scanning is more rapid and is in principle quite quantitative. Compared to radiography, gamma scanning is also insensitive to the presence of steel. Finally, gamma scanning might eventually be used in combination with pre-irradiated fuel loads to measure where a given portion of the initial fuel load froze in the channel. The gamma-scanning technique has been verified by comparing the fuel mass distributions obtained from different fission product chains with the fuel mass distribution obtained from more direct mass measurements.

To implement gamma scanning a lead shield and a collimator with a lead shutter were constructed. The field of view of the collimator was a transverse section through the TRAN package with an axial extent of ≈1 cm. A rail with a sliding carrier to support the TRAN package allowed the package to be positioned manually in front of the collimator with a repeatability of <2 mm. TRAN packages were scanned by counting for 300-1000 s at each of about 75 axial positions. These positions ranged from 1 cm to 15 cm apart, depending on the gamma intensity and its spatial variation. The intensity data were corrected for radioactive decay and for attenuation in passing through the varying wall thickness of the pressure vessel. The corrected intensity data were plotted as a function of axial position, and also integrated and normalized to provide information on the relative axial distribution of fuel.

5.1 Choice of Gamma Ray Line

The ability to infer the fuel distribution from a fission product distribution rests on a tight chemical bond between the molten fuel and the fission product nuclides during the freezing process. Initially the 1596 keV line of ^{140}La was chosen for scanning, based on the low background near this line, the high photon energy which minimized absorption and scattering, and the reasonable halflife of ^{140}La precursors (≈13 days). The consensus of several advisors familiar with chemistry and solid-state physics was that this fission product chain should remain bound to the fuel, even though the chain contained some volatile precursors with short halflives. However, comparison of the ^{140}La gamma scan for TRAN-1 with other methods of fuel mass measurement showed that serious discrepancies existed, even though there was general agreement between the ^{140}La gamma scan and the radiographs.

Figure 18 shows a typical corrected gamma intensity scan for the 1596 keV line, and the implied normalized fuel distribution. The large peak of emission at the base of the dump tank implies that a large fraction (≈35 percent) of the fuel passed completely through the freezing channel and was deposited on the walls of the dump tank (an erroneous conclusion).

Compared to the radiographs the gamma scan implied considerably greater axial variation of fuel density in the freezing channel, and the radiographs also showed little or no loose fuel material corresponding to the the large peak at the base of the dump tank. Finally, disassembly of TRAN-1 in the HCF revealed only ≈0.5 g of fuel deposited on the walls of the dump tank (Appendix C) rather than the 15 g expected from the 1596 keV gamma peak. Although up to 10 g of fuel were not accounted for during the TRAN-1 analysis in the HCF, it seemed very unlikely that 15 g of fuel deposited on the dump tank walls could be lost. It seemed more likely instead that the ^{140}La precursors might have become separated from the molten fuel during the freezing process. Therefore a search for alternative fission product chains that involved only non-volatile elements was begun.

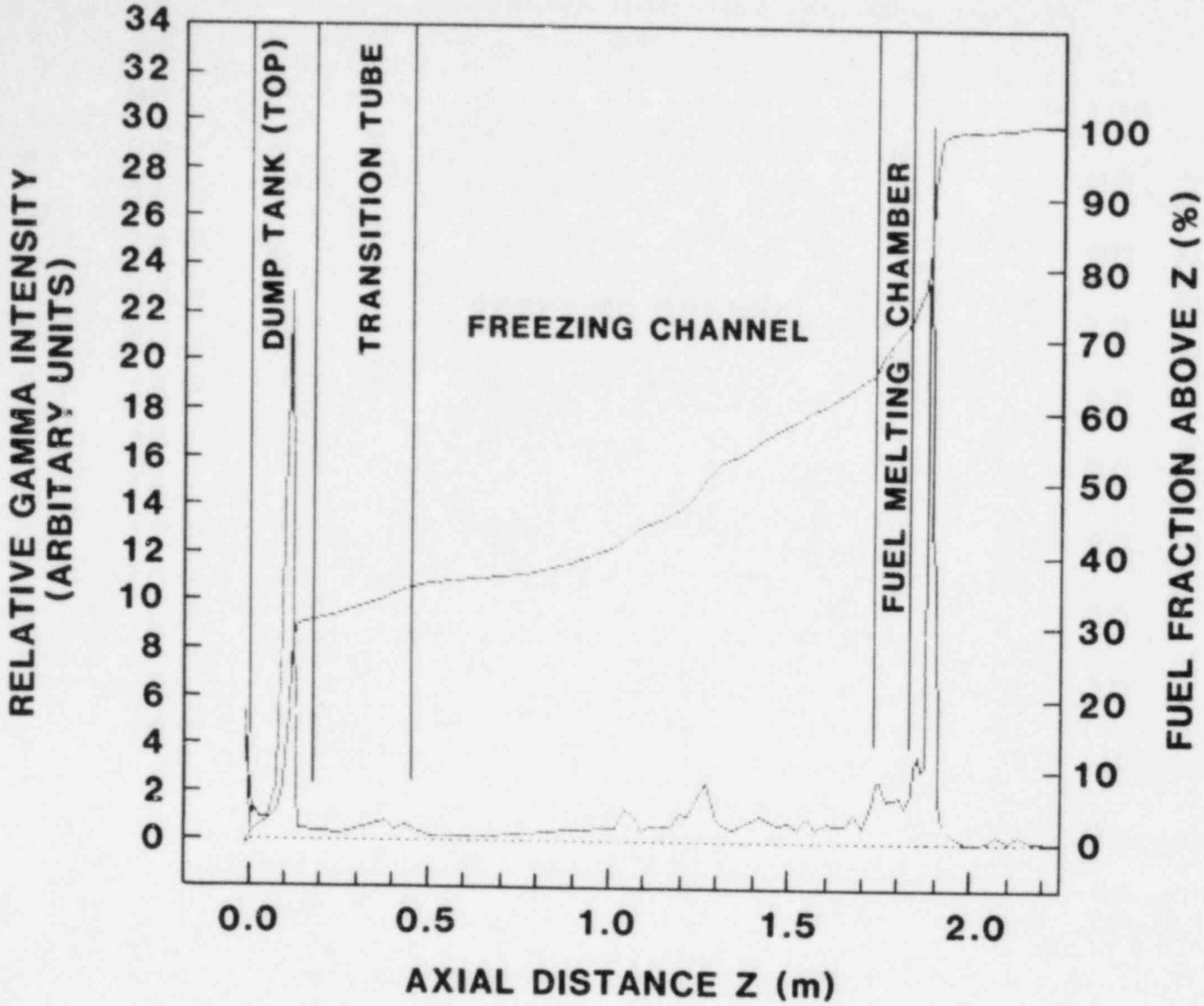

Figure 18 Final fuel distribution for the TRAN-3 experiment implied by the 1596 keV line of ^{140}La. (Erroneous distribution caused by the separation of the fission products from the fuel debris.)

5.2 Identification of Suitable Gamma Ray Lines

In addition to the chemical properties of a fission product chain, it seemed very important to have direct experimental evidence that a particular fission product line was associated closely with molten fuel. In the TRAN-3 radiographs a small isolated hollow sphere of fuel was observed in the gas passage below the fuel melting chamber. This isolated fuel mass was used to measure which gamma ray lines were associated with compact fuel masses, as distinguished from gamma ray lines associated with steel activation or with volatile fission products coating the interior surfaces of the pressure vessel. An axial

scan was made for several cm around this small fuel sphere, in which every intense gamma ray line in the spectrum was recorded. Four lines with reasonably high intensities and photon energies >500 keV were recorded, which were present only near the isolated fuel mass (the 1596 keV line was peaked in the region of the fuel mass, but also had a low-intensity "tail" emission on either side of the fuel mass). The four lines were: the 497.08 keV line of 39.4 day ^{103}Ru, the 756.72 keV and 724.18 keV lines of 64.0 day ^{95}Zr, and the 765.79 keV line of 35.0 day ^{95}Nb (Ref. 24).

Figure 19 shows a typical corrected gamma scan and normalized fuel distribution for the 765.79 keV line of ^{95}Nb, for experiment TRAN-3. The ^{95}Nb gamma emission corresponds very well with the abrupt end of the crust seen in TRAN-3 radiographs, and its relatively uniform intensity matches the uniform crust appearance. Because of the lower photon energies of these new lines, larger corrections must be made for absorption and scattering. These corrections are particularly important below the fuel melting chamber, where much fuel is usually found and where the steel walls are up to 4 cm thick and the geometry is complicated. Therefore additional checks on the fuel masses implied by the gamma scans should be made before quantitative results can be completely confirmed. However, at this time it appears that the lines of ^{103}Ru, ^{95}Zr, and ^{95}Nb give a reasonable and potentially very quantitative axial distribution of fuel mass. Results for TRAN-2 through TRAN-5 will be discussed below.

6. ANALYSIS IN HOT CELL FACILITY

The Hot Cell Facility (HCF) contains glove boxes and shielded boxes with remote manipulators for disassembly, sectioning, and microscopic examination of irradiated experiment packages. After being radiographed, the gas pressure inside the TRAN-2 through TRAN-5 packages was bled off slowly to ambient pressure through a small orifice and a filter to minimize material redistribution inside the freezing channel. Next, the insulation, electrical heaters, thermocouples, gamma ray detectors, and the pressure system were removed from the TRAN pressure vessel (referred to as the "fuel housing"). The bare fuel housing was then placed in one of the glove boxes, where the freezing channel and fuel melting chamber were sliced transversely and longitudinally into a number of sections, depending on which regions of the frozen fuel distribution were of greatest interest.

These sections were potted, the ends ground and polished, and then photographed through an optical microscope to measure the thickness and azimuthal symmetry of any UO_2 layers which were formed. Some samples were also etched to reveal the grain structure, and examined with a scanning electron microscope (SEM) and an electron microprobe, to look for evidence of molten steel. Materials such as UO_2 and steel can readily be distinguished with the SEM, and their chemical interactions studied. Micrographs of any loose fuel or steel debris can also be made, in an effort to distinguish between particles deposited from a vapor, and fine fractured debris resulting from breakup of a blockage.

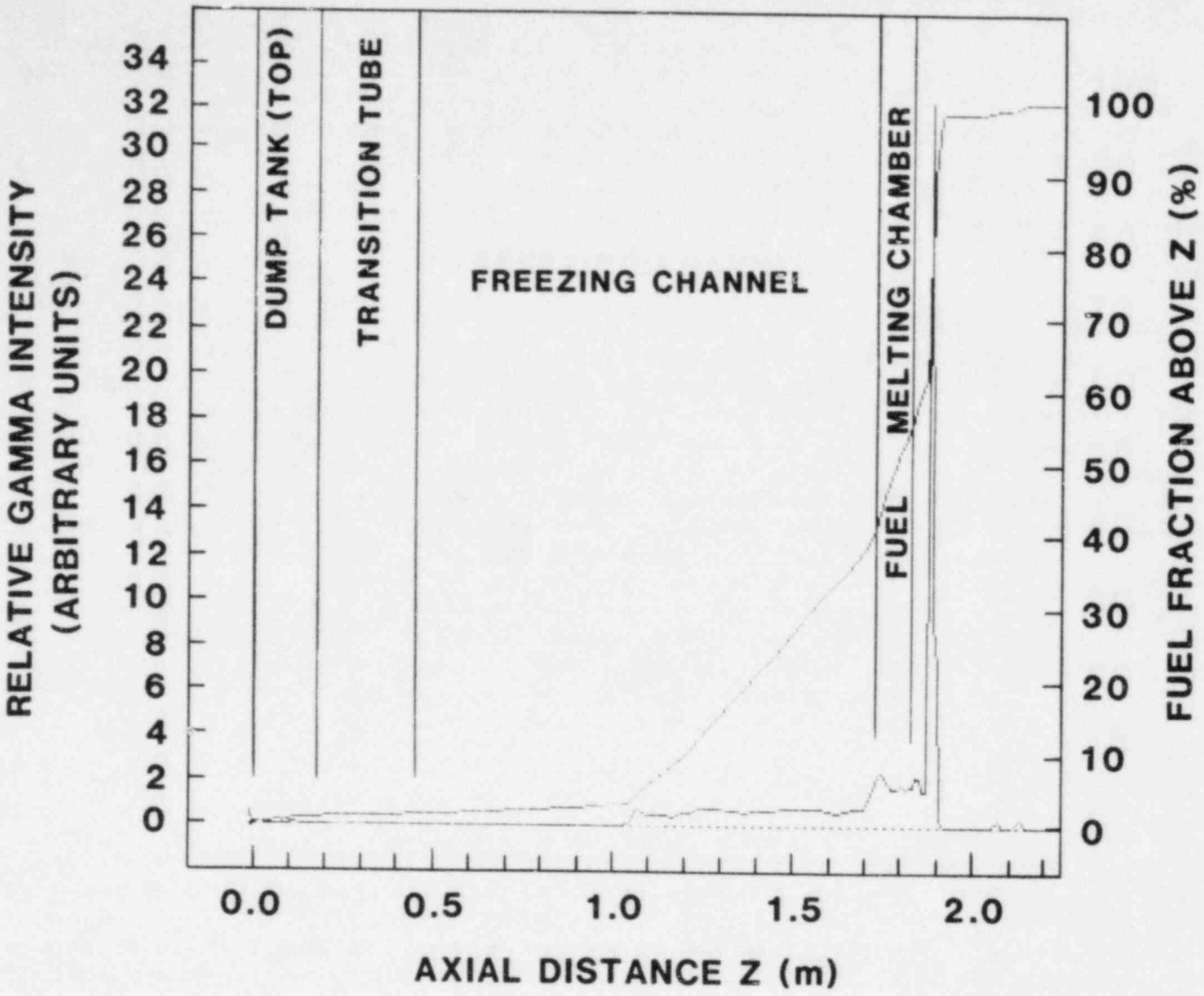

Figure 19 Final fuel distribution for the TRAN-3 experiment implied by 765.8 keV line of ^{95}Nb. (Correct fuel distribution.)

7. GRAVIMETRIC ANALYSIS

Finally, to measure the UO_2 mass distribution in TRAN-1 for comparison with radiographs and gamma scans, a gravimetric chemical analysis was made of all fuel debris adhering to the inner walls of the TRAN-1 fuel housing. This fuel debris was removed from all inner surfaces by immersing the fuel housing sections in concentrated nitric acid until no further UO_2 was removed. The resulting uranyl nitrate was dissolved in acetone and filtered to remove unwanted solids, then heated to 1160 K and dried in pre-weighed Pt crucibles to determine the total mass of UO_2. A similar procedure may be followed in later TRAN experiments, to confirm mass distributions implied by gamma scanning.

8. DATA RECORDING

The data recorded during a typical TRAN experiment fall into three main classes: (1) visually-observed and manually-recorded data (such as the slowly-varying temperature of the solenoid valve or the containment canister wall) which are related to proper operation of the experiment or experiment safety; (2) data recorded on stripchart recorders (the temperatures of the three temperature-regulating thermocouples); and (3) rapidly-varying transient data (temperature rise of the pressure vessel wall, fuel motion detector signals, pressure changes, a fiducial mark, and the reactor power signal). The transient data were processed by a data system which included preamplification of certain signals in DC differential amplifiers, then amplification of all signals to a standard signal range ($-3\ v < S < 3\ v$), automatic calibration of the net gain of each data channel, and recording of data either on an analog-to-digital converter (ADC) system with up to 32 channels, or on 26 channels of magnetic tape. The ADC system samples at rates up to 400 kHz, but has usually been used at rates of 4-40 kHz in TRAN experiments. A six-channel Visicorder is used to record a few basic signals to verify immediately that the experiment was successful.

The computerized ADC data system[25] permits the experimenter to transfer all raw data and the constants needed to analyze it to disk storage within a few minutes after the experiment has been performed. After taking this step to protect the data from accidental loss, the experimenter can analyze each channel at will, converting the data to engineering units and generating plots of the data in any time range of interest.

9. CALIBRATION OF FUEL ENERGY DEPOSITION

Several methods have been used to define the energy deposition in the 44 g of test fuel (11.1 percent enriched UO_2): (1) two-dimensional neutron-transport calculations employing a detailed geometrical model of the ACRR and the TRAN package; (2) dosimetry of a thin transverse slice of an actual test fuel pellet that was placed in the complete TRAN package and irradiated in the ACRR with a low-level pulse; (3) dosimetry of samples of uranium-loaded aluminum wire that were mounted at the center of the empty fuel melting chamber and irradiated with a full-sized ACRR pulse; (4) measurement of the ACRR pulse size required to approach the threshold of fuel melting; and (5) direct measurements of fuel temperature reached on a low-level ACRR pulse, interpreted with the aid of heat transfer codes.

Reasonably consistent results were obtained from methods (1), (2), (4), and (5). The uranium-loaded aluminum wire was judged not to be reliable for absolute measurements based on variations of the uranium content in the wire, and the uncertainties caused by neutron self-shielding inside the ≈8-mm-diameter test fuel pellets. The near-melting experiment in the ACRR is not practical because of expense and the difficulty of confirming fuel melting just as it begins to occur (the only data of this type were obtained unintentionally). Dosimetry on the transverse fuel pellet slice is a reasonably good method but is

cumbersome and does not take into account additional heating mechanisms such as gamma heating of the fuel. Thus far, the best method appears to be fuel temperature measurement on low-level ACRR pulses, which give very good agreement with the corresponding neutron transport calculations.[21]

The measurements of fuel temperature rise were made with the special fuel geometry shown in Figure 20. A special annular fuel pellet was made with a 0.13-cm-diameter hole along its axis, so that the junction of a 0.100-cm-diameter chromel/alumel thermocouple could be placed at the axial midplane of the fuel load. A typical temperature trace from such a thermocouple is shown in Figure 21 for an initial fuel temperature of ≈473 K. The measured rate of temperature rise is determined by the relatively loose coupling between the thermocouple and the fuel, and the rate of temperature fall was determined by heat losses out the sides of the fuel pellet into the steel pressure vessel. These calibration experiments were performed with exactly the same experiment package geometry as used in TRAN-2 through TRAN-5. By varying three parameters to match the observed temperature trace, the fuel energy deposition factor was determined from computer modeling of the thermocouple temperature.[26] These parameters represented the energy deposition coupling factor, the thermal coupling between the thermocouple and the fuel surrounding it, and the heat loss from the fuel to the melting chamber wall. The resulting energy deposition factor of 9.5 ± 0.5 J/g per MJ input compared very well with the calculated factor of 9.566 J/g-MJ.

The uniformity of energy deposition in the test fuel is also important when making parametric variations of fuel temperature. The calculated (axially-averaged) radial variation of energy deposition is shown in Figure 22 for the 11.1 percent fuel enrichment and 1.27 cm polyethylene thickness* used in the TRAN Series I experiments. The peaking of fuel temperature at the outer edge of the fuel will be reduced somewhat by heat loss to the melting chamber wall, and by heat transfer within the turbulent flowing fuel.

The axial variation of energy deposition was also measured with uranium-loaded aluminum wire in an empty Fuel Melting Chamber, for the conditions of TRAN-2 through TRAN-5 (Figure 23).

---

*A layer of polyethylene around the outside of the experiment was included to thermalize the neutron flux and thus raise the average energy deposition in the fuel pellets.

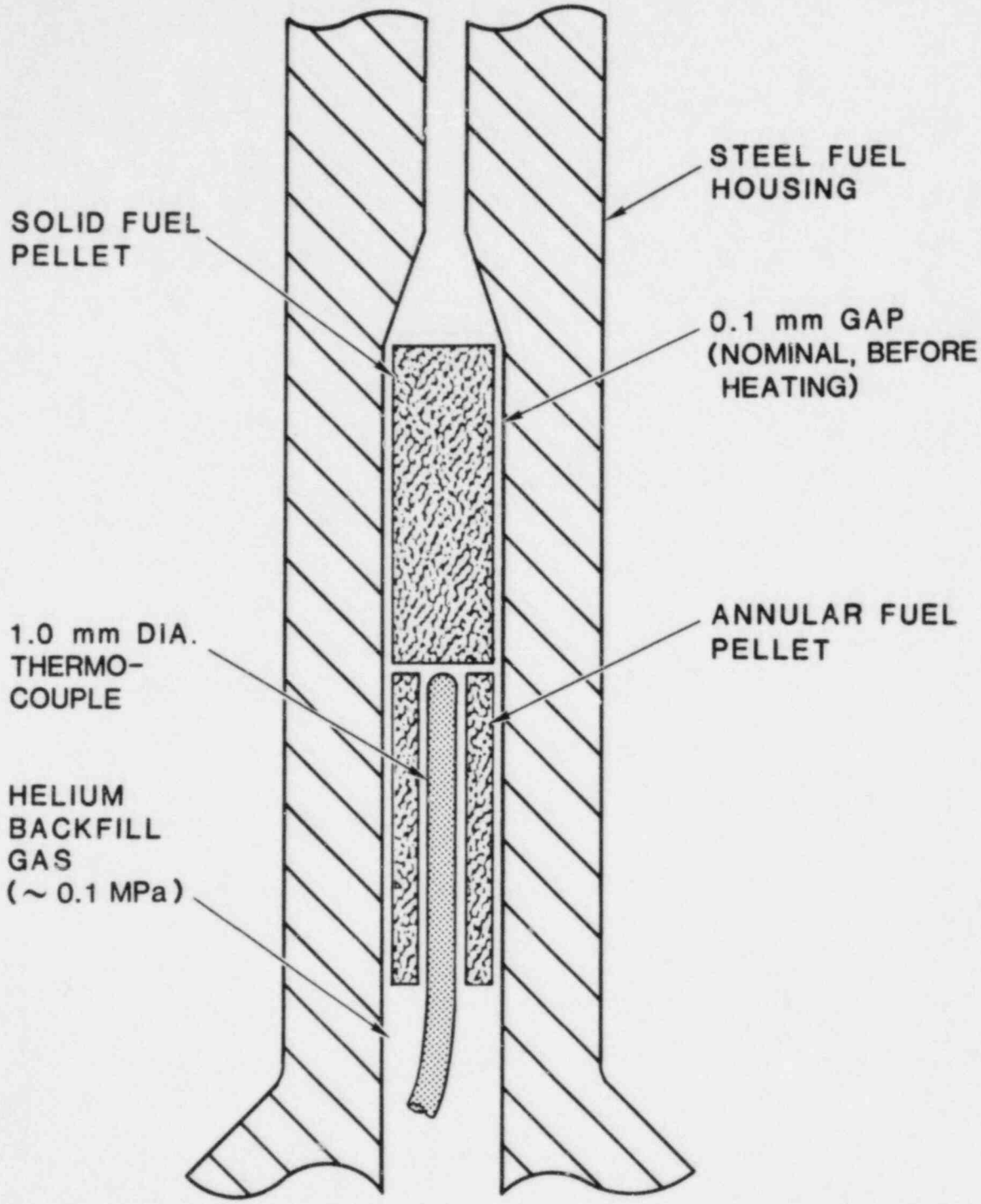

Figure 20 Special test fuel geometry used for the fuel energy deposition measurements.

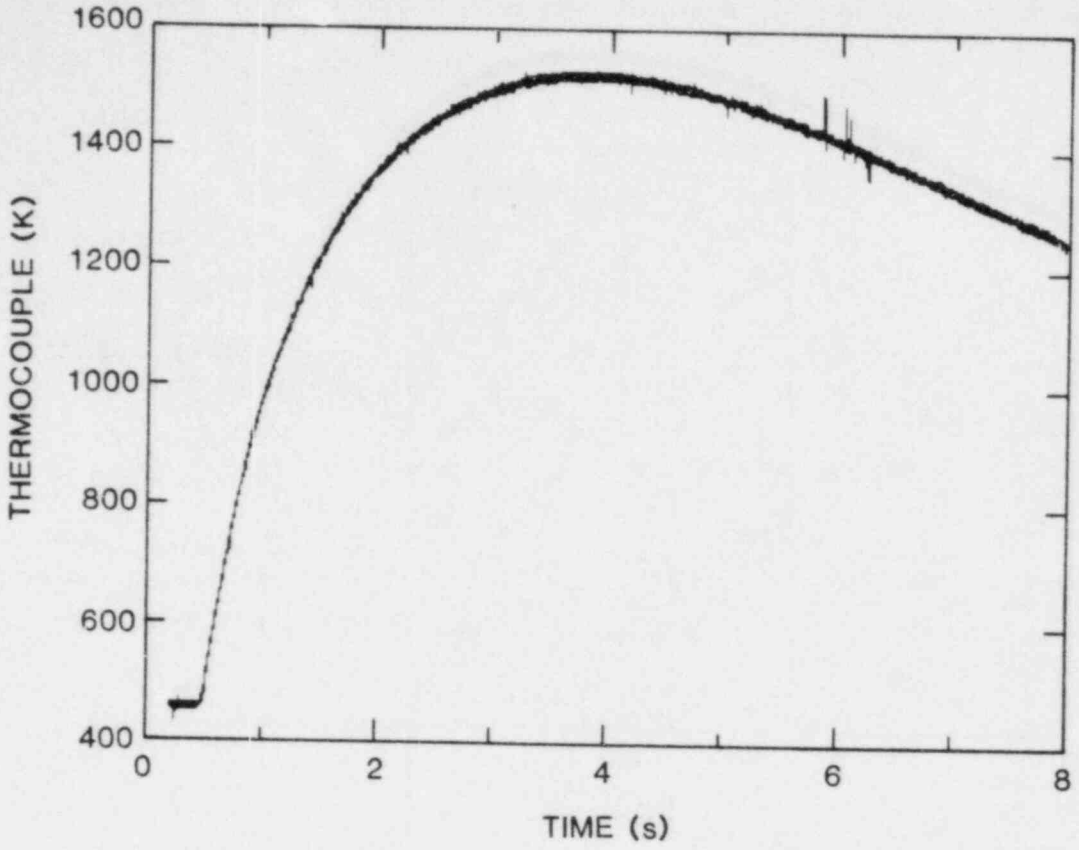

Figure 21 Typical temperature trace recorded during the energy deposition calibration experiment.

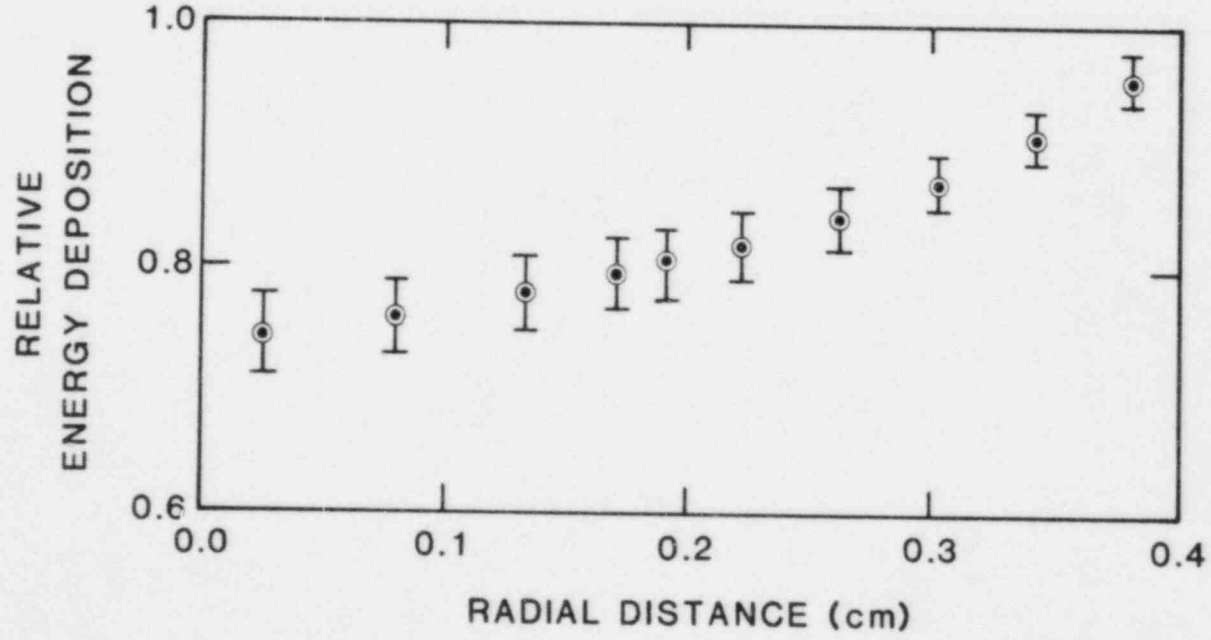

Figure 22 Calculated radial variation of the energy deposition in the fuel.

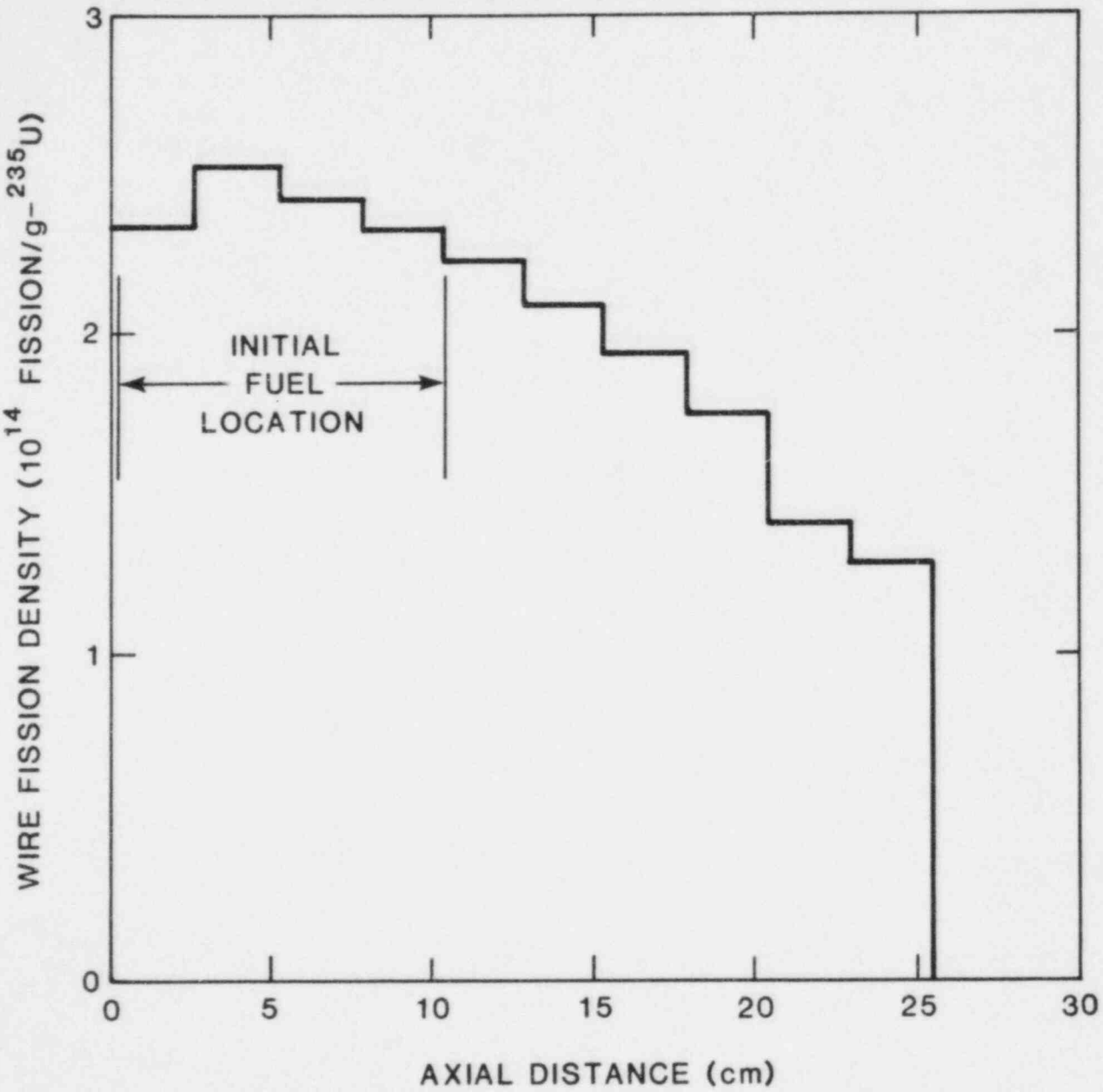

Figure 23 Axial variation of the energy deposition for the conditions of the TRAN-2 through TRAN-5 experiments.

APPENDIX C

RESULTS OF TRAN-1 EXPERIMENT

The purpose of TRAN-1 was to verify the experiment concept and to investigate the freezing of molten fuel at the low end of the steel and fuel temperature ranges of interest. It was performed at an initial steel temperature of 673 K, a driving pressure of 1.6 MPa, and a fuel temperature just above melt (ranging from 3138 K to 3473 K, depending on the initial axial location of the fuel mass of interest). Thermocouple data showed that the fuel moved almost completely out of the fuel melting chamber, indicating a long penetration of fuel into the freezing channel and an apparently successful experiment concept. The experimental data of TRAN-1 will be described in this section, organized in the order discussed in Appendix B. Time differences, Δt, quoted in the text are with respect to the peak of the ACRR power pulse, which corresponds approximately to the time of fuel melting in most experiments.

The dominant phenomenon observed in these lower-temperature experiments was the formation of a stable frozen fuel layer, which limited heat transfer from the bulk fuel flow to the steel wall. In TRAN-1 the layer was azimuthally quite uniform, fully-dense, and appeared to cover the entire channel surface at any axial location where it was present. The portion of the fuel layer nearest the steel wall was presumably deposited initially as a frozen crust under the bulk molten fuel slug. However, a portion of the layer appears to have resulted from the subsequent freezing of a liquid film deposited as the end of the finite-length slug of fuel passed up the channel. There was no evidence of steel melting or chemical interaction with the fuel in TRAN-1, although near the channel entrance the underlying steel was heated sufficently to cause grain restructuring. Large radial grains were observed in the fuel layer, with no obvious evidence of separate fuel-crust and fuel-liquid-film regions.

1. PRESSURE TRANSDUCER DATA FROM TRAN-1

Because of the unexpectedly rapid movement of hot fuel, two of the pressure transducers showed negative pressure excursions apparently caused by rapid heating of the pressure measuring diaphragm. Completely reliable pressure data were obtained only from the pressure transducer located at the He reservoir in the pressure system. The ACRR power peak occurred at 348 ms, so $\Delta t \equiv t - 348$ ms (except Figure 25, where $\Delta t \equiv t - 600$ ms).

The pressure transducer just below the fuel load went off scale at $\Delta t = +10$ ms, so no further useful data were obtained from this

transducer. The pressure transducer in the dump tank at the top of the apparatus registered the arrival of a small amount of hot material at Δt = +50 ms, which casts doubt on the subsequent data from this transducer also. The delay between the estimated time of fuel melting and the first appearance of hot material at the dump tank corresponds to a hot material velocity of >35 m/s. However, the dump tank transducer clearly indicates that no significant gas leakage around the fuel load occurred at early times, and that no significant gas pressure preceded the initial burst of hot fuel (although it is conceivable that gas may have closely accompanied the hot fuel).

On the other hand, the pressure transducer located at the He reservoir in the pressure system (see Figure 2) yielded reliable data for the driving pressure and gas flow into the freezing channel for the period of time when the solenoid valve was open (the first ten seconds of the experiment). Figure 24 shows the He reservoir pressure behavior for the first 0.5 s of the experiment, after correcting for electrical and radiation noise. Based on pressure equilibration measurements made with no fuel in the melting chamber, the pressure behavior should follow approximately the dashed line in Figure 24. Based on pressure measurements with a dummy fuel load, the initial pressure drop at 0.36 s in Figure 24 corresponds to the filling of the gas passage between the solenoid valve and the base of the fuel with helium.

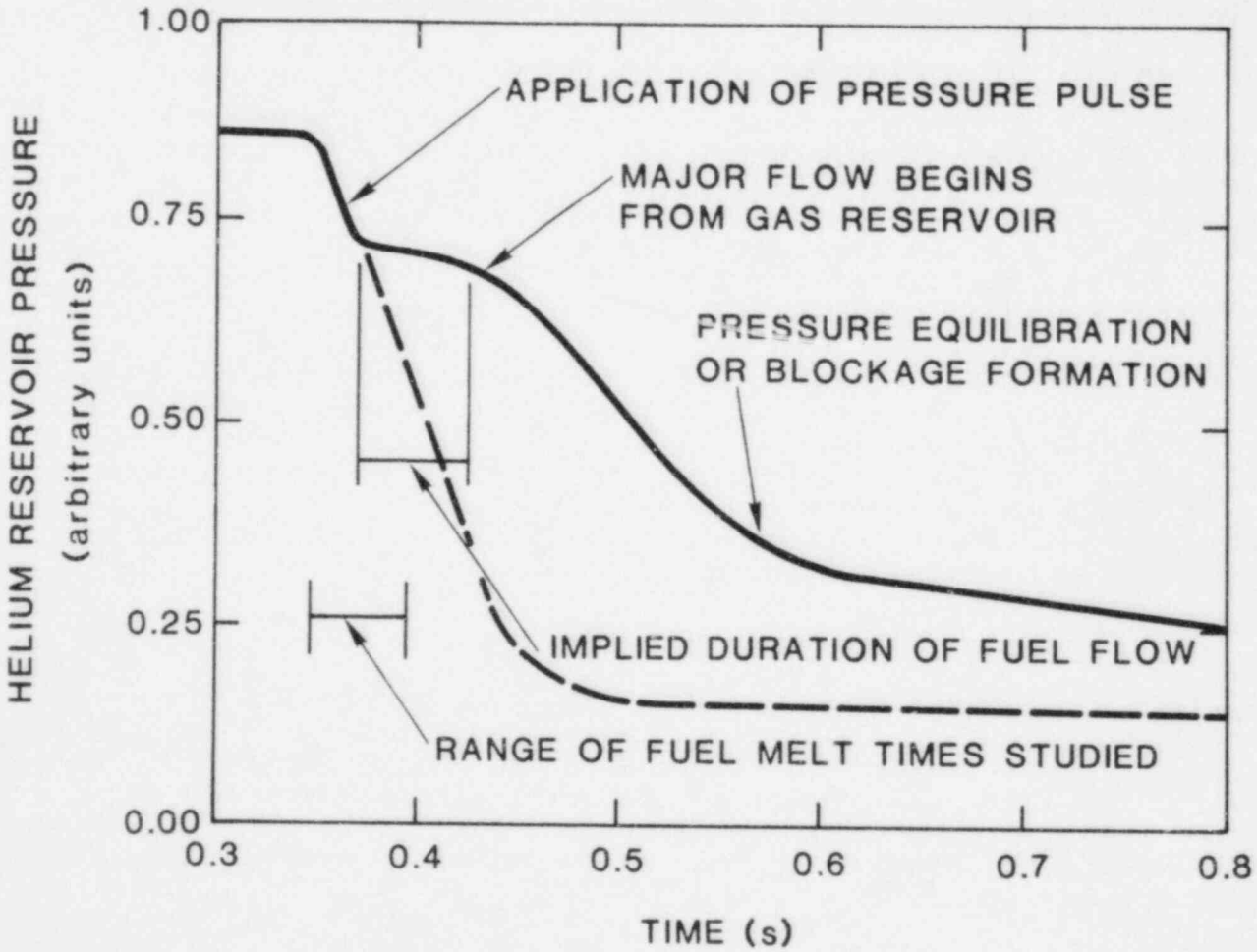

Figure 24 Helium reservoir pressure for the first 0.5 s of the TRAN-1 experiment.

The approximately steady pressure from 0.36 to 0.42 s (or Δt = 0.012 to 0.072 s) apparently corresponds to the flow of molten fuel up the freezing channel. At 0.42 s the channel opens up (a continuous slug of molten fuel is no longer present in the freezing channel), and gas begins to flow out of the pressure reservoir (corresponding closely to the somewhat uncertain dump tank pressure data in Figure 25). The gas flow* again decreases by a factor of ≈8 suddenly at ≈0.6 s (or Δt = +0.25 s). This new flow rate corresponds to only about five percent of the flow rate through an empty freezing channel. Thus it appears that an incomplete restriction was formed after much of the gas had flowed through the freezing channel. Figure 26 more clearly shows the abrupt change in gas flow rate at 0.6 s. The He tank pressure continues to fall slowly between 0.6 s and 2.5 s, after which it rises slightly over the remaining 7.5 s during which the solenoid valve is open.

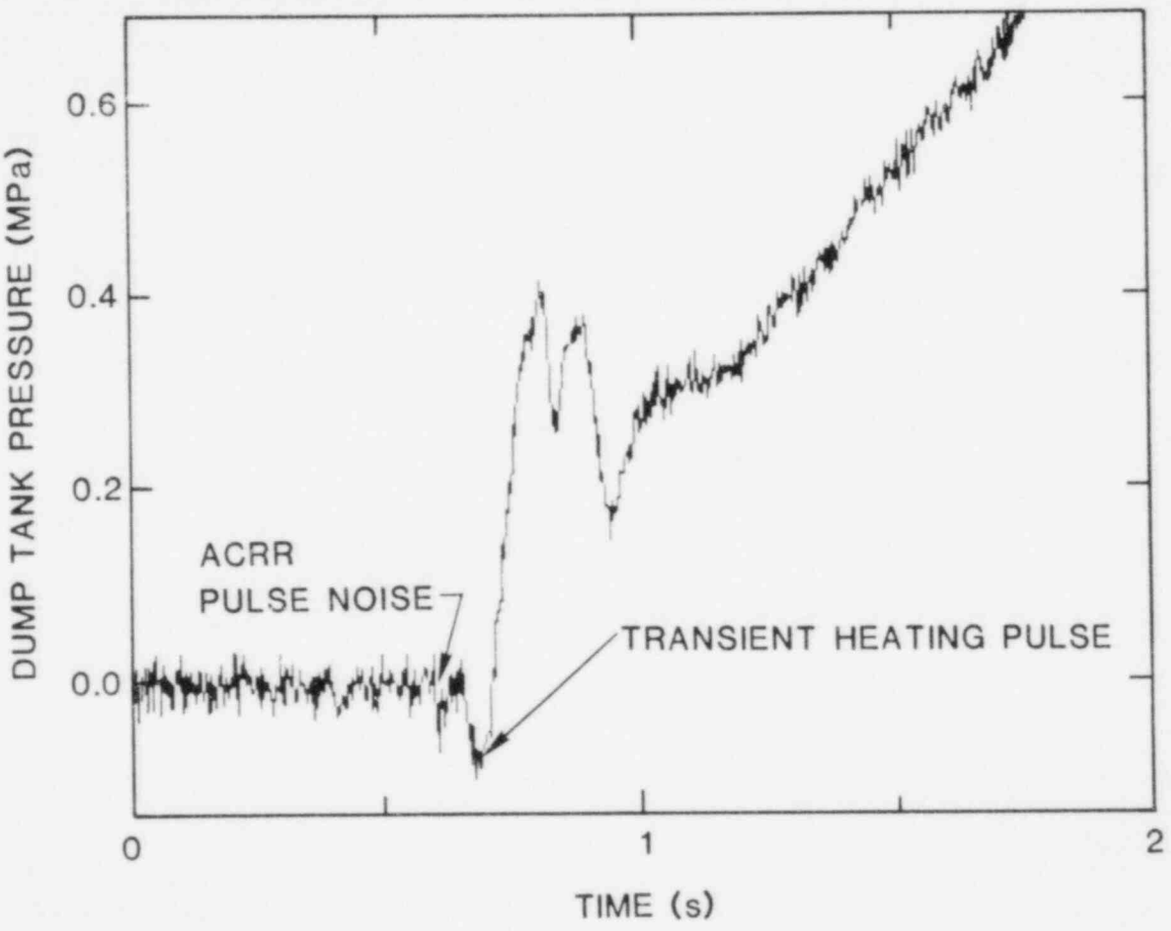

Figure 25 "Apparent" pressure in the dump tank beyond the freezing channel for the TRAN-1 experiment. (Pressures are questionable because of the heating of the transducer at 0.67 s.)

*Gas flow rates are inferred from the rate of pressure increase or decrease.

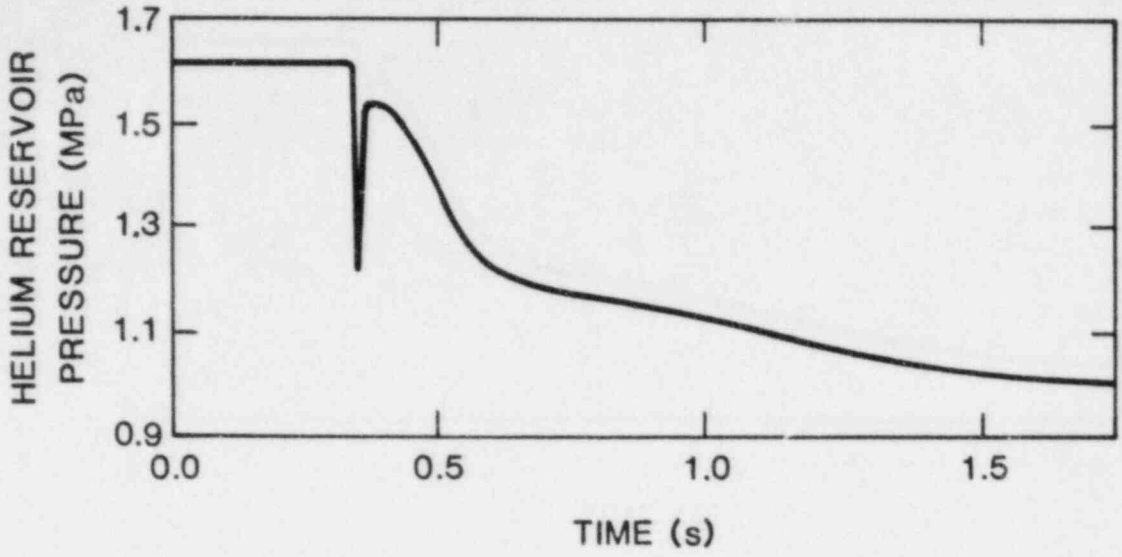

Figure 26 Helium reservoir pressure at later times, averaged over noise.

In summary, the gas flow data indicate a temporary filling of the freezing channel by the upward-moving column of fuel, then the opening of the channel accompanied by gas flow into the dump tank, and finally a porous flow restriction which persists for as long as gas flow data are available.

2. FUEL MOTION DETECTOR DATA FROM TRAN-1

No fuel motion detectors were included in the TRAN-1 experiment.

3. THERMOCOUPLE DATA FROM TRAN-1

Because of the large thermal mass separating the freezing channel from the thermocouples, thermocouple data have primarily been used to infer the approximate final location of frozen fuel. Based on the small temperature rise of the fuel melting chamber wall (peaking at ≈30 K after correction for gamma-ray heating), most of the fuel left the fuel melting chamber. The gamma-corrected temperature rises were 25 K and 20 K at 6.5 cm and 57.3 cm above the entrance to the freezing channel, respectively. These temperature rises correspond to the freezing of an amount of UO_2 which would partially fill the channel, which is consistent with other TRAN-1 data.

4. RADIOGRAPHY OF TRAN-1

When TRAN-1 was assembled, no special effort was made to collect the various instrumentation cables into neat bundles. As a result, the first radiographic images were very complex, with random criss-crossing of cables in the vicinity of the freezing channel. The TRAN-1 package was radiographed on two occasions: about one week after the experiment, and about four months later after remote manipulators in the HCF were used to remove the extraneous insulation, heater cables, pressure transducer cables, and thermocouple probes. Figure 27 shows the significant differences between these radiographs, which were presumably caused by handling with the manipulators. The stripping caused the frozen layer on the fuel melting chamber wall to flake off, apparently removed the two "blockages" seen in the earlier radiograph, and reduced the amount of loose fuel debris at the exit of the freezing channel. The length of frozen fuel layer, L_c, was estimated to be 50 cm in the first set of radiographs, but appeared to be 70±10 cm in the second set.

Because the final fuel distribution was seriously disturbed by the stripping process, on later experiments all cables were gathered into neat bundles separated from the freezing channel area, and the heaters, etc., were carefully stripped from the outside of the steel pressure vessel by hand before radiographs were made.

5. GAMMA SCANS OF TRAN-1

Detailed gamma scans of the 1596 keV line of ^{140}La were made for TRAN-1 using an axial resolution of ≈1.5 cm. However, this particular fission product appears to have become separated from the fuel so that gamma intensity does not accurately represent the final fuel distribution. The most dramatic discrepancy is a large peak of fission product emission near the base of the dump tank that appears to be associated with very little fuel. This result implies that perhaps 30 percent of the ^{140}I chain nuclides were separated from the fuel and were carried into the dump tank. Because the major He flow lasted about 1-1.5 s, the separation appears to have occurred during this time period.

6. EXAMINATION OF TRAN-1 IN HOT CELL FACILITY

TRAN-1 has undergone extensive post-irradiation examination in the HCF. Material was recovered from the dump tank, the freezing channel, and the melt chamber regions of the TRAN-1 fuel housing assembly. These materials were examined with optical and electron microscopy to determine their composition and structure, because this information may indicate how the materials were deposited. The freezing channel was also sectioned to determine the thickness and nature of the UO_2 crust, and to determine the condition of the steel wall beneath the crust.

Figure 28 shows that the crust was approximately uniform azimuthally but varied in thickness from ≈0.3 mm near the fuel melting chamber to

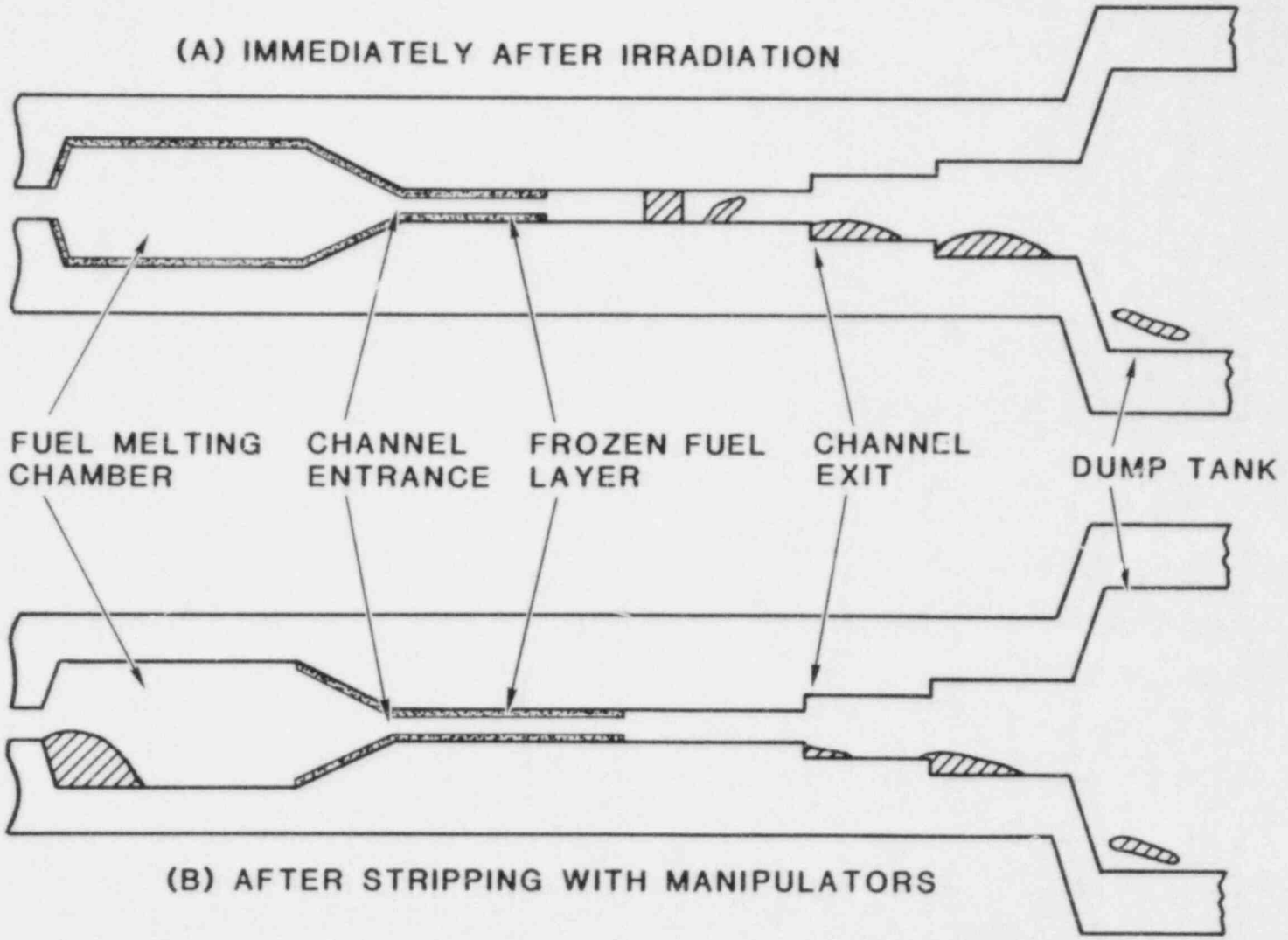

Figure 27 Schematic drawing of the fuel distributions in the TRAN-1 experiment before and after stripping with manipulators.

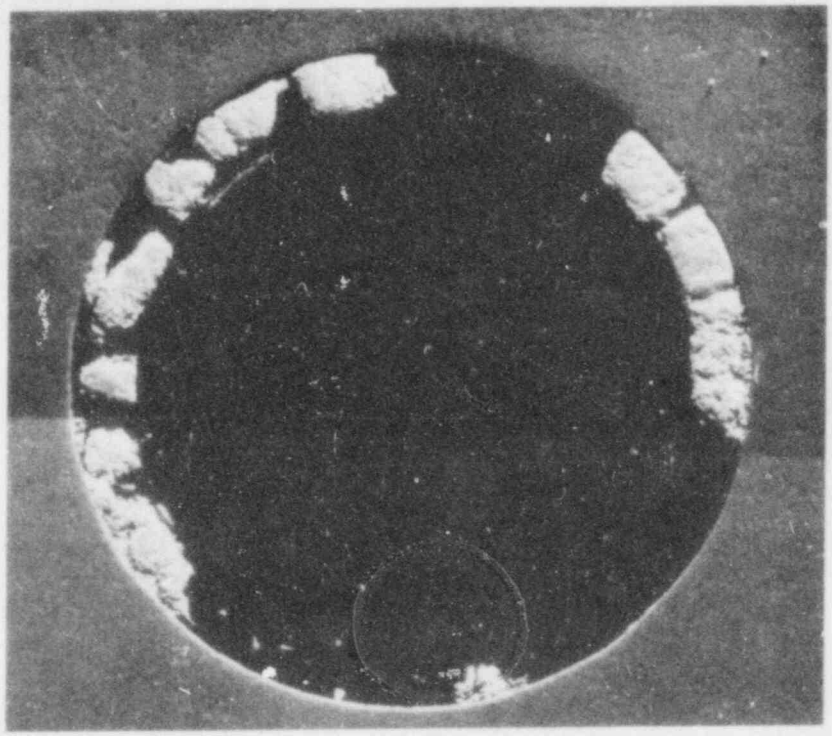

(a) 13.5 cm above the entrance

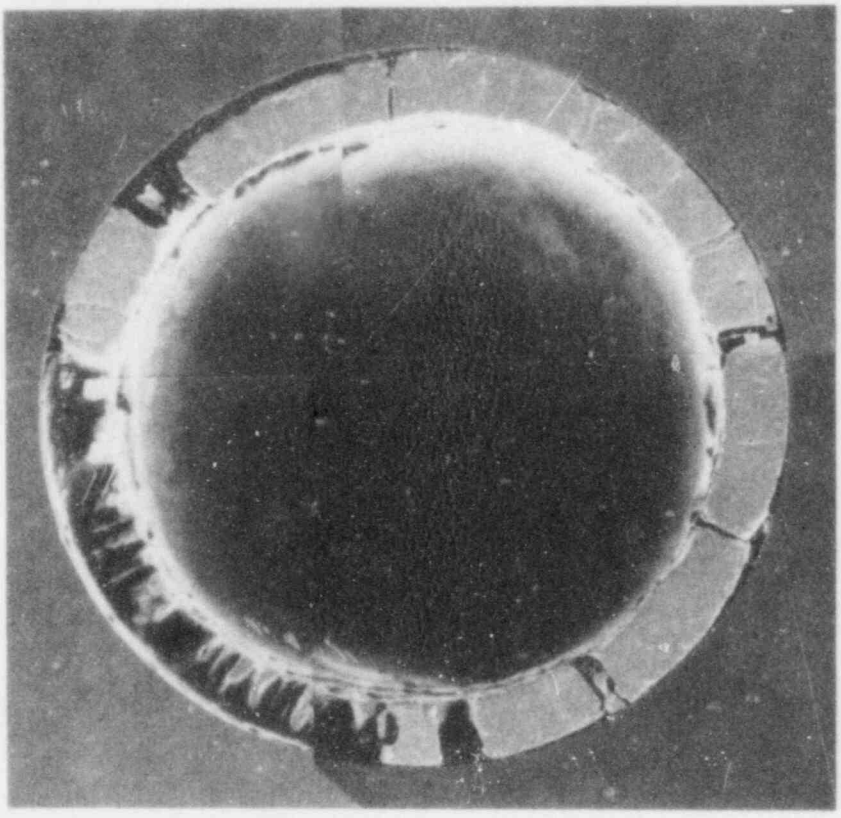

(b) 15.5 cm above the entrance

Figure 28 Fuel distribution in the freezing channel cross-sections of the TRAN-1 experiment. (1 of 2)

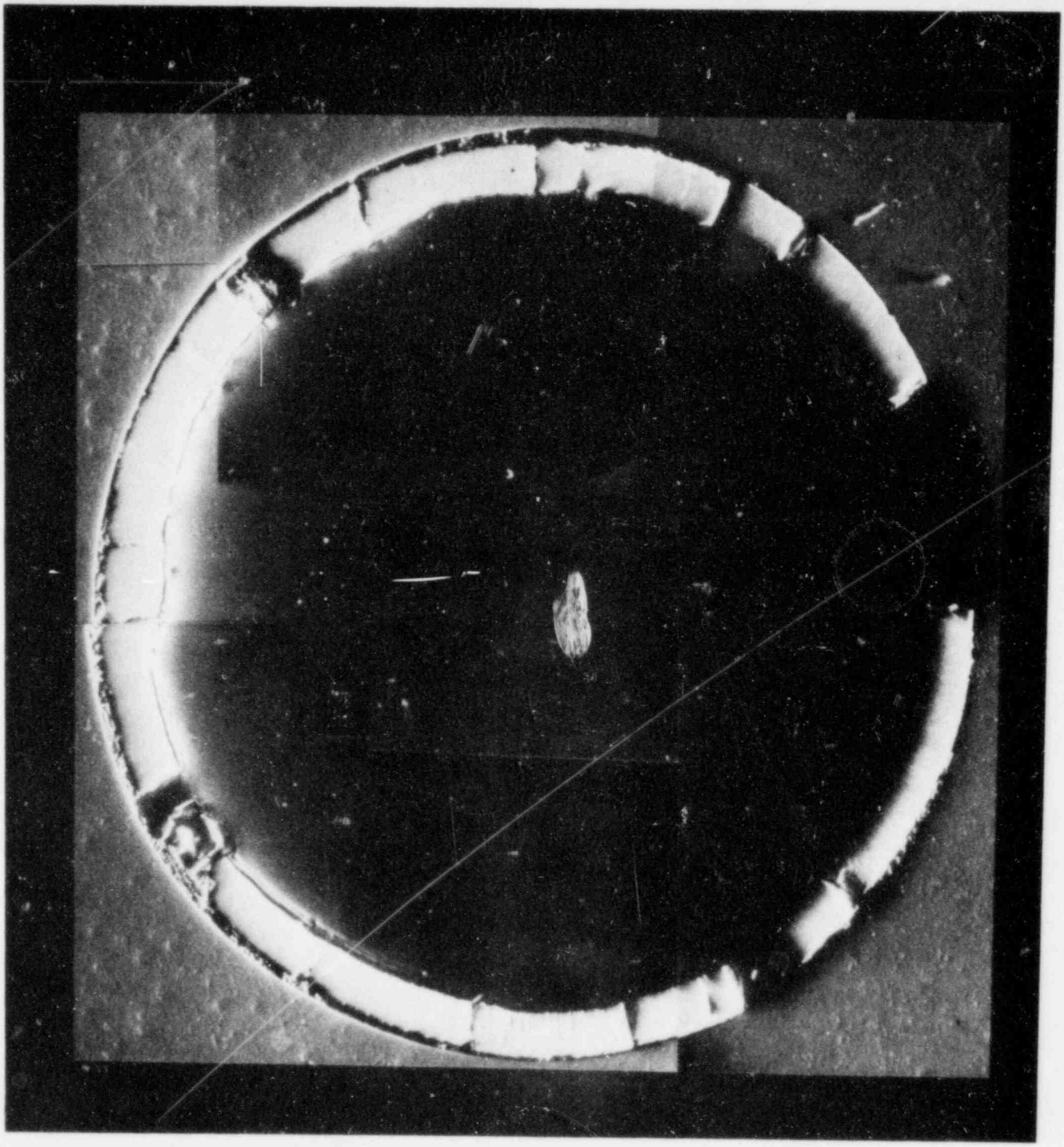

(c) 74.0 cm above the entrance

Figure 28. Fuel distribution in the freezing channel cross-sections of the TRAN-1 experiment. (2 of 2)

0.15 mm near the upper end of the crust. Large radially-oriented grains were visible in the UO_2 layer (Figure 28(b)), suggesting that the UO_2 was indeed liquid or vapor when deposited on the channel wall. A gravimetric analysis was made of the UO_2 mass contained in two 5-cm-long sections of the freezing channel separated by ≈50 cm. Assuming a linear variation of layer mass with distance along the channel, this gravimetric analysis confirmed the 0.15-0.3 mm layer thickness, and implied a total UO_2 mass of 12.3 g in the freezing channel.

No evidence of steel melting (based on absence of a "cast" grain structure in the steel), or chemical interaction between steel and UO_2 (based on sharp material boundaries observed in electron microprobe analysis) was seen (Figure 29). However, under the UO_2 layer near the entrance to the freezing channel, the steel was restructured into a fine, randomly-oriented grain pattern throughout a layer ≈20 μm wide. This restructuring was not found at the end of the UO_2 layer far from the channel entrance. It appears to have occurred around pre-existing damage sites caused by machining of the steel channel, and probably occurred in a very short time as the steel reached some threshold temperature (because no other restructuring was observed as a result of heating the steel to 673 K). The absence of steel restructuring far from the channel entrance is thus consistent with a decrease in the temperature of the molten UO_2 as it flowed up the channel.

Special attention was given to the material in the dump tank, because the large peak observed in the axial gamma scan implied that ≈10 g of fuel should be near the base of the dump tank, presumably in the form of a relatively uniform coating. A thin coating of fine UO_2 particulate was indeed observed on the face of the dump tank pressure transducer; this coating presumably caused the small negative pressure signal observed. However, the total mass of UO_2 removed from the dump tank side walls by chemical dissolution or scraping was only 0.209 g. Another small mass of UO_2 particles was discovered in a pile about 1 cm in diameter located at the center of the dump tank cover plate. This UO_2 was associated with a very small quantity of steel filings, and a large quantity of shattered organic material (Loctite, a leak sealant used on the valve at the base of the dump tank). Of the UO_2 particles in the pile about 1/3 were rounded in shape, and 2/3 had angular edges (Figure 30). The particle sizes ranged from <1 μm to ≈2 mm. Based on the shapes and sizes, some debris could have been deposited as a vapor or an aerosol, while other debris might have resulted from breakup of a UO_2 plug.

Finally, the UO_2 layers that had broken off the wall of the fuel melting chamber and the gas passage below the melting chamber were examined with an optical microscope. None of the original 80-percent-dense sintered material was found, indicating complete melting of the initial fuel load. Figure 31 shows evidence that a thin, relatively uniform UO_2 layer (≈0.1 mm thick) was laid down initially over the steel, followed in some areas by a thicker UO_2 layer with rounded edges and a random variation in thickness. This suggests that some UO_2 presumably drained from the fuel melting chamber down into the gas passage at late times.

(a) 200x scanning electron micrograph showing typical columnar grain structure in UO_2 layer

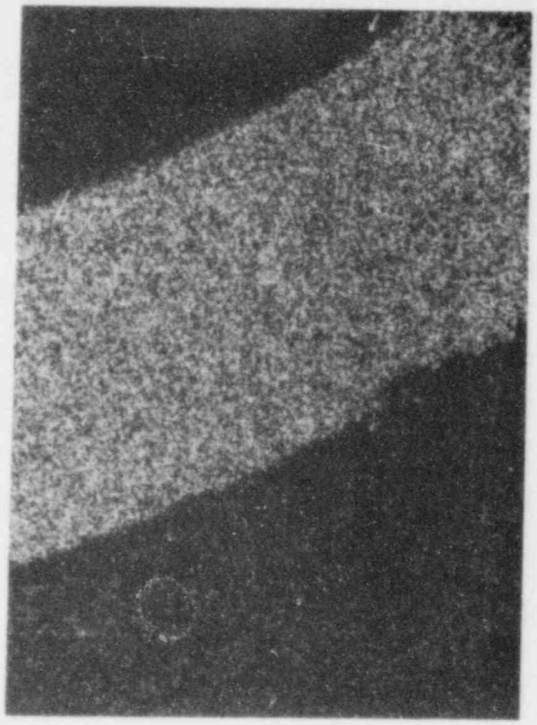

(b) U X-ray elemental distribution map of (a)

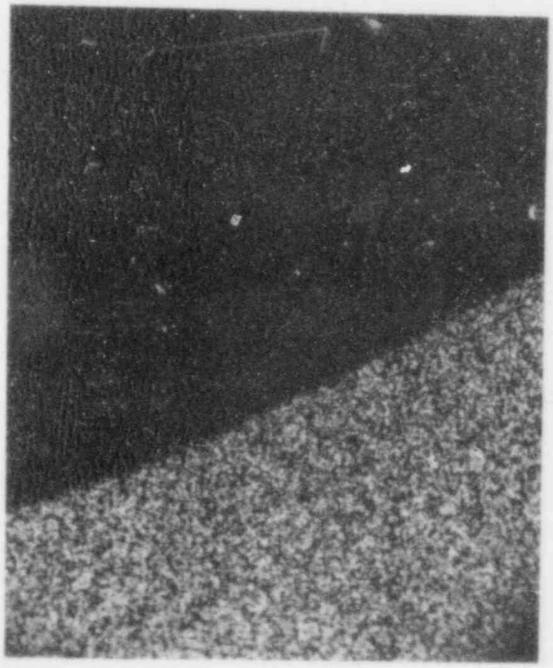

(c) Fe X-ray elemental distribution map of (a)

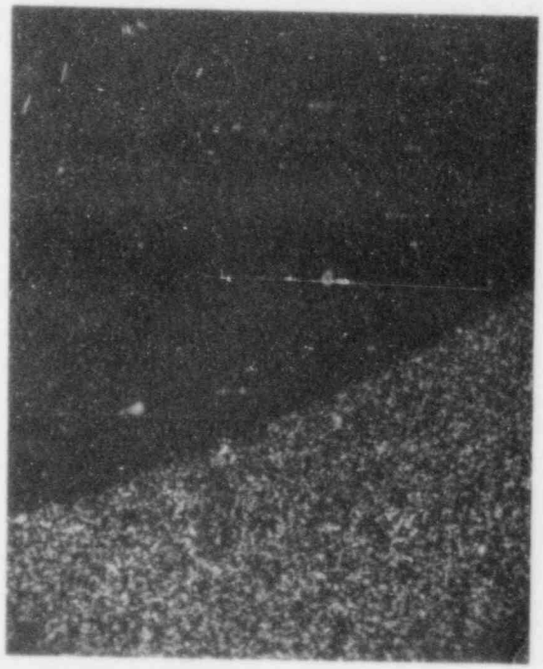

(d) Cr X-ray elemental distribution map of (a)

Figure 29 Details of the fuel crust structure in the TRAN-1 experiment showing the elemental distributions and the lack of interaction of fuel and steel.

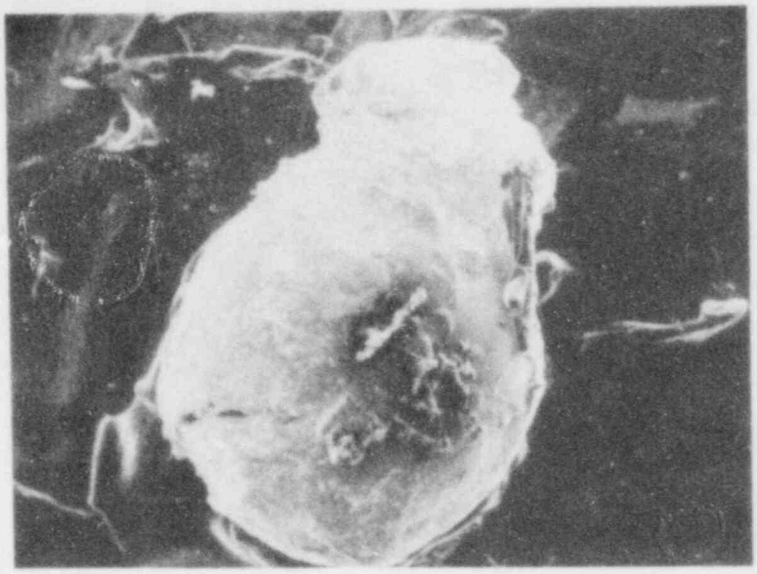

(a) 35x scanning electron micrograph of a hollow rounded particle

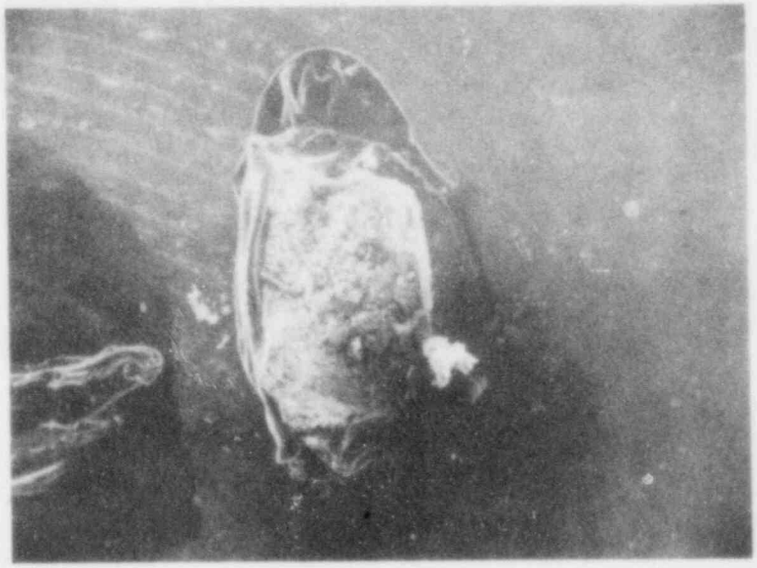

(b) 35x scanning electron micrograph of an angular particle

Figure 30 Representative rounded and fractured fuel particles from the dump tank cover plate of the TRAN-1 experiment.

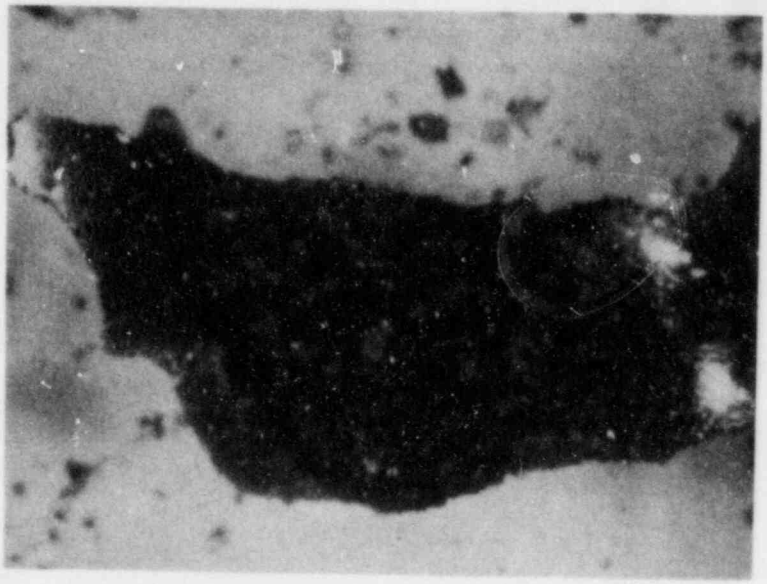

(a) A particle showing the two layers and the grain development (approximately 25x)

(b) Variation in layer thickness (approximately 25x)

Figure 31 Optical micrographs of the fuel crust layers from the melting chamber area showing the thin, uniform initial crust and thicker, rounded layer that has flowed back over the thin initial layer.

Table 8 summarizes the results of direct fuel mass measurements in TRAN-1. Of the initial 43.04 g of fuel, about 36.0 g or 84 percent has been accounted for. The missing 7 g may have been in the form of the fine powder seen at the exit of the freezing channel, and may have been lost during a poorly-controlled depressurization of the fuel housing or during the handling that occurred while manipulators were being used to disassemble the package.

Table 8. Direct Fuel Mass Measurements in the TRAN-1 Experiment

Location	Loose Debris (g)	Gravimetric Analysis (g)	Total (g)
Fuel Melting Chamber and Below	16.12	4.23	20.35
Freezing Channel	0.0	14.15	14.15
Dump Tank	1.28	0.21	1.49
	Total directly-weighed fuel		36.0

7. INITIAL FUEL AND STEEL CONDITIONS IN TRAN-1

Based on the measured energy deposition coupling factor (Section 9 of Appendix B) and the measured axial variation in energy deposition shown in Figure 32 (which applies to the conditions of TRAN-1 only), the (adiabatic) initial fuel temperature could have ranged from the melting temperature at the lower end of the fuel column (≈3138 K) to 3473 K at the upper end of the column, with an average of ≈3173 K. Fuel melting is estimated to have occurred at 355 ms near the middle of the fuel column, or about 8 ms before the driving pressure was applied.

The steel temperature was well regulated at 673 K, but estimates of the axial variation around the locations of the regulating thermocouples were not available. Some difficulties were experienced with heater tape reliability. Later experiments revealed that the heater tapes degraded rapidly when used above 873 K in a He atmosphere over a conducting substrate.

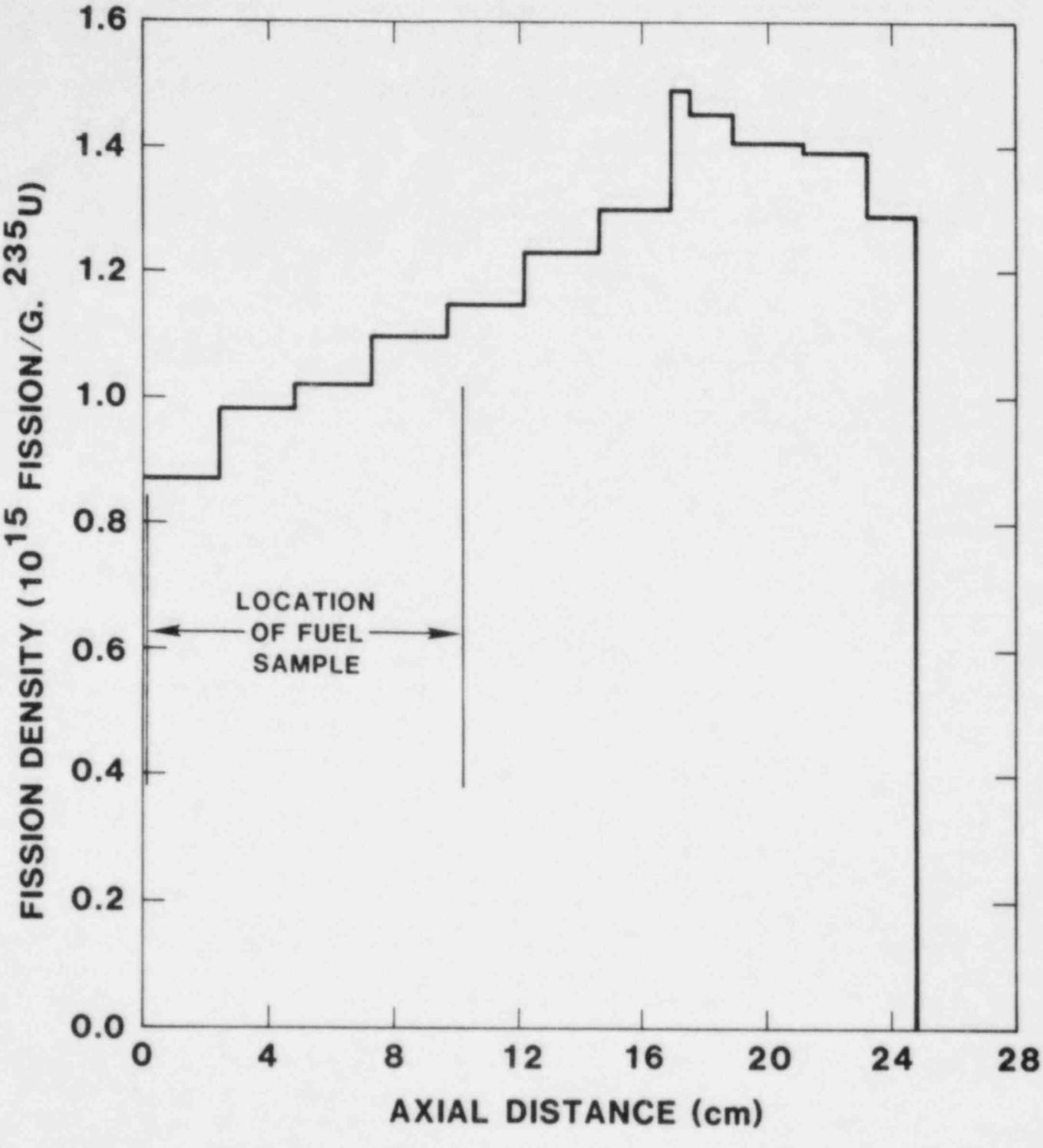

Figure 32 Measured axial variation of the energy deposition in the fuel and at the entrance to the freezing channel, for the TRAN-1 experiment only.

APPENDIX D

RESULTS OF TRAN-2 EXPERIMENT

Because no evidence of steel melting was found in TRAN-1, the TRAN-2 experiment was designed to enhance steel and fuel melting by increasing the initial fuel and steel temperatures, and by reducing the driving pressure so that the contact time between fuel and steel was increased. The parameters intended for TRAN-2 were: T_F = 3973 K, T_S = 873 K, and P_D = 1.0 MPa. The experiment was unintentionally performed in two stages: an initial experiment (TRAN-2/AE) in which the fuel was not even melted and therefore did not flow into the freezing channel, and a second experiment (TRAN-2/R) in which complete fuel melting and a fuel temperature of ≈3723 K were achieved. The unexpectedly low energy deposition in TRAN-2/AE resulted from a conservative philosophy of choosing reactor pulse size, combined with reliance on uranium-loaded aluminum dosimetry wire to provide absolute energy deposition data. The principal error in energy deposition measurement appears to have resulted from the considerable uncertainty in the uranium content of the dosimetry wire.

Radiographs of TRAN-2/AE showed that the initial fuel load had expanded axially by ≈10 percent, and that severe fuel cracking had occurred, but that no fuel had flowed into the cone-shaped transition region of the freezing channel. Therefore the TRAN-2 fuel housing was simply pumped out, the He reservoir was refilled, and the package was re-irradiated with a higher ACRR pulse (194 MJ, vs. 134 MJ for TRAN-2/AE). The results of this second experiment (TRAN-2/R) will be the primary focus of this section, but occasional references to TRAN-2/AE will be made, for the following reason: because of the relatively small difference in reactor power level between the two experiments, but the large difference in the amount of fuel motion that occurred, approximate calibrations of several diagnostic methods can be obtained.

1. PRESSURE TRANSDUCER DATA FROM TRAN-2

Because the pressure transducer near the base of the fuel melting chamber was destroyed by hot fuel so early in the TRAN-1 experiment, in TRAN-2 and all subsequent experiments this transducer was relocated to just above the solenoid valve. This relocation has protected the valve from damage but has not completely eliminated heating effects, at least as judged by some of the erratic and apparently non-physical signals recorded at late times.

The ACRR power peaked at 322 ms for the TRAN-2/R experiment, so $\Delta t \equiv t - 322$ ms. As shown in Figure 33, the dump tank transducer indicated

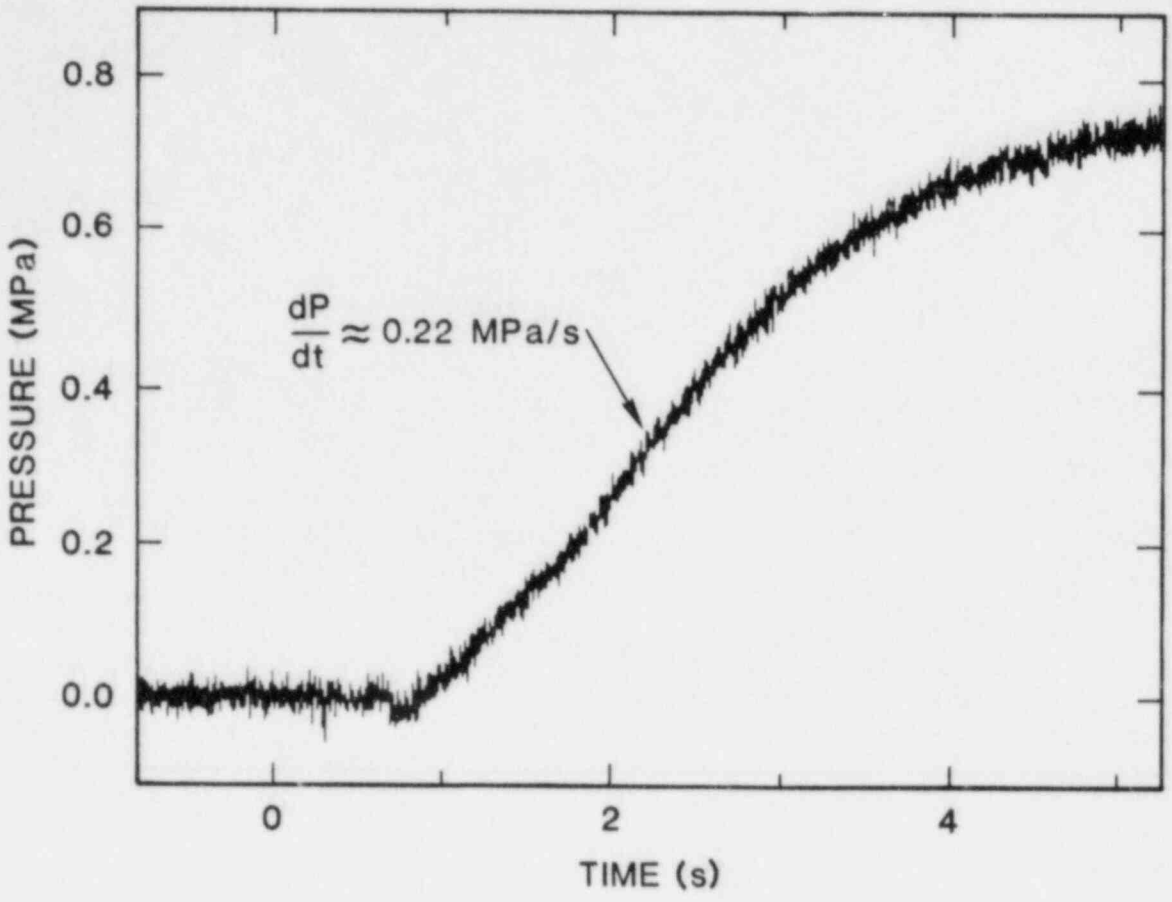

Figure 33 Dump tank pressure history in the TRAN-2/R experiment.

no significant gas flow for $\Delta t < +0.4$ s, at which point a very slow pressure rise began ($\approx$0.22 MPa/s, or 10 percent of the empty-channel pressure drop rate). Correspondingly, the helium reservoir pressure transducer indicated a similar pressure fall rate (Figure 34).

These data therefore imply the formation of a tight blockage to gas flow for $\approx$0.4 s, followed by a gradual gas flow for the next $\approx$5 s. The time at which gas began to flow may indicate when the blockage began to shrink and crack away from the channel walls.

2. FUEL MOTION DETECTOR DATA FROM TRAN-2

The lack of fuel motion in experiment TRAN-2/AE allowed for a possible calibration of the fuel motion sensitivity of the platinum self-powered detectors. To correct for differences in the ACRR pulse shape between the two experiments, at each point in time the signal from each fuel motion detector was divided by the normalization detector signal at that time. The resulting normalized signals for the two experiments could then be compared, referencing times to the peaks of the ACRR pulses. A representative pair of normalized signals for TRAN-2/R and TRAN-2/AE is shown in Figure 35 for the self-powered detector located 11.5 cm above the entrance to the freezing channel.

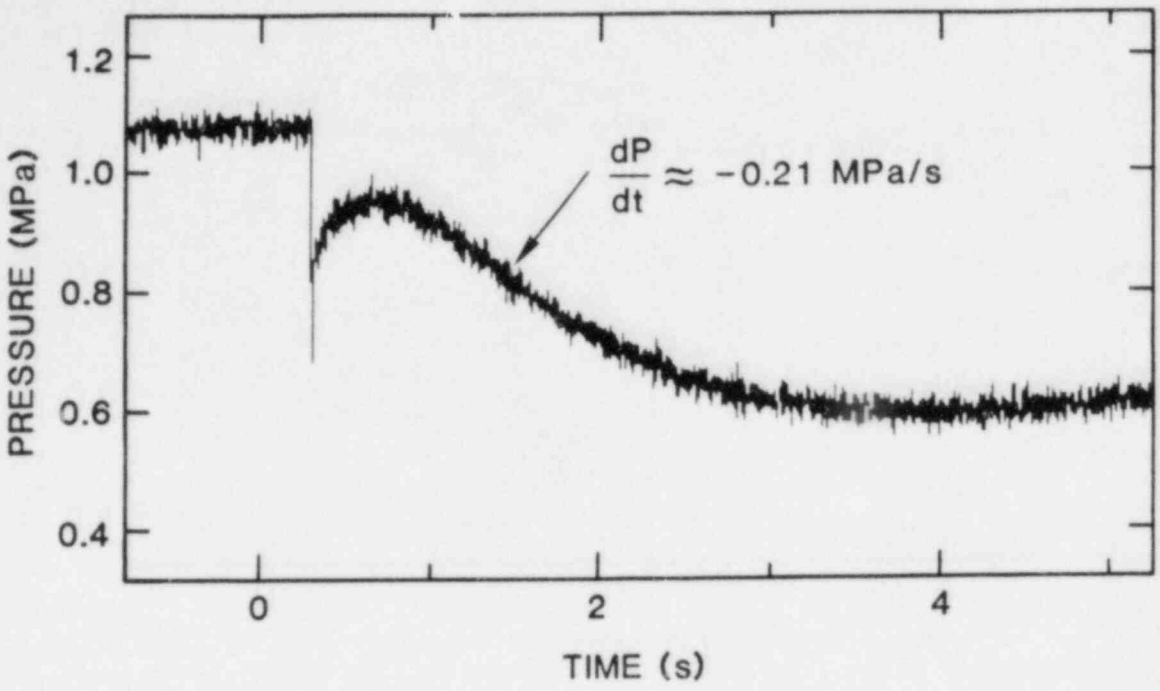

Figure 34 Helium reservoir pressure history in the TRAN-2/R experiment.

The signal ratio is near one and is very noise-free for about the first 15 ms after the ACRR pulse peak, but over the next 10 ms degenerates rapidly into random noise. Some of this noise was caused by the finite resolution of the analog-to-digital converter used to record the data. There may be a small difference between the two normalized signals beyond 20 ms after the ACRR pulse; however, this difference is nearly swamped by noise. Therefore no quantitative estimate of fuel motion sensitivity could be made on experiment TRAN-2. A complex computer model of the geometry of all nearby gamma emitters would also be required to analyze these data in detail for confirmation of fuel motion.

Additional data have been taken from TRAN-3 and TRAN-4 to check operation of the detectors at higher temperatures, and to give further cases for analysis. The detectors appear to be quite durable, are relatively noise free, and can operate at high temperatures, but their sensitivity to fuel motion is unknown at present.

3. THERMOCOUPLE DATA FROM TRAN-2

A comparison of the thermocouple data from TRAN-2/AE and TRAN-2/R shows the difference that would be expected from the differences in fuel motion. That is, when fuel does not move, the melting-chamber-temperature rise is larger, and only gamma heating is observed in the freezing channel. When fuel moves into the freezing channel, the melting-chamber-temperature rise is smaller, and a small, delayed temperature rise is observed in the freezing channel. Table 9 shows the temperature rises observed in TRAN-2/R and TRAN-2/AE.

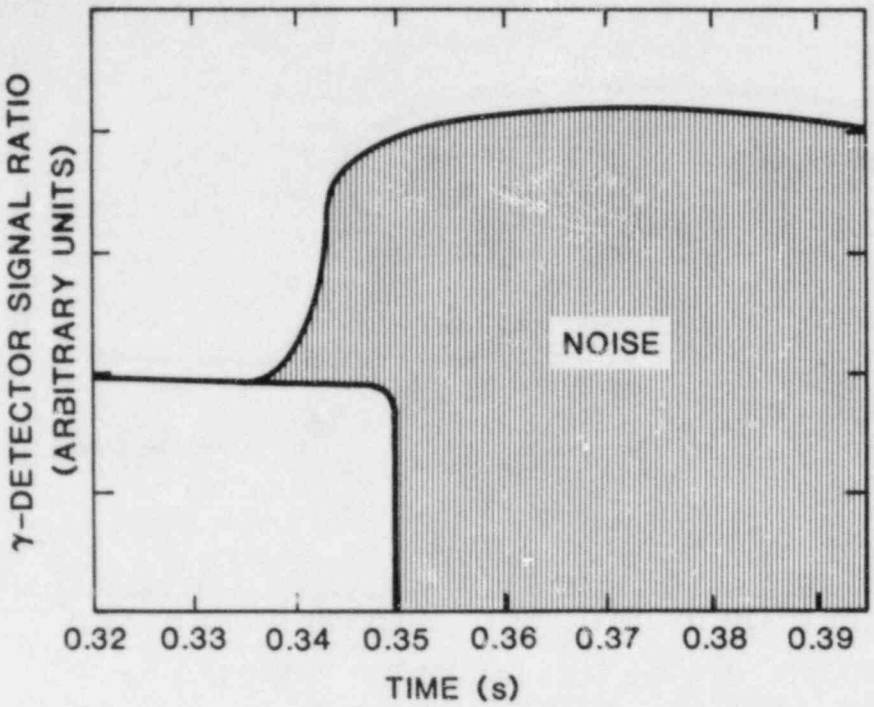

(a) TRAN-2/R

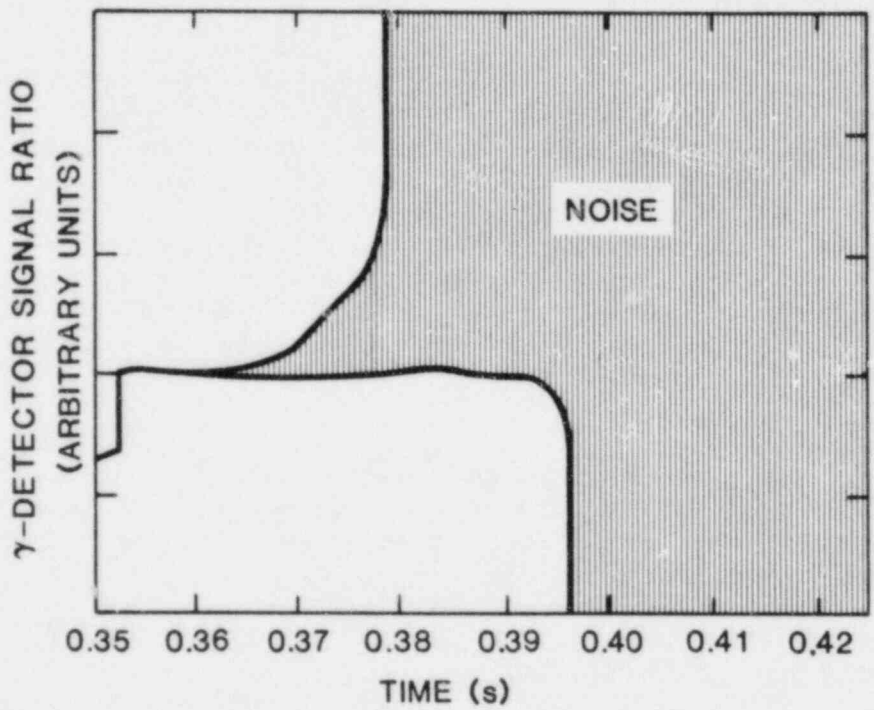

(b) TRAN-2/AE

Figure 35 Signal from the gamma detector located 11.5 cm above the entrance to the freezing channel for the TRAN-2 experiment.

Table 9. Measured Temperature Rises Caused by Gamma Heating and Fuel Freezing

	TRAN-2/AE		TRAN-2/R	
	ΔT_γ	ΔT_f	ΔT_γ	ΔT_f
Melt Chamber	43	174	33	103
Freezing Channel	5	0	5	14

4. RADIOGRAPHY OF TRAN-2/R

As stated above, the radiographs of TRAN-2/AE showed no fuel in the freezing channel. However, the radiographs of TRAN-2/R showed a relatively uniform frozen fuel layer on the walls of the fuel melting chamber and the first 87 cm of the freezing channel. A small partial blockage was located 14 cm above the freezing channel entrance, and there may have been a small enlargement of the channel diameter over the 2-3 cm near the channel entrance (Figure 36, top). Near the middle of the long frozen layer there were a few places where the layer appeared to have flaked off (Figure 36, middle). At ≈8 cm above the upper end of the frozen layer were located two well-defined, dense blockges ≈7 mm long, separated by an ≈8 mm long space containing some lower-density debris (Figure 36, bottom). Finally, a small amount of loose debris was seen at the exit of the freezing channel, where small horizontal ledges could have allowed some debris to collect during the time the experiment was vertical.

These radiographic observations are consistent with a fairly long slug of molten fuel moving up the freezing channel, leaving behind a frozen crust or a thin liquid fuel layer or both. Near the time of slug depletion, the material near the leading edge of the fuel slug apparently cooled sufficiently such that a blockage formed. This blockage seals off the flow of gas until it has cooled and cracked away from the channel wall. At this point gas begins to flow, and could conceivably move the blockage debris upward a few cm to its present resting place. The radiographs do not provide any information about the possible mechanism for the blockage formation. However, the post-irradiation examination in the HCF did provide some possible explanations (see section 6).

5. GAMMA SCANS OF TRAN-2

The 765.8 keV line of ^{95}Nb produced the best signal-to-noise ratio when TRAN-2 was rescanned using the less volatile fission product chains. Figure 37 shows the corrected gamma intensity and the implied normalized fuel distribution. The two blockages were very clearly seen at Z = 0.8 m, and the fuel crust in the freezing channel was seen to be relatively uniform. In agreement with the radiographs, a small amount of fuel was located beyond the end of the freezing channel. According to Figure 37, about 50 percent of the initial fuel load

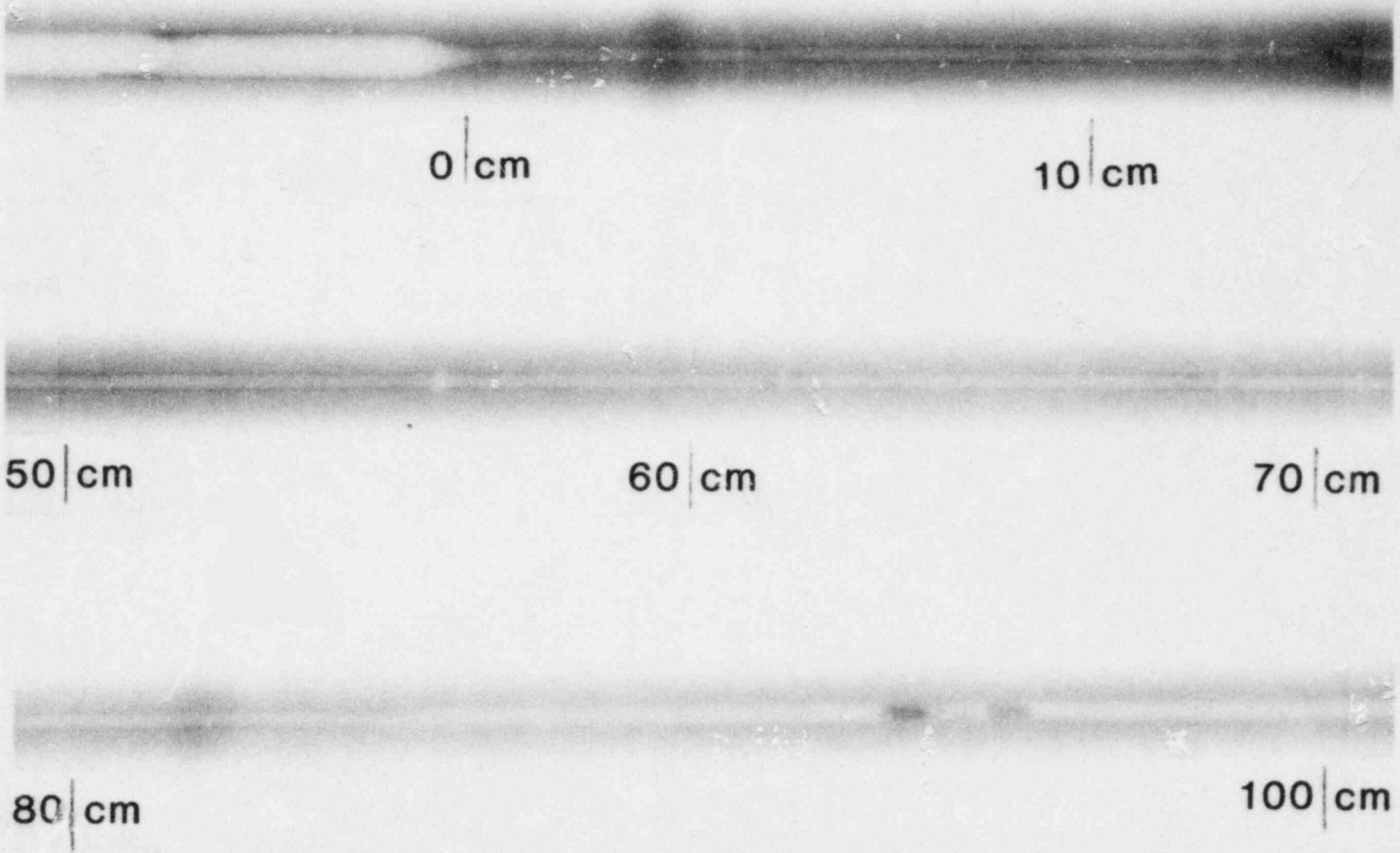

Figure 36 Radiographs of the TRAN-2/R experiment.

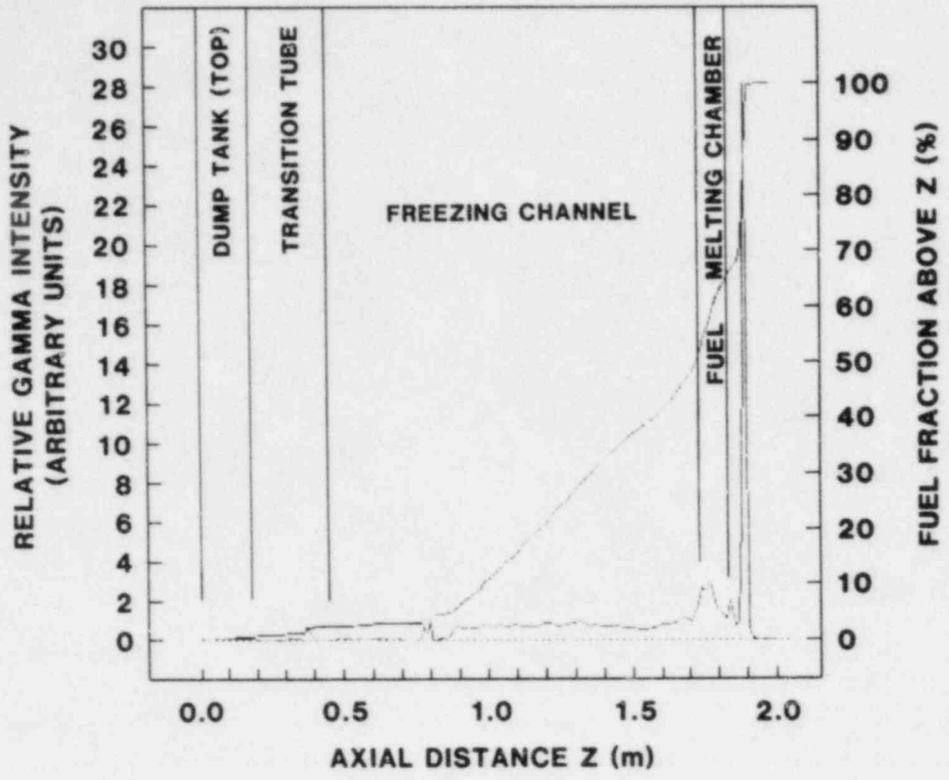

Figure 37 Gamma scan of the TRAN-2/R experiment.

froze in the freezing channel or beyond, about 15 percent remained in the fuel melting chamber, and the remaining 35 percent froze in the gas passages below the fuel melting chamber. Similar overall results were obtained with the 497.08 keV line of ^{103}Ru, although the signal-to-noise ratio was noticeably worse.

6. EXAMINATION OF TRAN-2 IN HOT CELL FACILITY

The TRAN-2/R fuel housing was sectioned transversely at the fuel melting chamber (Figures 38 (a) and (b)), at the transition section between melt chamber and freezing channel (Figure 38(c)), and at 3 cm, 12 cm, and 18 cm above the entrance to the freezing channel (Figures 39 (a) through (c)). Longitudinal cuts were made at the entrance to the freezing channel (Figure 40), through the two blockages (Figures 41 and 42), and through the upper portion of the fuel crust (Figures 43 and 44).

In contrast to TRAN-1, TRAN-2 displayed a melted and refrozen steel layer outside the fuel crust near the entrance to the freezing channel (Figures 38 and 39). The fuel crust was quite thick, and had a smooth inner surface but a rough outer surface where the fuel contacted the molten steel. Figure 40 shows the onset of this rough boundary (along with a thickening of the fuel crust) at the entrance to the freezing channel. There was no evidence of large grains in the fuel crust, and

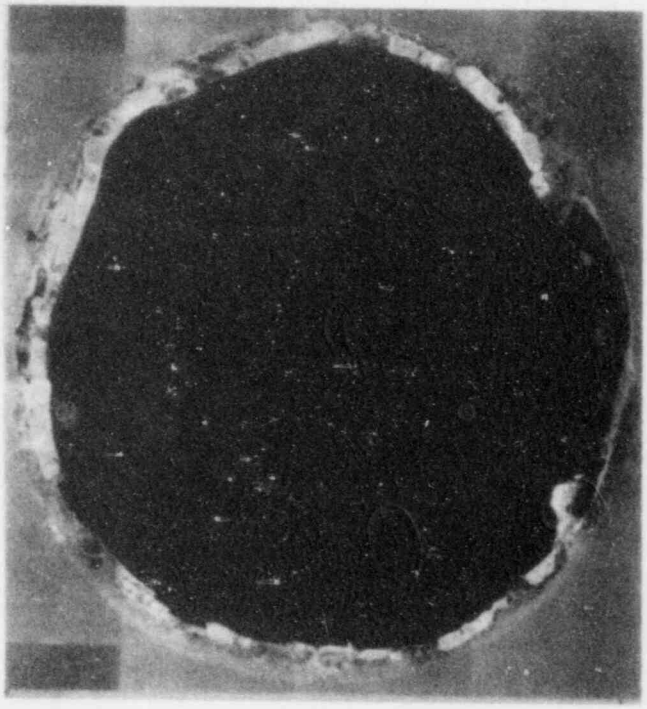

(a) 5.8 cm below the top of the melt chamber

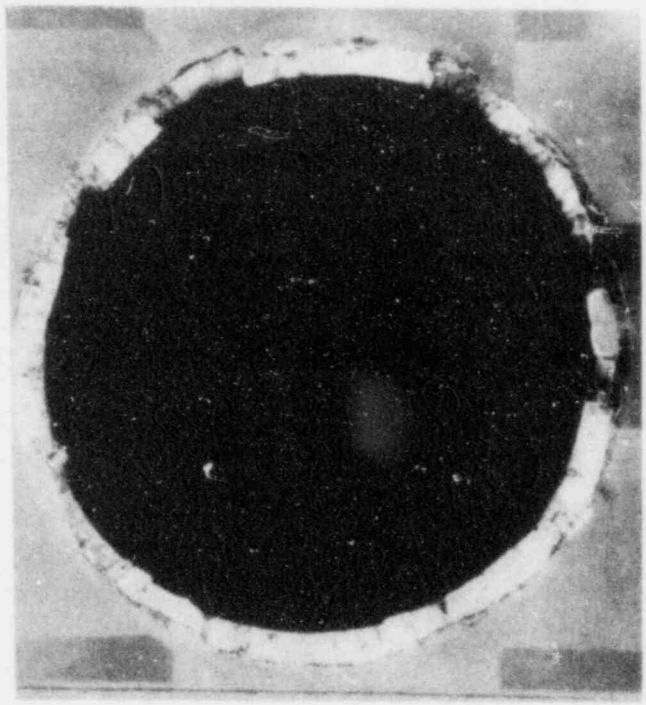

(b) 2.8 cm below the top of the melt chamber

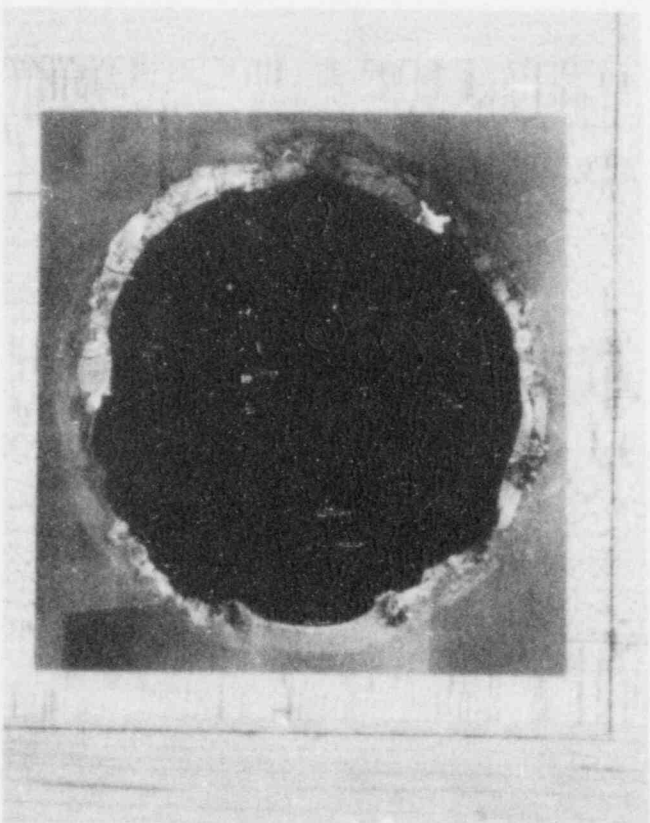

(c) transition region

Figure 38 Channel cross sections in the melt chamber and the transition region of the TRAN-2/R experiment. (≈10x)

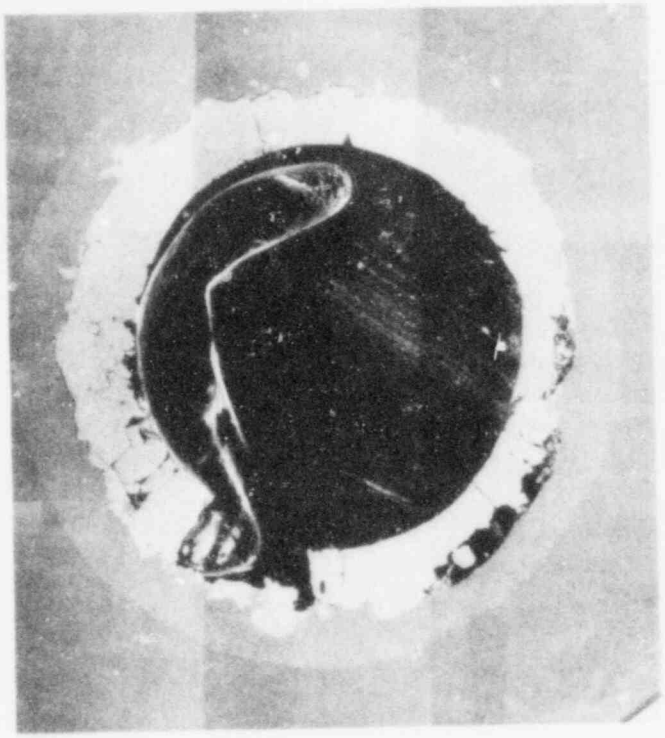

(a) 1.8 cm above the inlet (≈20x)

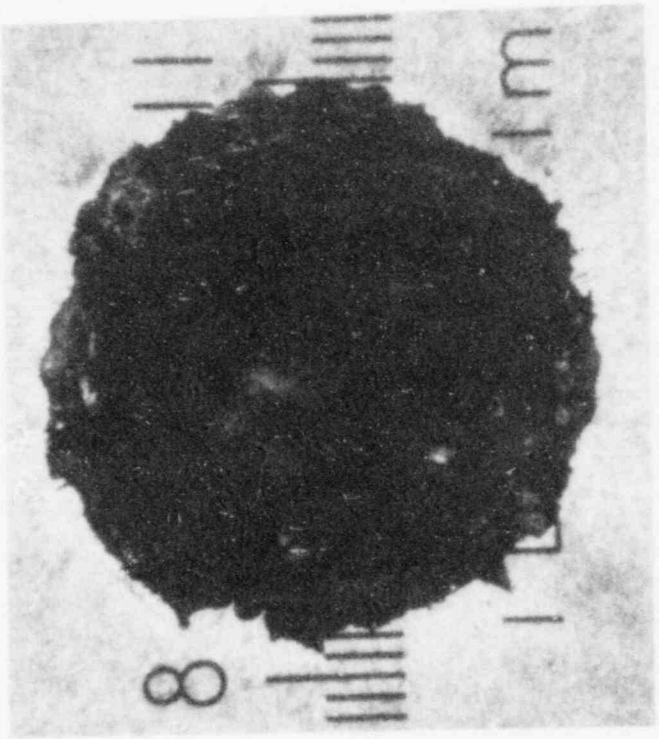

(b) 15.3 cm above the inlet (≈25x)

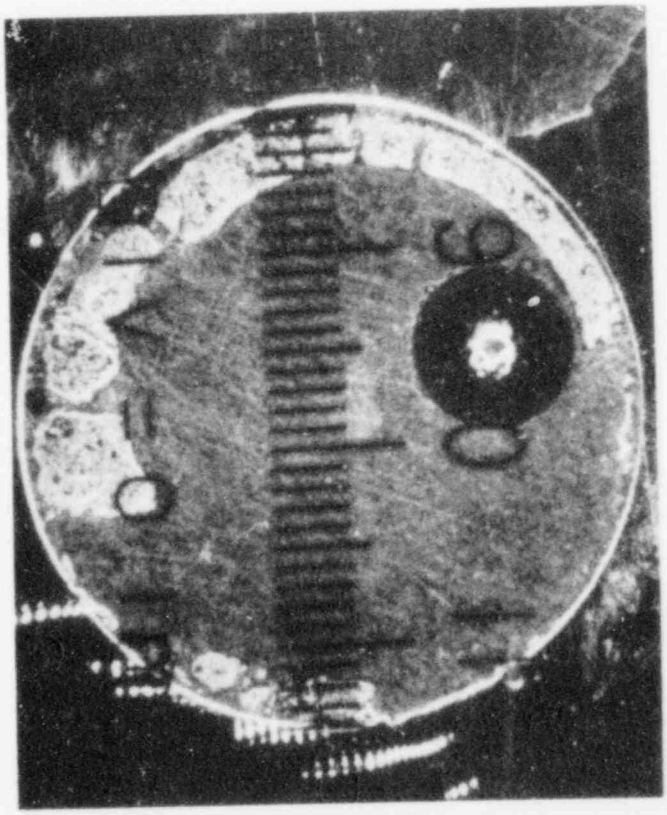

(c) 21.3 cm above the inlet (≈25x)

Figure 39 Channel cross sections in the freezing channel of the TRAN-2/R experiment.

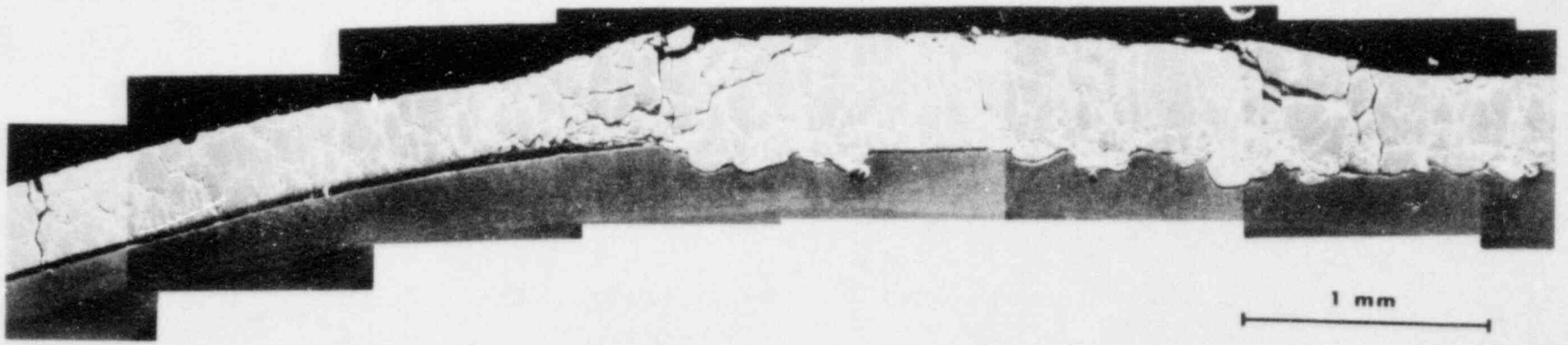

Figure 40 Longitudinal cut in the upper part of the fuel melting chamber of the TRAN-2/R experiment.

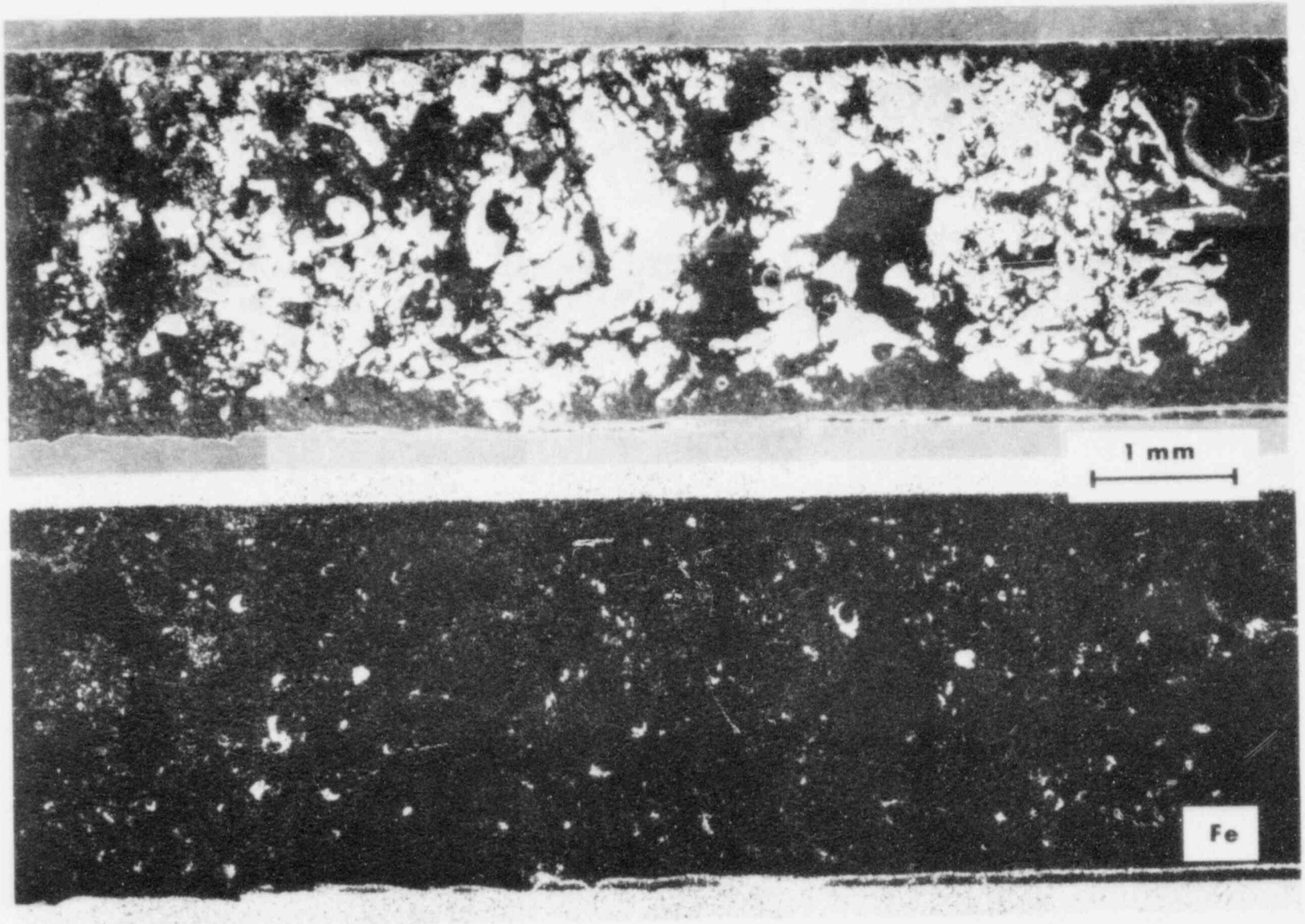

Figure 41 Longitudinal cut through the upper blockage of the TRAN-2/R experiment.

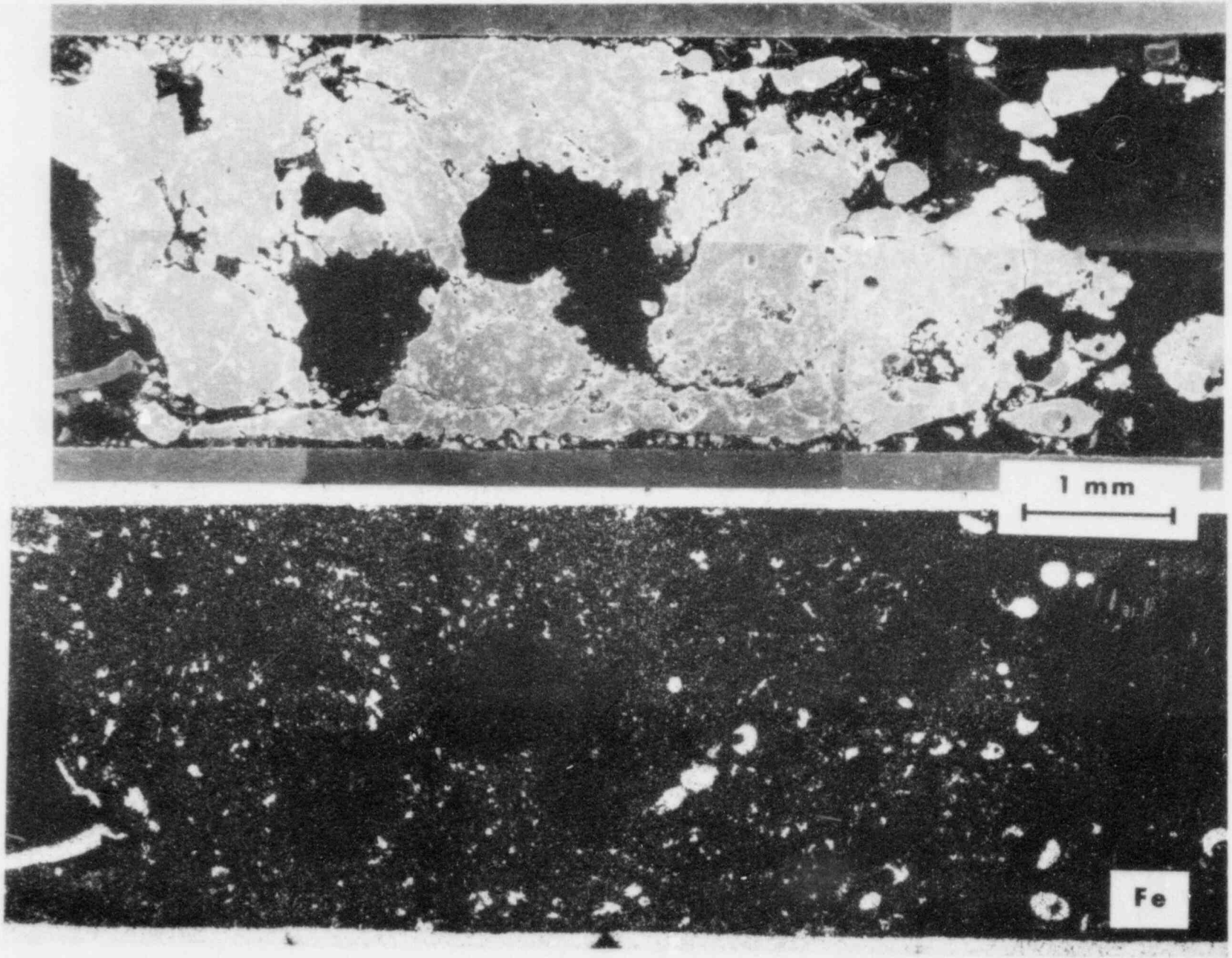

Figure 42 Longitudinal cut through the lower blockage of the TRAN-2/R experiment.

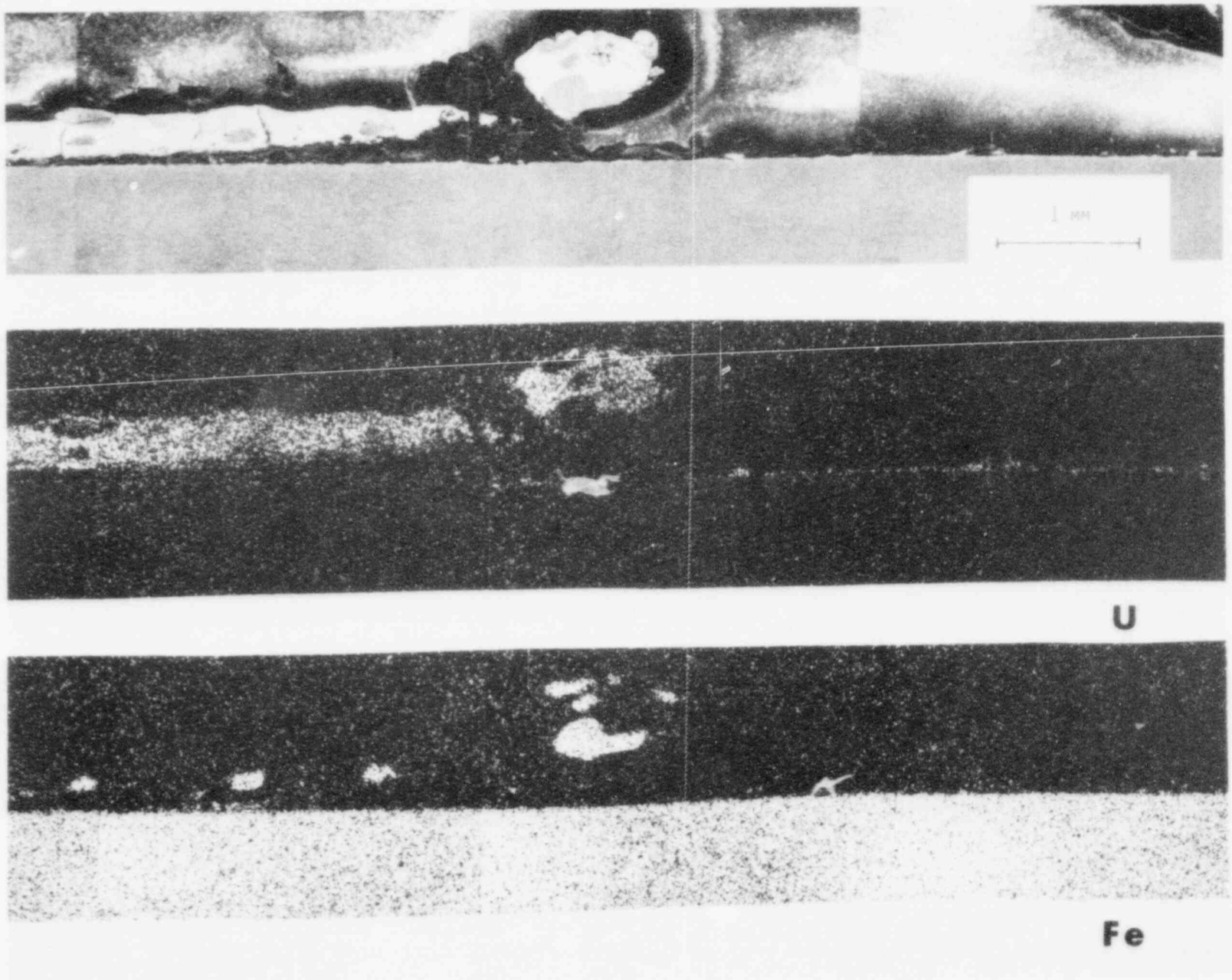

Figure 43 Longitudinal cut through the upper part of the fuel crust of the TRAN-2/R experiment. (Side 1)

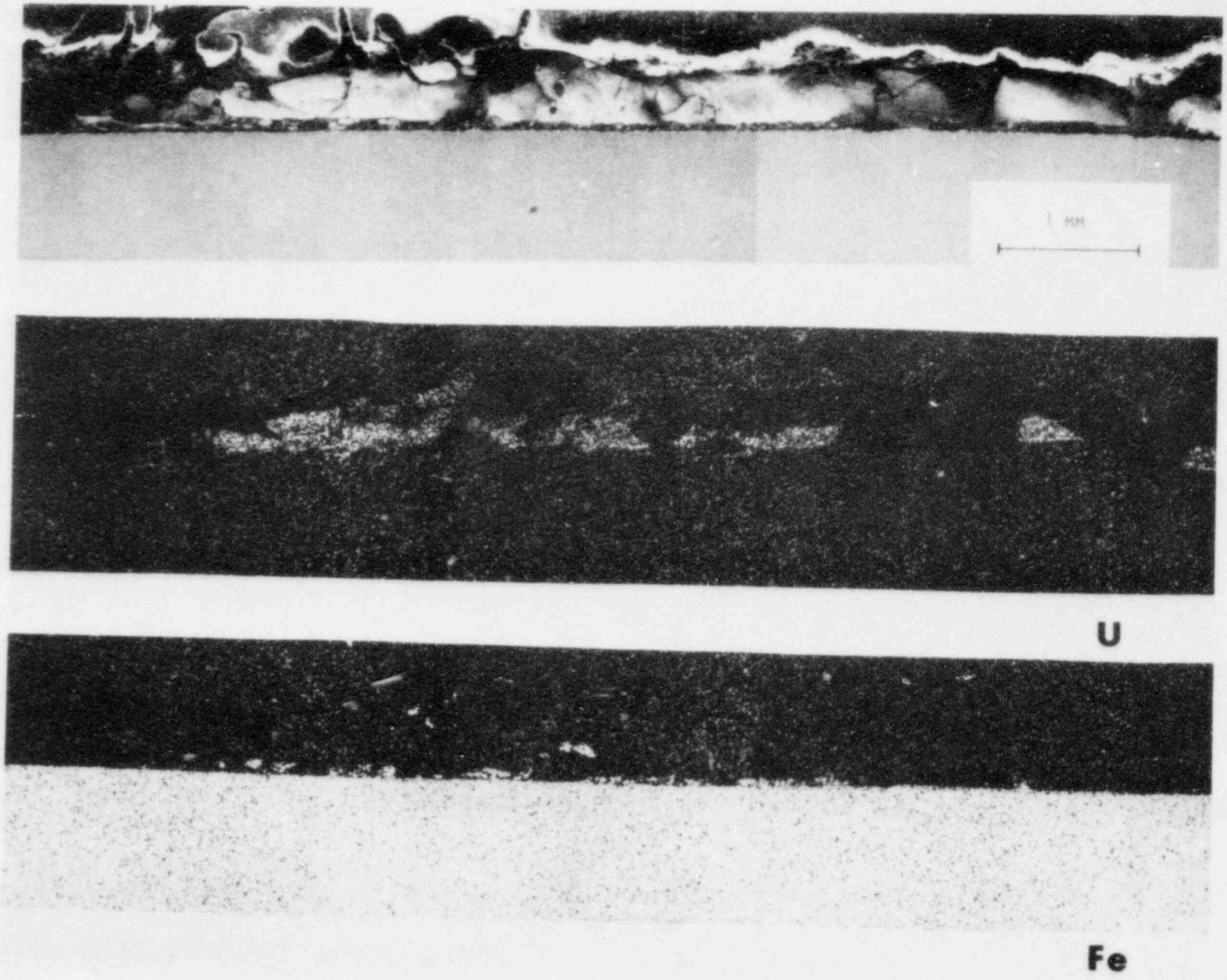

Figure 44 Longitudinal cut through the upper part of the fuel crust of the TRAN-2/R experiment. (Side 2)

no evidence of steel mixed into the fuel. A few isolated chunks of fuel were observed in the molten steel layer. The outer boundary of the melted and re-frozen steel layer was nearly circular.

Longitudinal sections through the two blockages (Figures 41 and 42) revealed that they were composed mainly of fuel, with a small steel admixture in the form of isolated globules. The fuel in the blockages nearly filled the channel cross-section. More voids were found in the blockage farther from the entrance. Based on quantimeter area measurements, both the upper and lower blockages contained about 20 volume percent steel, but the void fraction of the lower blockage was 40 percent versus 60 percent for the upper blockage.

A longitudinal section through the upper end of the crust also showed a significant amount of steel in the fuel crust, in the form of isolated steel globules (Figures 43 and 44). Thus the crust composition near the blockages resembles the blockage composition rather than the crust composition near the channel entrance. Compared to TRAN-4, the steel globules in TRAN-2 do not appear to contain any frozen fuel precipitate.

Based on the high steel content and the porous nature of these blockages, it appears that steel ablation and entrainment may have played an important role in the TRAN-2 blockage formation.

7. INITIAL FUEL AND STEEL CONDITIONS IN TRAN-2

The measured axial variation in energy deposition for the conditions of TRAN-2 through TRAN-5 is shown in Figure 23. The measured energy deposition coupling factor together with the ACRR pulse size indicates a fuel temperature ≈3720 K, which is fairly constant along the initial fuel column. The 1.0 MPa driving pressure was applied at $\Delta t = -6.5$ ms, or well before fuel melting (in contrast to TRAN-1). The initial steel channel temperature was quite constant along the channel, with an average temperature of ≈860 ±10 K.

APPENDIX E

RESULTS OF TRAN-3 EXPERIMENT

Experiment TRAN-3 was performed on July 30, 1981, at a driving pressure difference of 1.0 MPa (no backpressure in the freezing channel), a fuel temperature ≈3770 K, and an initial steel temperature of 943 ± 33 K averaged along the freezing channel. Because massive steel melting had not been observed in TRAN-2, the goal of TRAN-3 was to raise the steel temperature to 1073 K where rapid steel melting was very likely. However, the glass-wrapped heater tapes used in these early experiments began to fail, and TRAN-3 was performed hastily as the temperature was falling. In TRAN-3 care was taken to apply the driving pressure very close to the time of fuel melting, but no earlier.

1. PRESSURE TRANSDUCER DATA FROM TRAN-3

The ACRR power peaked at 326 ms, so $\Delta t = t - 326$ ms. The driving pressure pulse of ≈1.0 MPa was fully applied to the fuel at $\Delta t \approx -10$ ms, and gas flow into the dump tank began at $\Delta t = +90$ ms (Figure 45). An increase in the gas flow from the reservoir appeared to occur at $\Delta t = +130$ ms (Figure 46). However, the dump tank and pressure reservoir transducers indicated a pressure discrepancy at 8 s of about 0.38 MPa, which is somewhat larger than would be expected based on estimates of transducer errors. In addition, the pressure appears to be lower in the reservoir than in the dump tank at about 2 s, which is difficult to reconcile with the steadily increasing pressure in the dump tank. Because these discrepancies are not understood at present, it seems best to rely on the dump tank transducer, which shows very little evidence of radiation noise. For $\Delta t > 100$ ms the pressure transducer just above the solenoid valve showed a large, erratic signal decrease, which indicated transient heating of the transducer face (Figure 47).

The initial phase of pressure equilibration in the dump tank was complete at $\Delta t = 0.35$ s, which indicates a gas flow rate only 25 percent as large as for an empty flow channel. Final pressure equilibration occurred at $\Delta t \approx 5$ s (probably including gas heating effects). Thus, molten fuel appeared to block the gas flow for 80-120 ms, but the freezing channel then opened up partially, and a tight blockage was not formed.

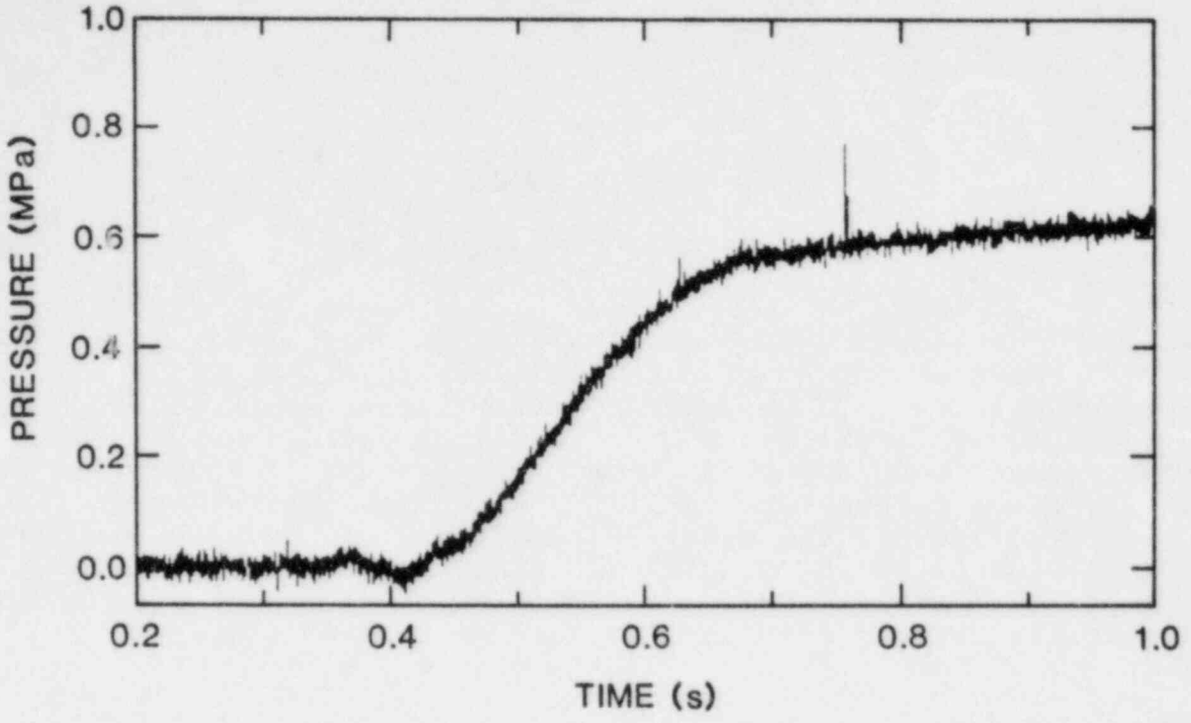

Figure 45 Short-term dump tank pressure in the TRAN-3 experiment.

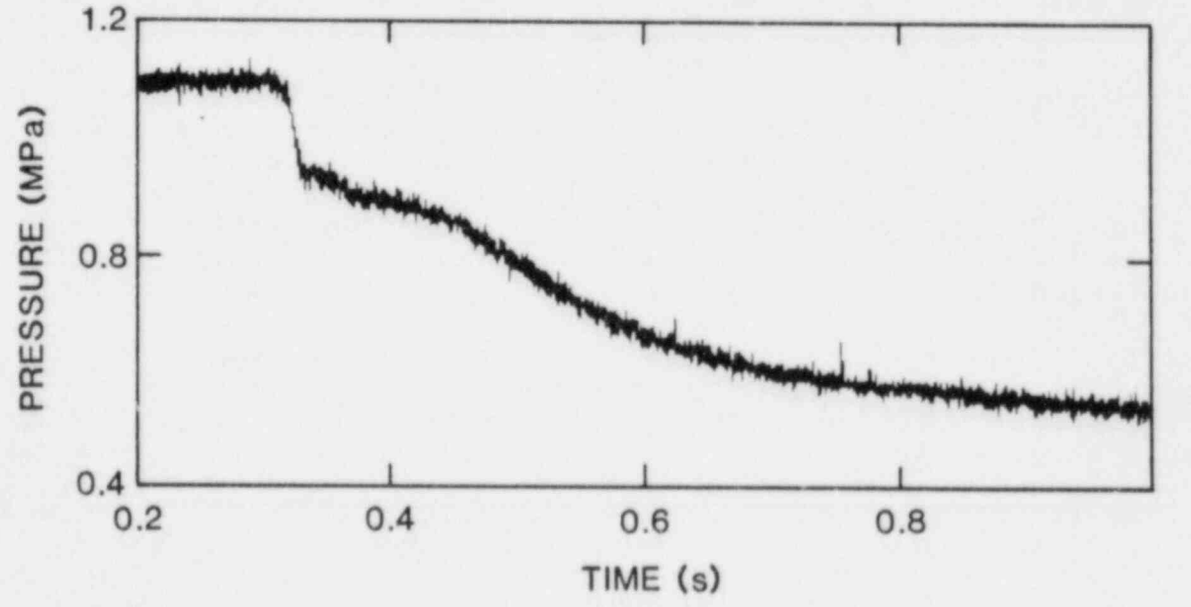

Figure 46 Short-term helium reservoir pressure in the TRAN-3 experiment.

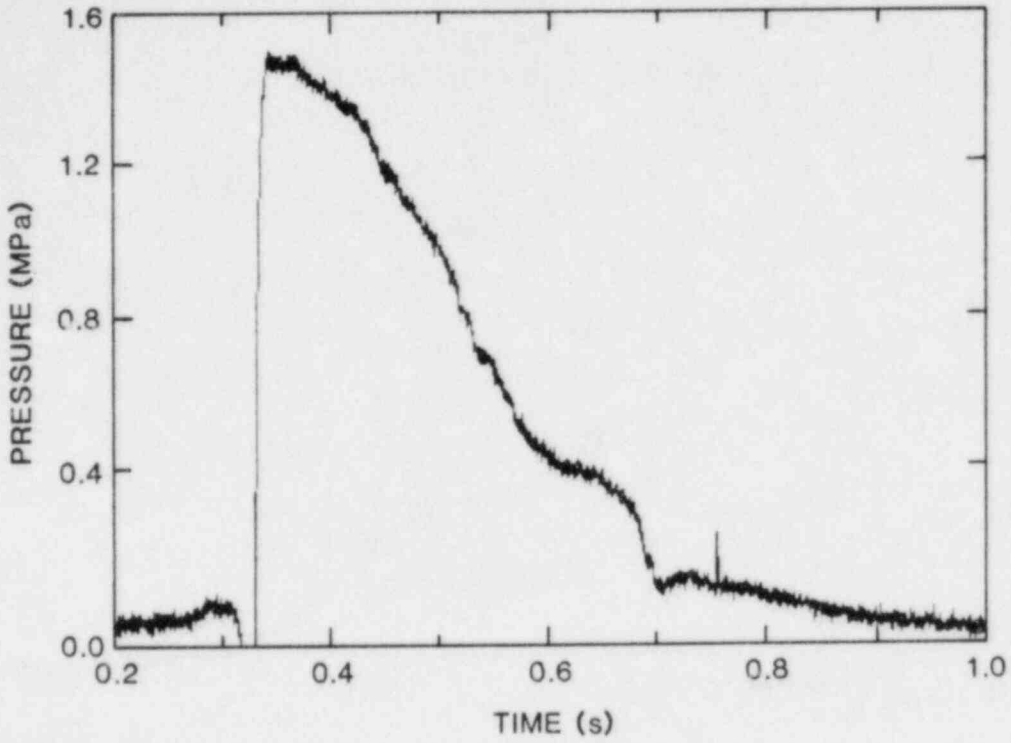

Figure 47 Short-term melting chamber pressure in the TRAN-3 experiment.

2. FUEL MOTION DETECTOR DATA FROM TRAN-3

For -0.015 s $< \Delta t < 0.015$ s the fuel motion detector signals resembled the TRAN-2/R signals, but the peak amplitudes ranged from 5 to 24 percent lower, the average decrease in peak signal being 12 percent. The normalization detector signal decreased by only 5 percent, which might result from variations in the ACRR power. An overall decrease in signal intensity might also result from the somewhat higher initial steel temperature of the TRAN-3 experiment (943 K vs. 873 K for TRAN-2/R). Differences between individual detectors could result from slightly different detector placement on the fuel housing, or changes in detector characteristics caused by handling (during removal from TRAN-2/R and re-installation on TRAN-3). An additional factor in comparing TRAN-3 with TRAN-2/R is that axial expansion of the fuel by ≈10 percent had already occurred before the TRAN-2/R experiment.*

From the above discussion, it appears difficult to rely on absolute signal levels without careful pre-calibration of the detectors under actual operating conditions. Therefore, differences in signal shape at late times ($\Delta t > 0.025$ s) were also examined. The signal shapes were compared to the late-time ACRR power signal (Figure 48) and the

*Axial expansion caused by fuel cracking occurred during TRAN-2A/E. Thus, the fuel in TRAN-2/R had a higher (≈10%) porosity than the fuel in TRAN-3.

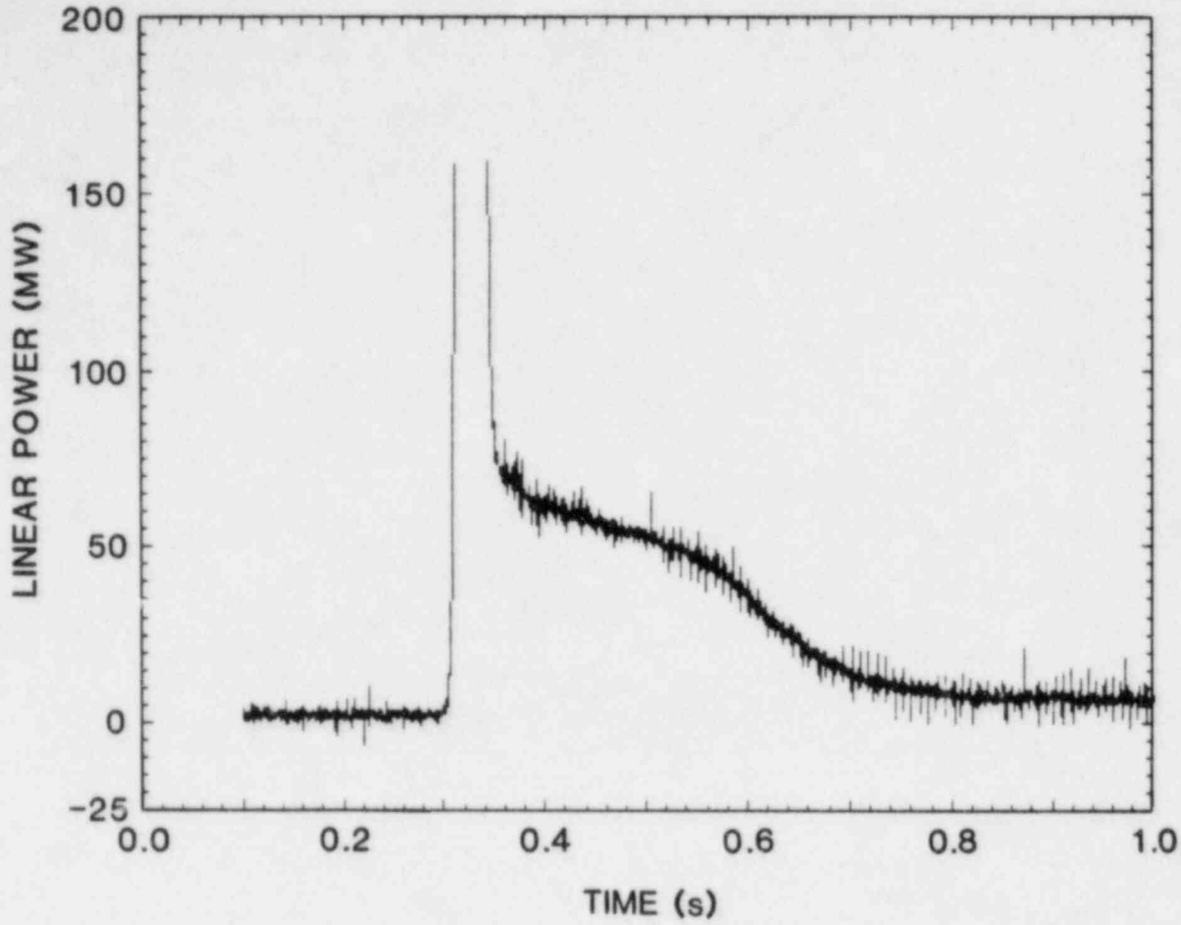

Figure 48 ACRR power at the tail of the ACRR pulse.

late-time normalization detector signal (Figure 49), which have similar shapes. Relative to these two signals, the fuel motion detector located 11.5 cm above the entrance to the freezing channel showed a broad peak at $\Delta t \approx 0.15$ s (Figure 50). The signal from the detector located at the exit of the freezing channel (Figure 51) resembled the normalization detector signal within the experimental noise. The detectors at the top and bottom of the fuel melting chamber were not recorded with sufficient precision to see late-time signal shapes.

In summary, the fuel motion data contain excessive noise such that the late-time signals are difficult to interpret. Hence, care must be taken to amplify the signals so that they can be read with greater precision by the ADC. Although there are indications of fuel motion into the freezing channel, detailed analysis must be performed to confirm the detection of fuel motion.

3. THERMOCOUPLE DATA FROM TRAN-3

After correcting for gamma heating, the temperature rises of thermocouples located at the fuel melting chamber, at 11.5 cm, and at 39.4 cm above the entrance to the freezing channel were 67 K, 20 K, and

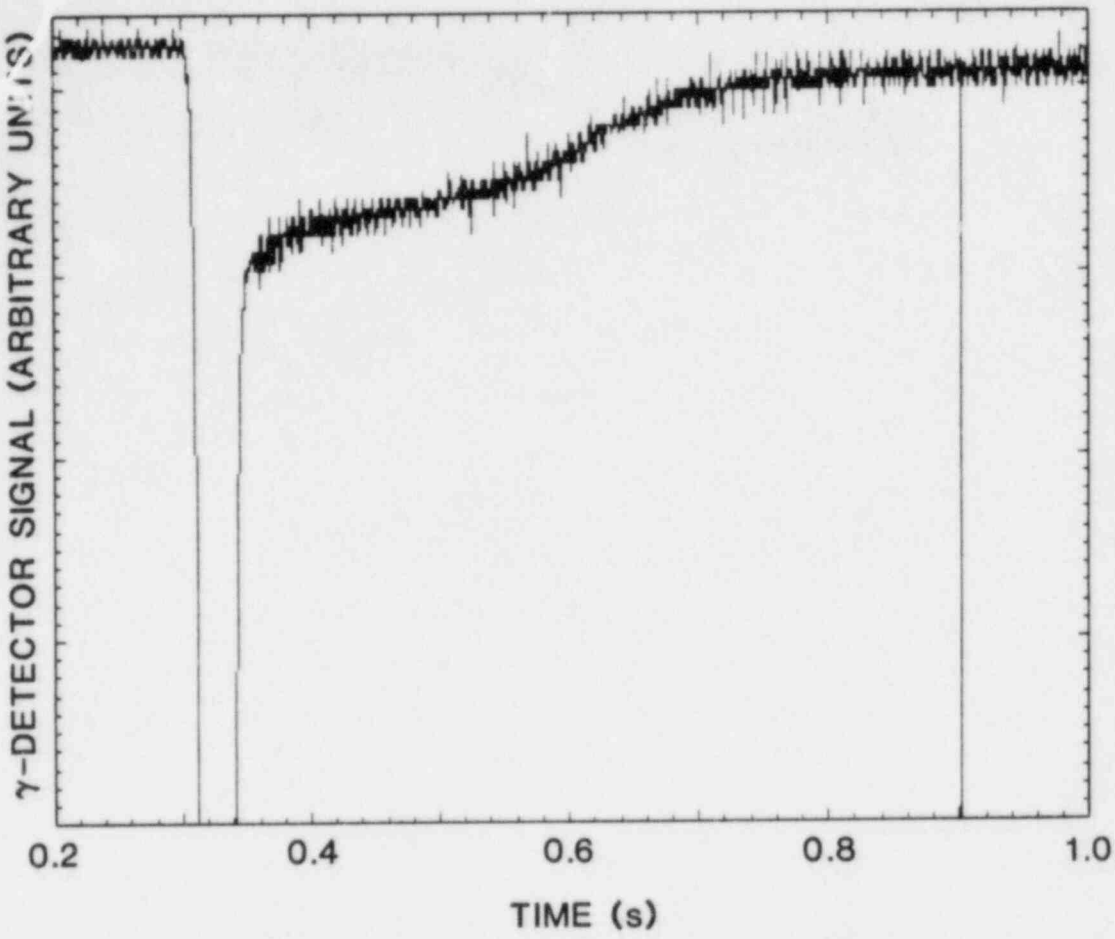

Figure 49 Normalization detector signal at the ACRR pulse tail.

19 K, respectively. The 67 K temperature rise is consistent with most of the fuel leaving the fuel melting chamber, and the 20 K temperature rises are consistent with UO_2 freezing and filling part of the freezing channel.

4. RADIOGRAPHY OF TRAN-3

Radiographs of TRAN-3 showed a frozen layer (presumbly UO_2) extending 67 cm into the freezing channel, with no obvious blockages. Below the fuel melting chamber, hollow spheres of fuel apperared to have come to rest in the exit of the solenoid valve, and in the pressure transducer housing just above the solenoid valve. These spheres may have caused the transient heating that was observed in the signal trace of the pressure transducer located just above the solenoid valve. The three spheres ranged in diameter from 3.0 to 3.5 mm. Little or no debris was observed beyond the freezing channel exit or in the dump tank. The frozen UO_2 layer was uniform except for some thickness variations and

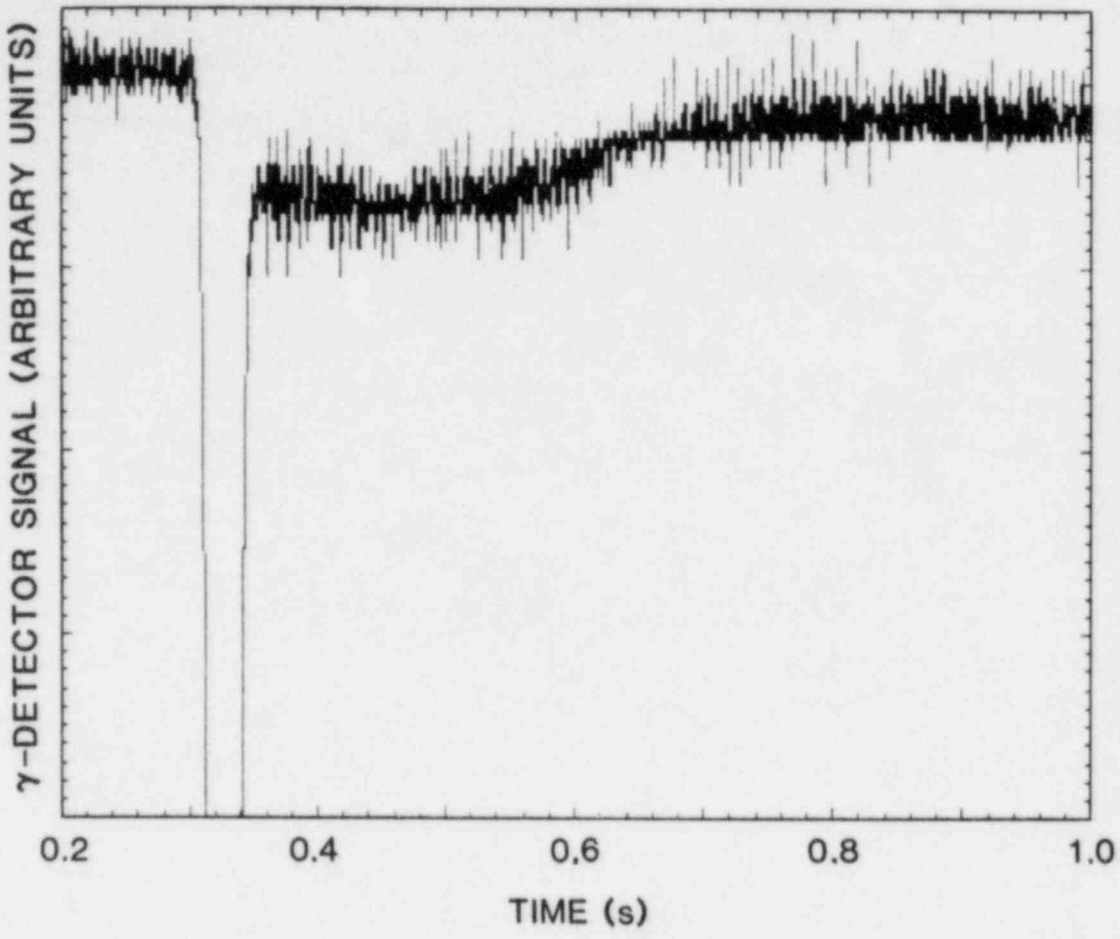

Figure 50 Signal from the fuel motion detector located at 11.5 cm above the freezing channel entrance.

axial gaps in the layer, in the ≈20 cm near the leading edge of the crust. There was some evidence of widening of the freezing channel near the entrance from 3.2 to ≈3.8 mm diameter.

5. GAMMA SCANS OF TRAN-3

As described in Appendix B, Section 5, the small fuel spheres observed in the pressure transducer housing of TRAN-3 were used to identify which gamma ray lines were most characteristic of fuel. Using two of these four lines, scans were made of the TRAN-3 fuel distribution (Figures 52 and 53). In contrast to the scan made with the 1596 keV line of ^{140}La (Figure 54), these scans were in good agreement with the radiographs, showing a relatively uniform fuel layer extending 68.7±1.2 cm from the entrance of the freezing channel, with only a small amount of fuel debris beyond the exit of the freezing channel. About 40 percent of the fuel was located beyond the entrance to the freezing channel, somewhat lower than the 50 percent estimated for TRAN-2/R. Because the pressure pulse was applied at $\Delta t = 0$ in TRAN-3, or nearly at the time of fuel melt, it is possible that some early

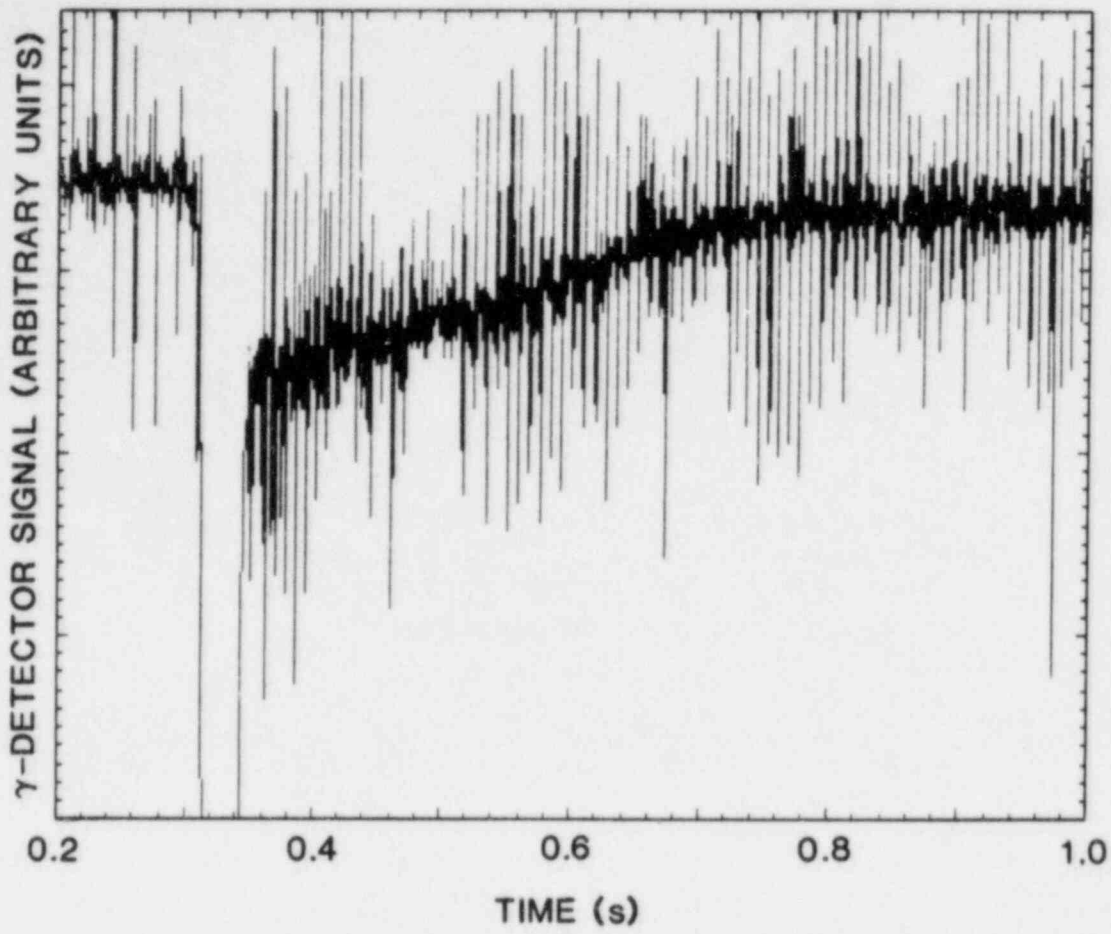

Figure 51 Signal from the fuel motion detector located at the exit of the freezing channel.

downward fuel dispersal occurred, resulting in less fuel available for entry into the freezing channel.

6. EXAMINATION OF TRAN-3 IN HOT CELL FACILITY

It has not been decided whether to examine TRAN-3 in the HCF, in view of the financial constraints and the relatively simple characteristics of the frozen fuel structures observed in radiographs. If it were examined, emphasis would be placed on the nature of any debris in the dump tank, on the evidence for possible steel melting near the entrance to the freezing channel, and on the nature of the fuel debris below the fuel melting chamber (in an effort to determine when and how the fuel flowed down into this region). It might also be of interest to examine the upper end of the frozen fuel layer for evidence of fuel splashing or the existence of a transient blockage near the leading edge of the flow.

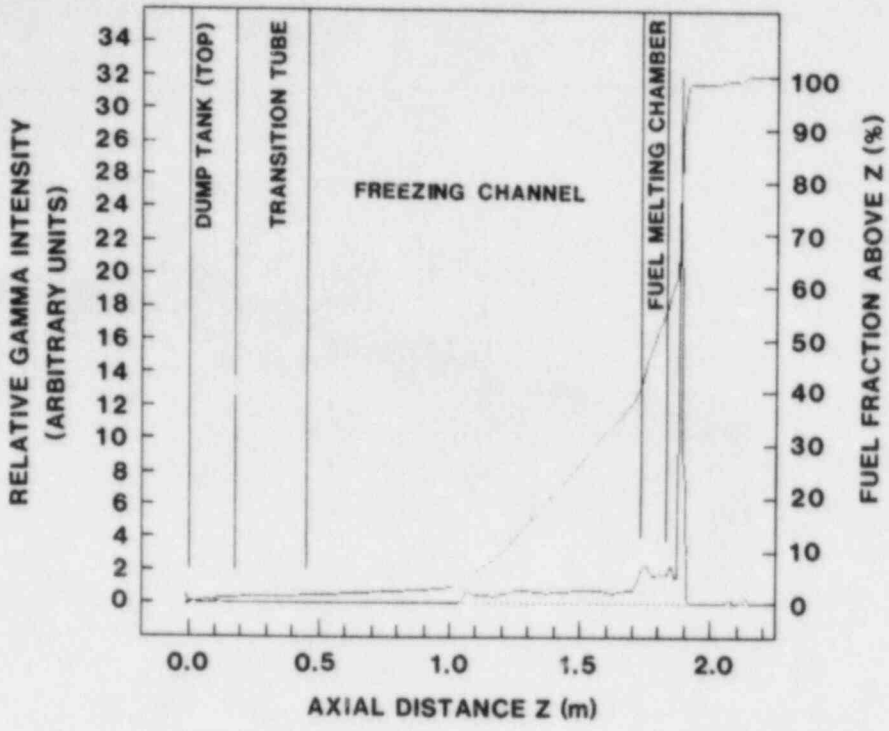

Figure 52 Gamma intensity and the normalized fuel distribution for the TRAN-3 experiment using the 765.8 keV line of ^{95}Nb.

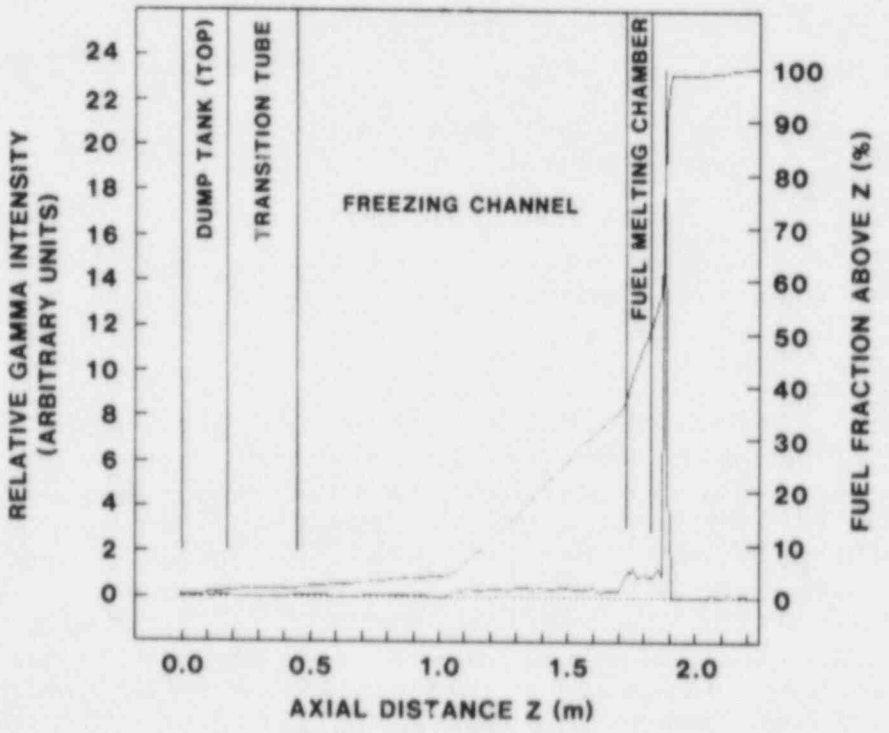

Figure 53 Gamma intensity and the normalized fuel distribution for the TRAN-3 experiment using the 497.1 keV line of ^{103}Ru.

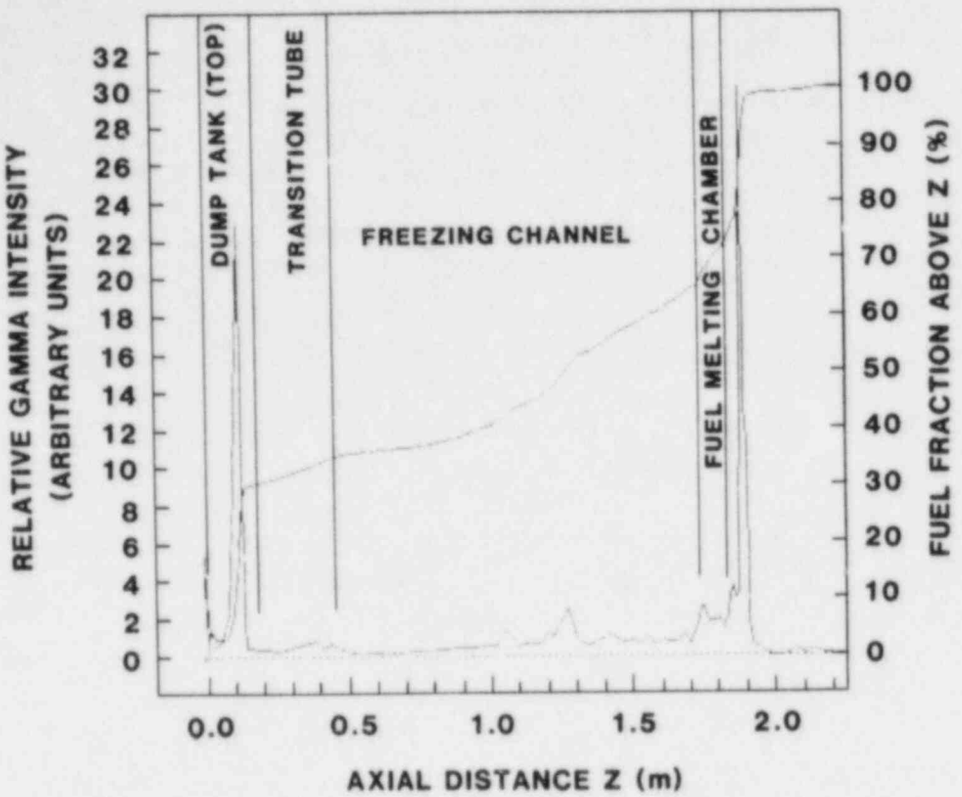

Figure 54 Gamma intensity and the normalized fuel distribution for the TRAN-3 experiment using the 1596 keV line of ^{140}La. (incorrect fuel distribution)

7. INITIAL FUEL CONDITIONS IN TRAN-3

Based on the fuel-temperature rise measurement, the fuel temperature in TRAN-3 was estimated to be ≈3770 K. Because the pressure pulse was applied near fuel melting (for an average element of fuel), fuel disruption and dispersal may have occurred earlier at the ends of the fuel column. Any fuel which flowed downward out of the fuel melting chamber is unlikely to be forced back into the freezing channel by the applied pressure pulse. Therefore a reduced amount of fuel could have been forced into the freezing channel.

If a short slug of fuel enters the freezing channel, the slug would be quickly depleted by crust formation and liquid film deposition. Therefore the true freezing and plugging behavior of a very large mass of fuel may not have been observed in TRAN-3. Because no gas flow past the fuel load was observed in the first three TRAN experiments, it was decided to apply the driving pressure well before fuel melt in TRAN-4 and TRAN-5, to maximize the amount of fuel pushed into the freezing channel. Although this might result in some additional uncertainty in the fuel temperature, the characteristic freezing and plugging behavior of a very large mass of fuel might be more readily observed.

8. INITIAL STEEL CONDITIONS IN TRAN-3

Because the glass-fiber-insulated heater tapes were failing, the experiment was performed as some portions of the freezing channel were beginning to cool down from temperatures > 973 K. Figure 55 shows a plot of the steel temperature at the beginning of fuel flow, including the effects of transient gamma heating. The average temperature was 943±33 K. New heaters of a different type were installed on later experiments.

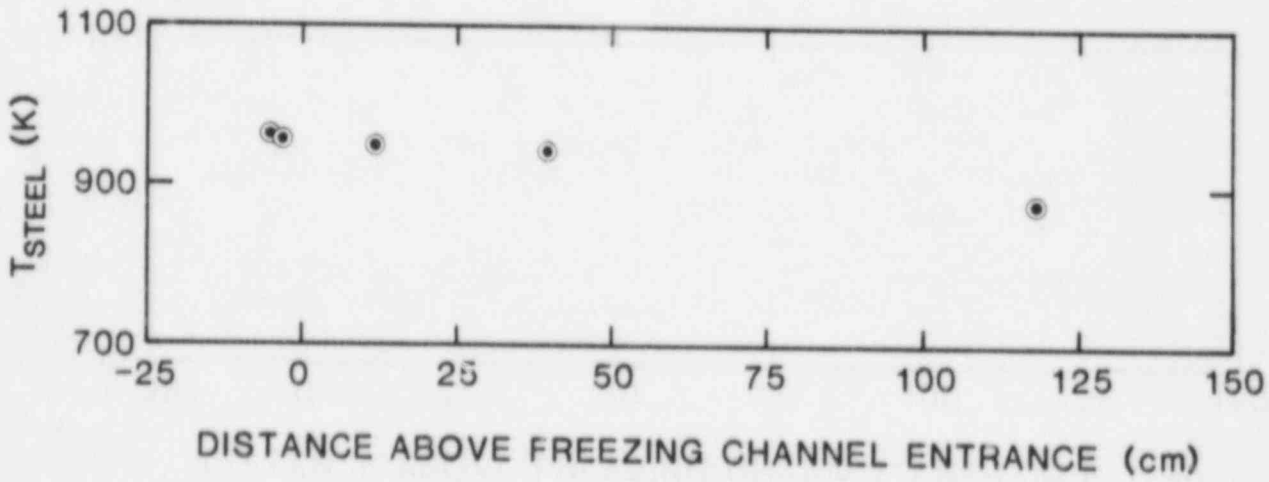

Figure 55 Initial steel temperature along the freezing channel for the TRAN-3 experiment.

APPENDIX F

RESULTS OF TRAN-4 EXPERIMENT

The TRAN-4 experiment was performed on December 7, 1981 at an initial steel temperature of 1170 K, an initial fuel temperature of ≈3800 K, and a driving pressure of 1.0 MPa, with no significant backpressure in the freezing channel or the dump tank. The purpose of this experiment was to investigate phenomena which might be expected when instantaneous steel melting occurs. Calculations by Hayden[15] had previously shown that such instantaneous melting might be expected at initial steel temperatures above 1100 K. New coaxial heaters were installed to permit reliable operation at much higher steel temperatures. To maximize the mass of fuel available for flow into the freezing channel, the driving pressure was applied well before the onset of fuel melting (earlier experiments had indicated little or no leakage of gas past the fuel load). An unchanged driving pressure and an unchanged, high fuel temperature were chosen to maximize steel melting and to provide direct comparison with preceding experiments conducted at lower steel temperatures (TRAN-2 and TRAN-3). In good agreement with Hayden's calculations, the posttest radiographs and analysis of TRAN-4 in the HCF demonstrated extensive steel melting and removal, accompanied by radically new fuel/steel interaction phenomena.

As stated previously, the phenomena of fuel-steel interaction in the higher-temperature range were quite different. Most of the information on these phenomena was obtained by examination of TRAN-4 in the HCF. A fuel crust was still observed, but near the channel entrance it lay over a region of melted and frozen steel ≈0.1 mm thick. The outer surface of the molten steel layer was relatively circular in cross-section, but the inner surface showed azimuthally-varying thickness, and in some cases narrow peaks of steel projecting toward the channel axis. The outer surface of the fuel often conformed closely to the curved steel surface, implying that the fuel was still molten at the time of formation of the steel "waves". Near the channel entrance much of the molten steel had been removed, leaving narrow, isolated steel peaks at several azimuthal locations. The fuel crust did not appear to have the clear, radially-oriented grains seen in TRAN-1. At one axial location a pure steel layer ≈0.14 mm thick was found between two fuel layers 0.2 and 0.4 mm thick. At another axial location a steel layer was found lying over a thick fuel crust. Careful examination of some cross-sections revealed a few isolated droplets of fuel and steel that were intimately mixed, possibly representing a eutectic phase. However, most of the cross sections in TRAN-4 were consistent with entrainment or removal of steel in relatively large, continuous sheets rather than intimate mixing of fuel and steel particulate. In some cross sections the fuel appeared to be less than fully dense.

1. PRESSURE TRANSDUCER DATA FROM TRAN-4

The ACRR power peaked at 328.5 ms, so $\Delta t = t - 328.5$ ms. The pressure pulse was fully applied by $\Delta t = -35$ ms. Based on data from the helium reservoir (Figure 56) and dump tank (Figure 57) pressure transducers, significant gas flow into the dump tank began no later than $\Delta t = 130$ ms. Radiation noise in the pressure transducers obscured the early details of the gas flow, but it is conceivable that some gas flow may have begun as early as $\Delta t = 5$ ms. Gas flow continued until $\Delta t = 1.7$ s, with an abrupt flow decrease at $\Delta t = 0.5$ s. Based on a small negative transient observed at the dump tank pressure transducer, the main gas flow was again preceded by a mass of hot material which was associated with little or no gas. This hot material arrived at the dump tank at $\Delta t = 40$ ms. At $\Delta t = 160$ ms the pressure transducer just above the solenoid valve began to display erratic negative signal changes, typical of those caused by heating of the transducer diaphragm. This appears to indicate late-time drainage of molten material from the fuel melting chamber down to the solenoid valve region.

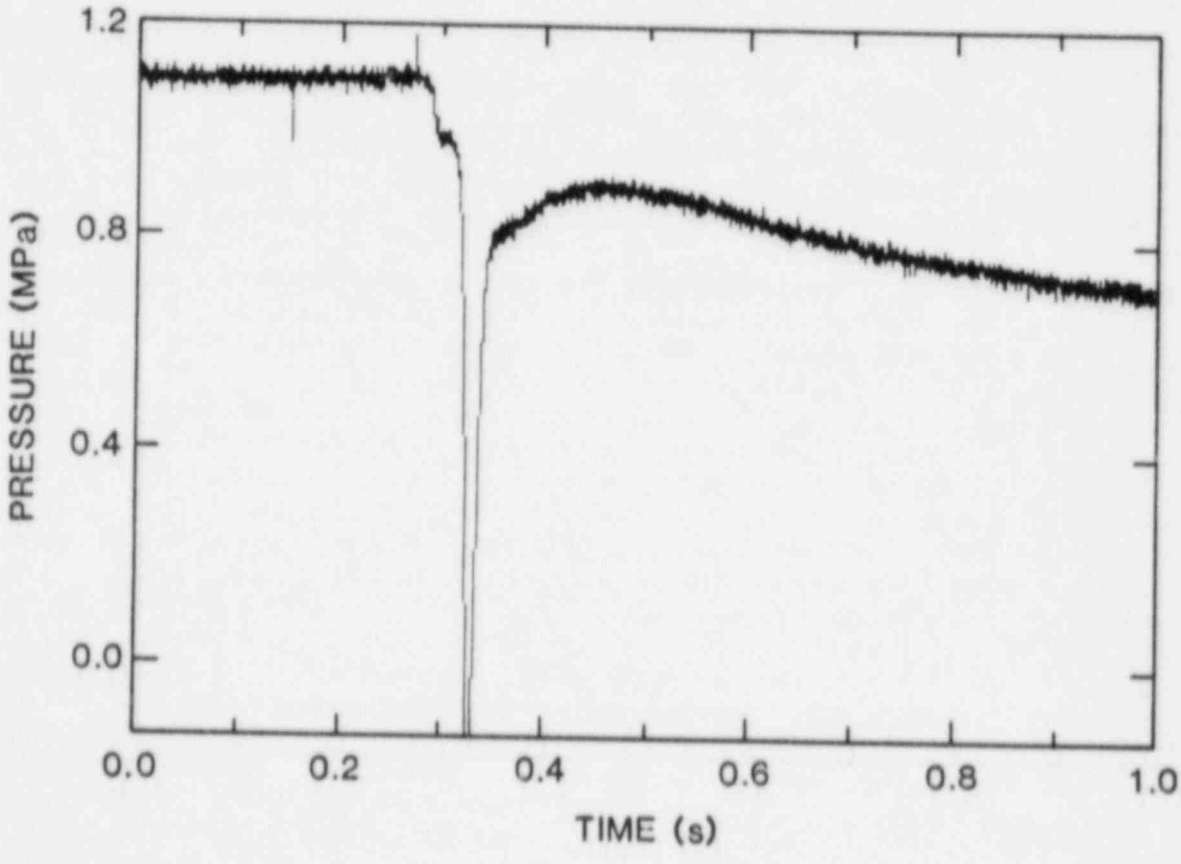

Figure 56. Short-term helium reservoir pressure in the TRAN-4 experiment.

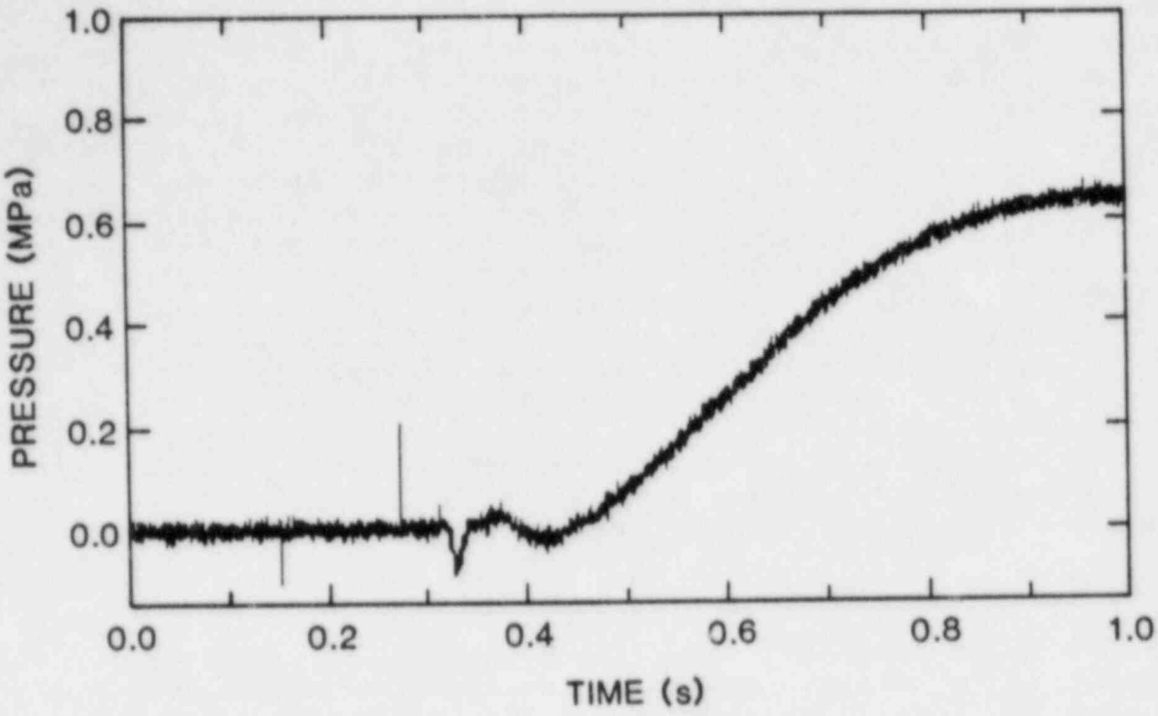

Figure 57 Short-term dump tank pressure in the TRAN-4 experiment.

2. FUEL MOTION DETECTOR DATA FROM TRAN-4

Detailed fuel motion data were recorded for TRAN-4, but funds have not been available to analyze the data. A cursory examination of the data showed that at least one detector (located at 11.5 cm above the entrance to the freezing channel) shorted out near the peak of the ACRR pulse. It is not clear whether this failure was an indication of a temperature limit on detector operation, or merely the result of repeated bending of the detectors during removal and re-installation on three different TRAN experiments.

3. THERMOCOUPLE DATA FROM TRAN-4

The accuracy of the thermocouples at these higher temperatures was checked during the testing of the new coaxial heaters, by comparing the temperatures measured through the data system, with direct measurements of thermocouple output voltage, and with the temperature as recorded by a Doric Type K thermocouple readout unit. Good agreement was obtained among all measurements.

The average initial steel temperature measured at six points along the fuel melting chamber and freezing channel was 1170 ± 40 K. Peak transient temperature changes (after correction for immediate gamma ray heating) were 6 K at 39.4 cm above the entrance to the freezing channel, and 0 K at 99 cm above the channel entrance, indicating frozen fuel only in the lower part of the freezing channel.

4. RADIOGRAPHY OF TRAN-4

Radiographs of TRAN-4 showed extensive steel removal near the channel entrance, and a complex shape of the fuel crust, including large variations in the apparent crust thickness and some regions in which material might have filled the channel completely. Particularly observed were: (1) A much shorter crust length (48 cm vs. the 67 cm seen in TRAN-3); (2) an abrupt decrease in crust thickness at 26 cm above the channel entrance; (3) large amounts of steel removal in the first 5 to 8 cm of the freezing channel; (4) a much thicker crust in the lower 26 cm of the freezing channel (0.7 mm vs. the 0.3 mm seen in previous experiments); (5) no blockages at the end of the crust, but a region from 8 to 17 cm which appeared to be nearly filled with low-density material; and (6) a large fuel accumulation in the upper half of the fuel melting chamber. Based on these radiographs, locations were chosen for transverse cuts through the TRAN-4 freezing channel. No loose debris was observed beyond the end of the fuel crust or in the dump tank in these radiographs.

5. GAMMA SCANS OF TRAN-4

The radiographs of TRAN-4 showed such interesting fuel/steel interactions that immediate disassembly in the HCF was advisable. Therefore a rather cursory gamma scan was made of TRAN-4, with only enough data taken to confirm a fuel crust length comparable to that observed in the radiographs (for example, no data were taken in the dump tank region). A fuel crust length, L_c, of about 48 cm was derived from the gamma scan. In some regions the gamma intensity appeared to change less rapidly than the average density seen in the radiographs, which is consistent with relocation of molten steel. A large fraction of the fuel (about 30 percent) was observed in the fuel melting chamber, with strong axial variations in its distribution. This would also be consistent with draining of molten fuel back into the melting chamber from part of the fuel freezing channel. A large fraction of the fuel (about 30 percent) was also observed below the fuel melting chamber, in agreement with previous experiments. A plot of the gamma intensity and resulting implied relative fuel distribution is shown in Figure 58.

6. EXAMINATION OF TRAN-4 IN HOT CELL FACILITY

The evidence of significant steel melting in TRAN-4 and a radically different appearance of the UO_2 crust argued for immediate study of TRAN-4 in the HCF. Based on the radiographs, the fuel housing was sectioned transversely at specific locations. In TRAN-4 clear evidence of steel melting and interaction with fuel was observed, in contrast to earlier results at lower steel temperature. Some of the unique phenomena observed at various axial locations include "foamy" UO_2 crusts with roughly spherical inclusions of steel, a "fluted" interface between the UO_2 crust and the underlying steel, and alternating layers of UO_2 and steel. In this section, the principal results are described and photomicrographs of representative cross-sections are shown. A complete report has been written on the types of crusts and fuel/steel interactions observed.[27]

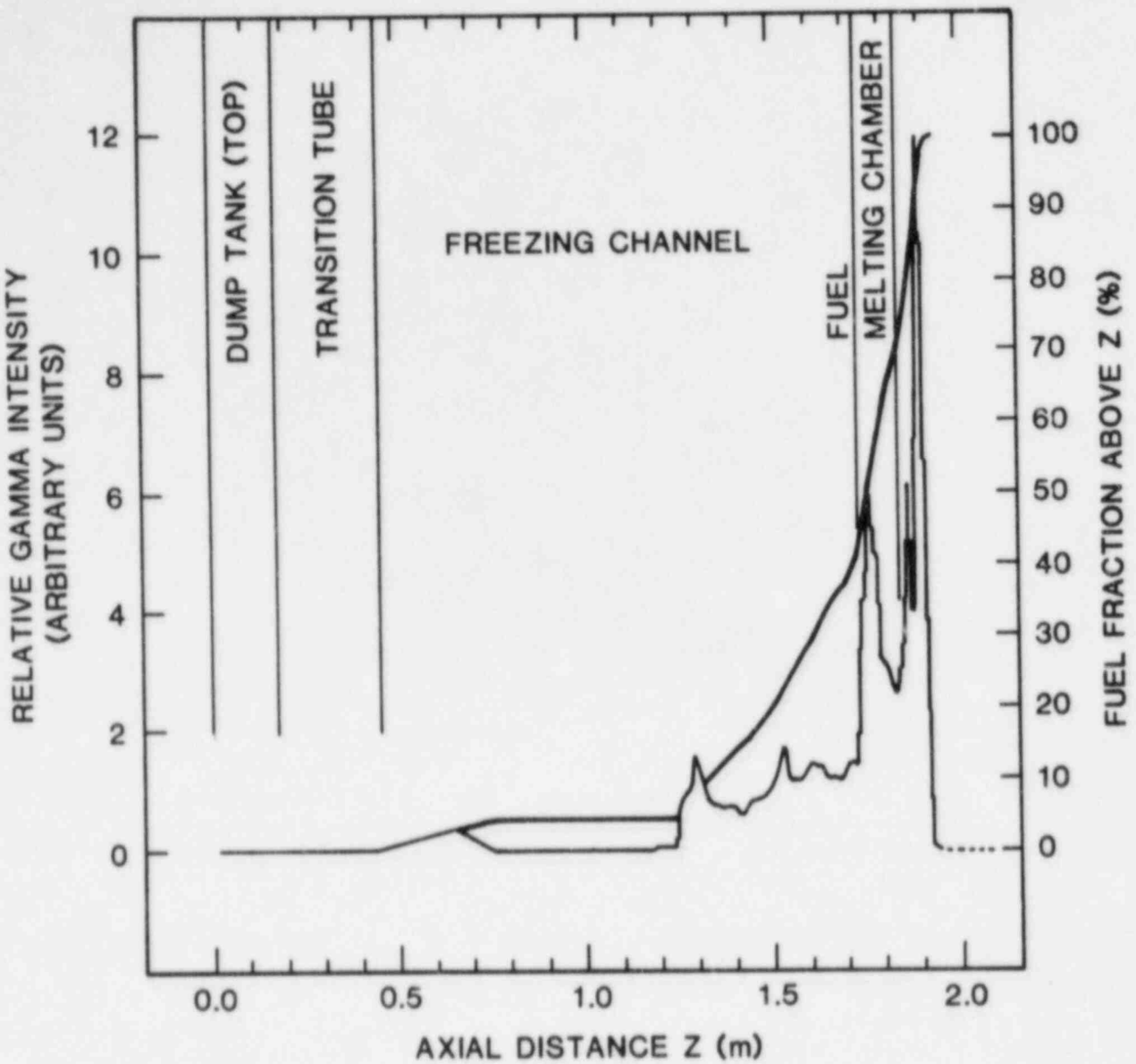

Figure 58 Gamma intensity and the normalized fuel distribution for the TRAN-4 experiment using the 497.1 keV line of ^{103}Ru.

Figure 59 shows a cross-section 0.2 cm below the entrance to the fuel freezing channel, in the cone shaped transition region. At the outer edge of the figure the coarse-grained structure of the as-fabricated wall is seen. A region of fine-grained steel, which appears to be melted and re-frozen, is visible around part of the central hole. The outer boundary of this fine-grained steel region is approximately circular, but the inner boundary shows fingers and sheets of steel, or contact with fragments of UO_2 crust. It appears that the molten steel has been stripped off the wall in thin sheets by fluid instabilities over some azimuthal regions, leaving behind the fingers or islands of molten steel. Over other azimuthal regions, the UO_2 crust may have protected the molten steel from removal. It is interesting to note that the UO_2 crust does not appear to contain any steel.

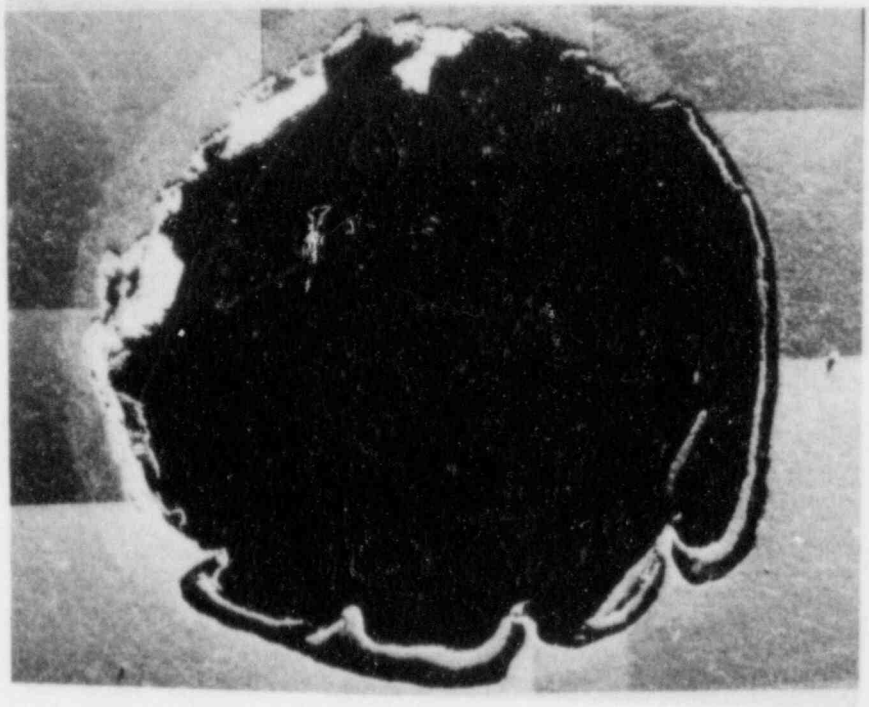

Figure 59 Cross-section through the end of the cone-shaped transition at the entrance to the freezing channel of the TRAN-4 experiment.

Figure 60 shows a cross-section at 9.8 cm above the entrance to the freezing channel. The roughly circular outer boundary of the melted and re-frozen steel is clearly visible, and there are large azimuthal variations in the steel layer thickness. A thick UO_2 crust is present, but the large radially-oriented grains seen in TRAN-1 are not visible, and the crust appears to have interacted with the steel at one point along its outer boundary. A few inclusions of molten steel may be present in the UO_2, but there appears to be no fine-scale mixing of fuel and steel.

Figure 61 shows a cross-section at 12.8 cm above the entrance to the freezing channel. Although a thick UO_2 crust is visible, the underlying steel layer has broken through it in several azimuthal locations, apparently because of fluid instabilities. The high curvature of the fuel/steel boundary, the close contact between the fuel and steel, and the relatively unfractured condition of the UO_2 next to the steel indicate that the boundary was formed while the bulk volumes of the two materials were still molten. Sheets of molten steel are visible on the inside surface of the UO_2 crust. Several small globules of mixed fuel and steel about 0.1 mm in diameter are visible inside the fuel crust, but again there is no evidence of fine-scale mixing of fuel and steel.

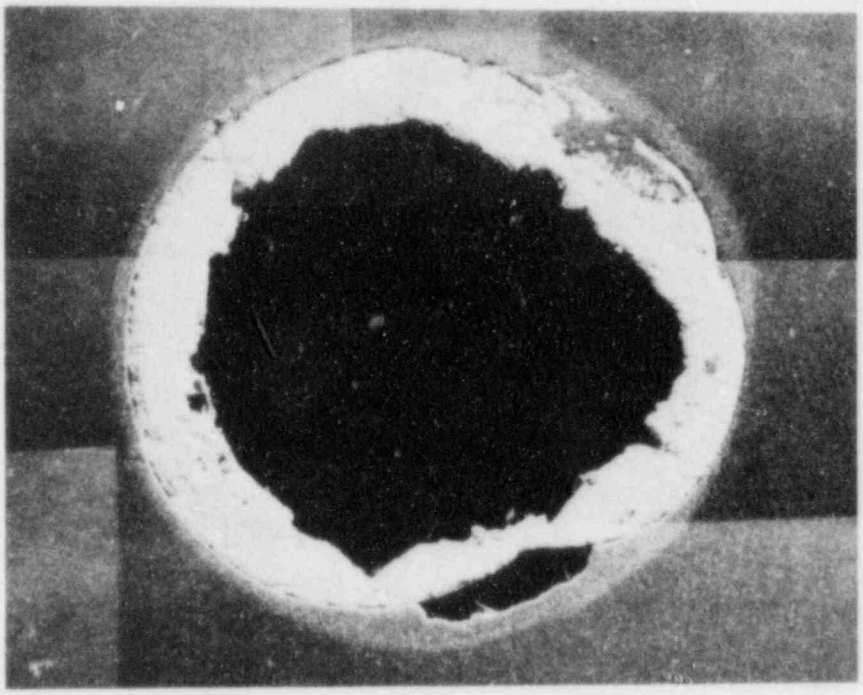

Figure 60 Cross-section at 9.8 cm above the freezing channel entrance of the TRAN-4 experiment.

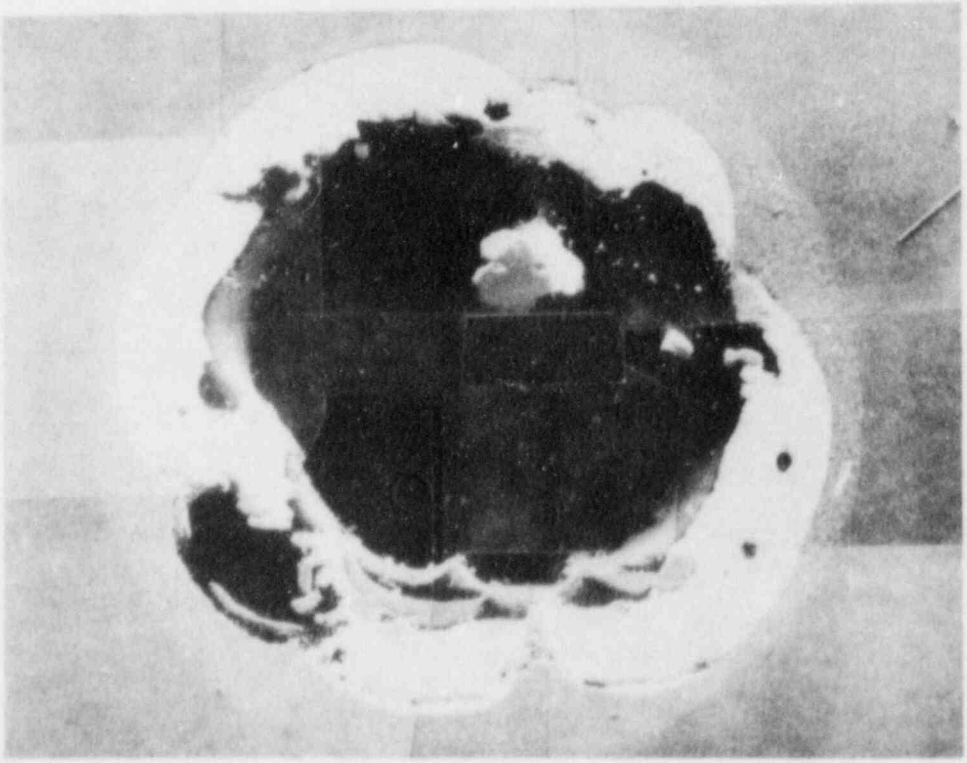

Figure 61 Cross-section at 12.8 cm above the freezing channel entrance of the TRAN-4 experiment.

Figure 62 shows a cross-section at 24.1 cm above the entrance to the freezing channel. An almost continuous outer fuel crust is visible, containing a number of globules of mixed fuel and steel. Toward the center of the channel there is an almost continuous layer of steel, although the layer thickness is highly variable and the layer contains some fuel crust particles. Finally, there is a thick fuel crust covering about half of the steel layer, which has a much more irregular outer boundary than inner boundary. Because this inner crust is not highly fractured, it appears to have assumed its curved shape while it was almost totally molten.

Near the end of the fuel crust observed in radiographs, a section showed a thick fuel crust, with a thick steel layer lying over its inside surface, suggesting that steel remained molten much longer than the fuel, and was moved around by the flowing gas. At much higher locations in the freezing channel, sections showed a few fragments of crust and thin layers of molten steel, which may have been deposited by the flowing gas. Although there was not much evidence of fuel on the side walls of the dump tank, about one gram of mixed fuel and steel was observed on the top cover of the dump tank. This accumulation of debris was composed of two types: a finely-divided loose black powder which appeared to have been sprayed radially outward over the cover plate, and a compact mass of mixed fuel and steel about 1 cm in diameter and a few mm thick which adhered strongly to the center of the cover plate. The particle sizes in this mixed mass were so small that it was impossible to resolve fuel particles from steel. However, based on earlier work, some of the particles might have been steel globules or spheres with frozen fuel adhering to them (see Figure 63).

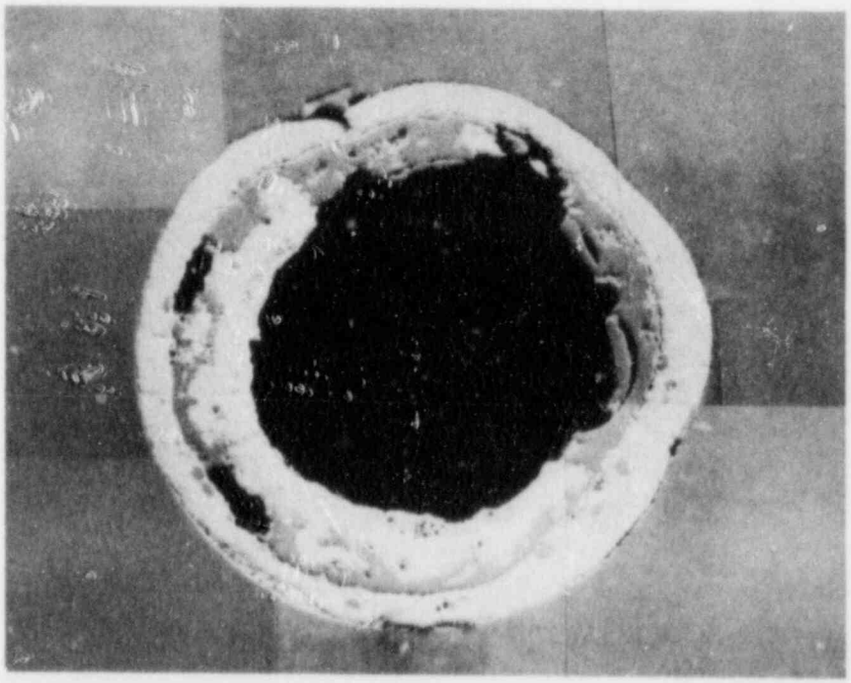

Figure 62 Cross-section at 24.1 cm above the freezing channel entrance of the TRAN-4 experiment.

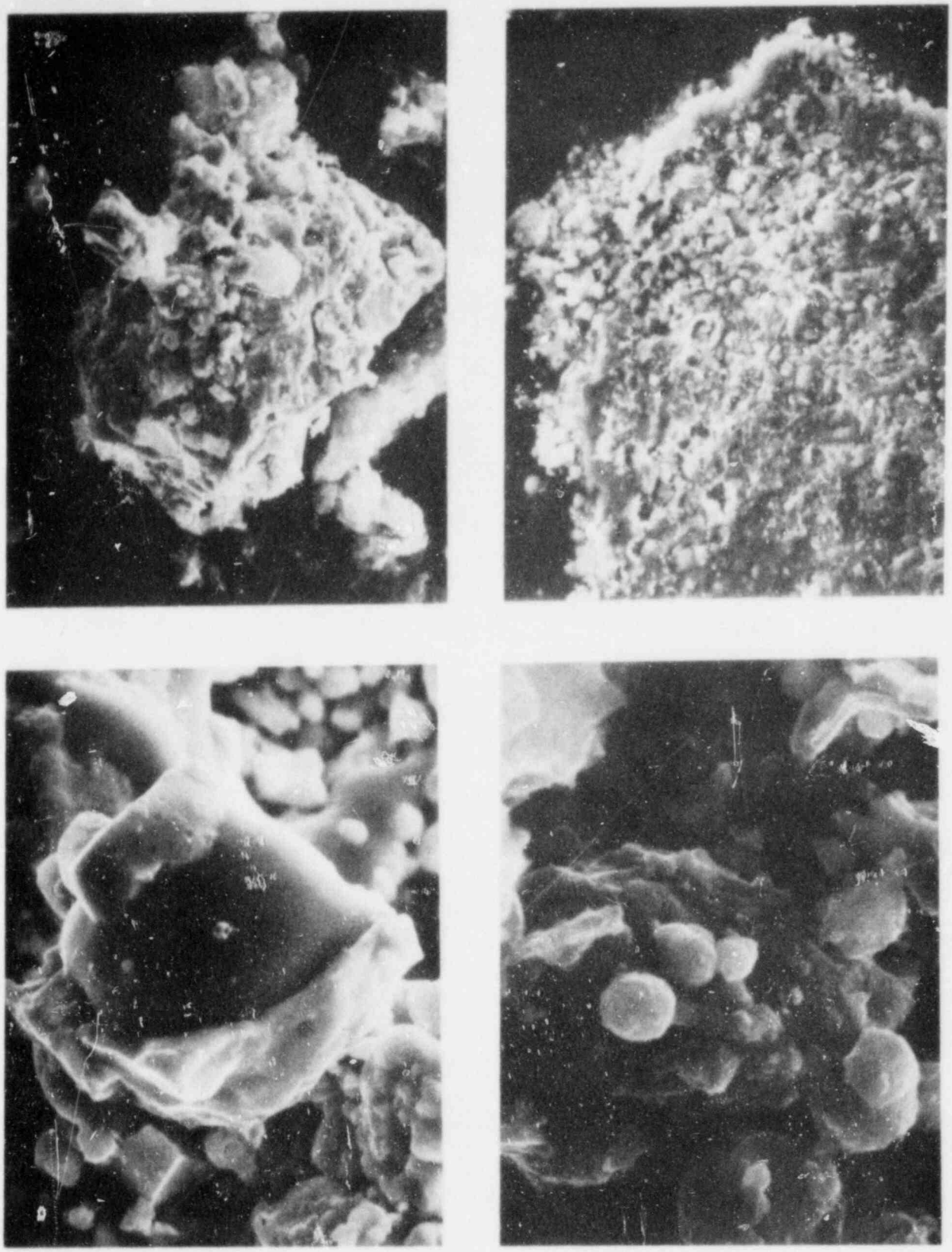

Figure 63 Representative particles taken from the mixed debris at the center of the dump tank cover plate of the TRAN-4 experiment.

Longitudinal cuts were made along two short sections of the freezing channel, beginning at axial locations -0.2 cm and 24.1 cm above the entrance to the freezing channel. These longitudinal cuts are shown in Figures 64 and 65. The lower cut shows a very complex crust shape with molten steel filling the entire cross-section of the cut at two axial locations, which would imply complete blockage of the channel. However, the steel may have flowed into this position after pressure equilibration or there may have been a tortuous path through this region which may have permitted some gas flow. This steel blockage was very difficult to see on the radiographs. The upper longitudinal section shows a clearly-defined meniscus of frozen steel, which indicates steel draining, because it is concave toward the upward direction.

An interesting structure was observed in some of the isolated globules of steel which were sometimes found in thick UO_2 crust regions. Figure 66 shows two such steel globules with very different appearances. The larger globule (about 100μ in diameter) appears to be mostly steel, but a small amount of UO_2 has apparently precipitated out of the steel in the form of a grid-like structure. It appears that the original globule was a steel/UO_2 eutectic with a low UO_2 content. The smaller globule appears to have been mostly UO_2, with a small amount of steel, and the UO_2 has precipitated out in the form of a coral-like structure. These mixed UO_2/steel globules have been observed only in TRAN-4 thus far, suggesting that a minimum steel or fuel temperature is required to form the eutectic.

In the fuel melting chamber the fuel crust was highly variable in thickness, and appeared to have been distorted away from the underlying steel wall in some regions. At some points the crust seemed to terminate in teardrop-shaped globules of fuel, which could be indicative of fuel draining back into the fuel melting chamber. Finally, in the region below the fuel melting chamber where much of the fuel has typically come to rest, "wavelike" melting of the underlying steel was observed in some areas.

7. INITIAL FUEL AND STEEL CONDITIONS IN TRAN-4

Based on the measured ACRR power traces and the shot size data provided by ACRR operations, the adiabatic fuel temperature at the end of the ACRR pulse was 3773 ± 150 K. The pressure was applied about 30 ms before fuel melting, to maximize the amount of fuel available to flow up the channel. However, the rapid onset of gas flow through the channel may indicate that the penetration distance was controlled by depletion of fuel, and not by freezing mechanisms. The initial steel temperature as measured by seven thermocouples located along the freezing channel was 1169 ± 33 K. The measured axial variation of channel temperature is shown in Figure 67. The new heaters worked very reliably.

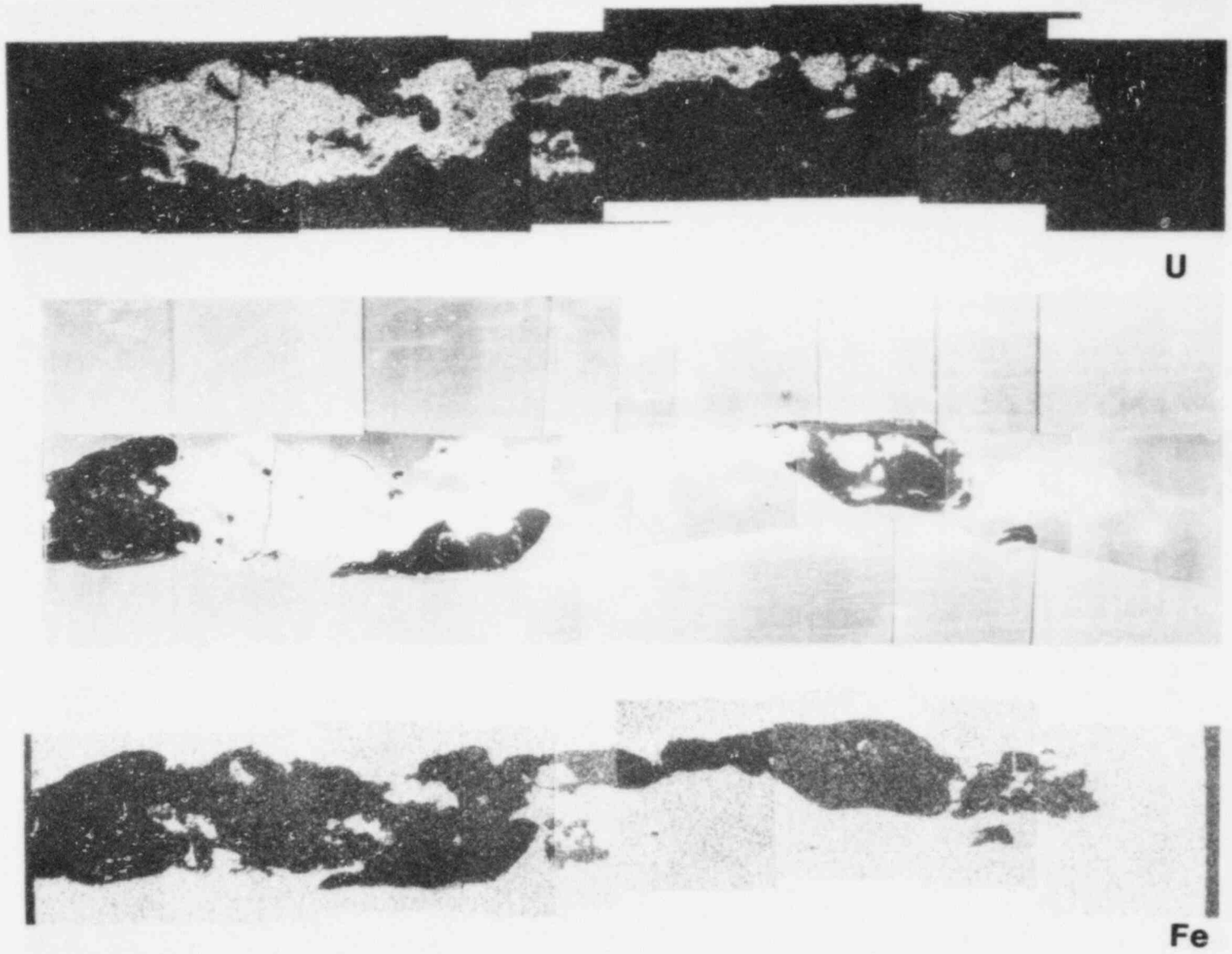

Figure 64 Longitudinal cut through the freezing channel from -0.2 cm to 2.8 cm above the freezing channel entrance of the TRAN-4 experiment.

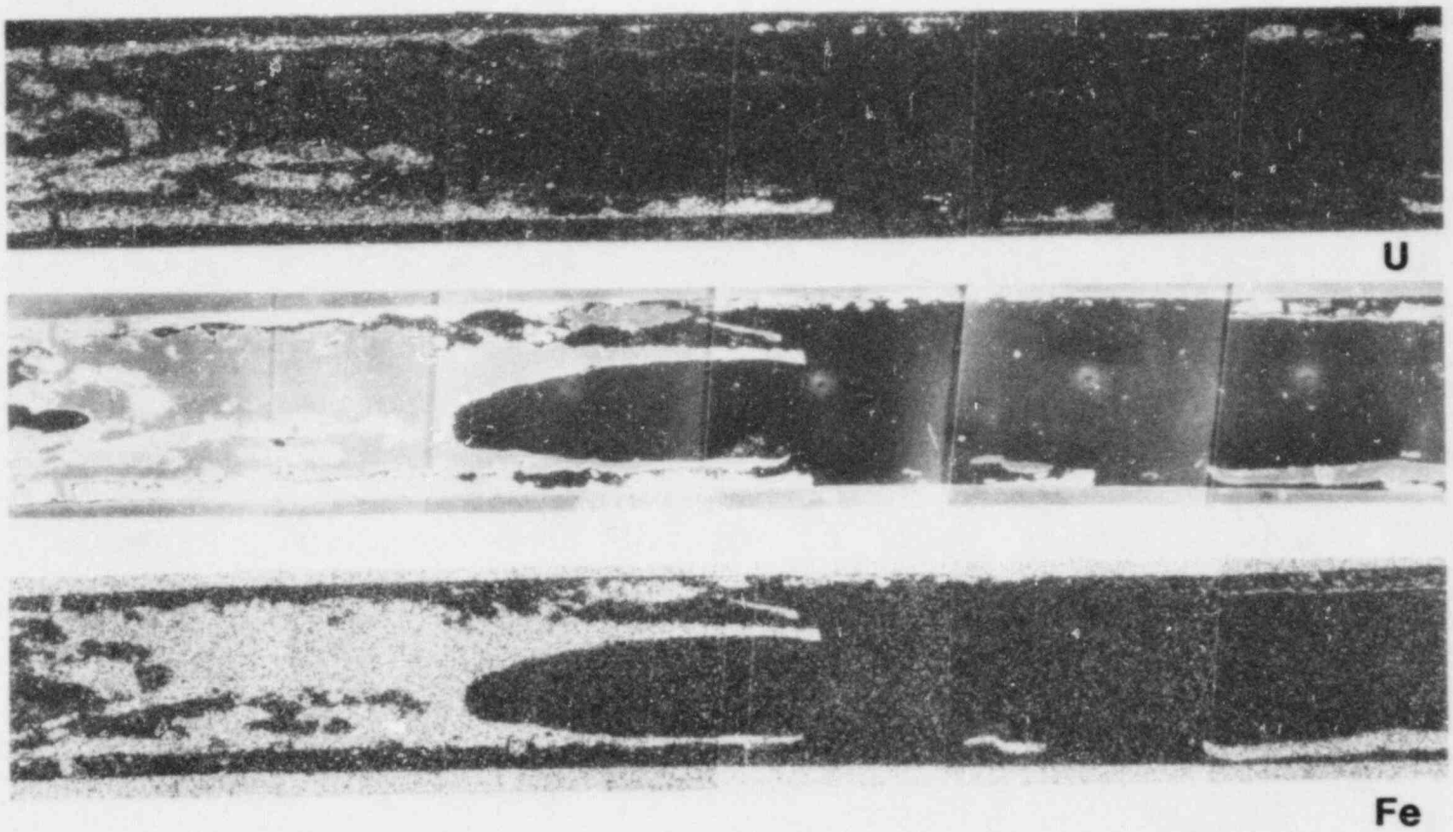

Figure 65 Longitudinal cut through the freezing channel from 24.1 cm to 27.1 cm above the freezing channel entrance of the TRAN-4 experiment.

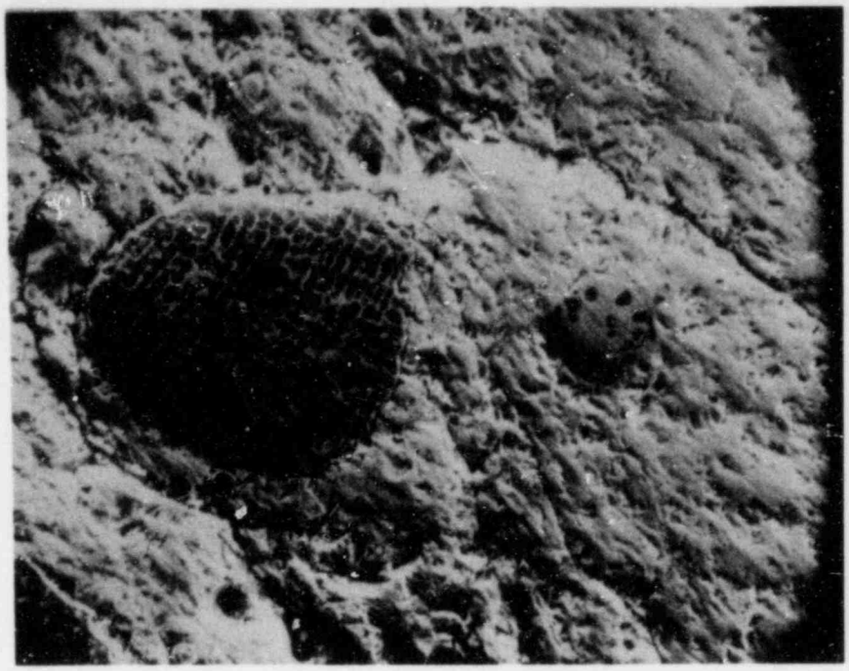

Figure 66 Mixed steel/UO_2 globules observed in the UO_2 crust at 24.1 cm above the freezing channel entrance.

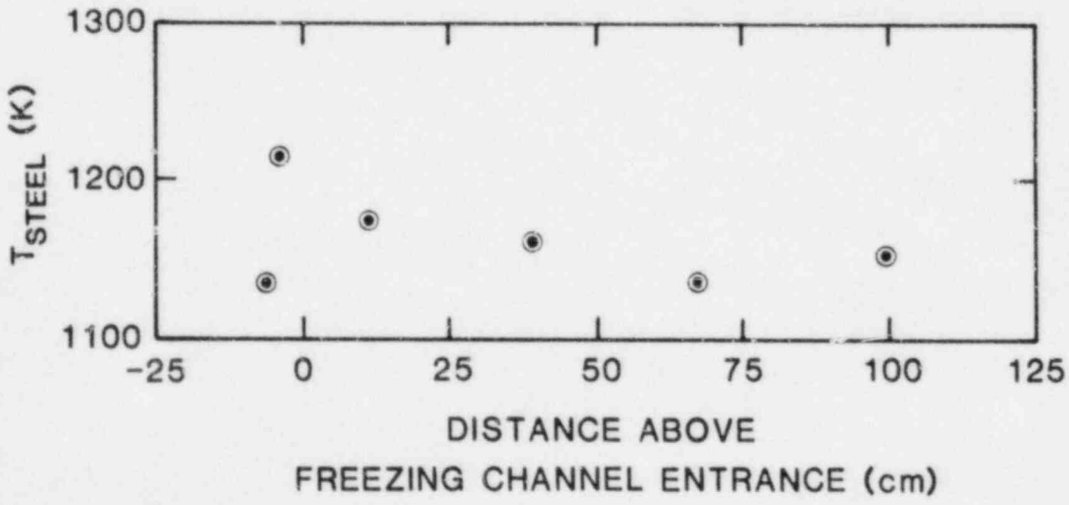

Figure 67 Axial variation of the initial steel temperature, including gamma heating.

APPENDIX G

RESULTS OF TRAN-5 EXPERIMENT

Experiment TRAN-5 was performed at the same initial fuel and steel conditions as TRAN-4, but was designed to approximate the conditions expected during the CRBR LOF Transition Phase more closely. Therefore a much lower driving pressure difference was selected (0.3 MPa). The observation of the finely-divided fuel debris in the dump tank had also raised the question of whether boiling of the leading edge of the fuel flow might dominate the freezing process. Therefore boiling of fuel was prevented by placing an initial backpressure of about 0.2 MPa of helium in the fuel melting chamber, freezing channel, and dump tank regions.

Unfortunately, when TRAN-5 was performed a large transient pressure pulse of about 0.3 MPa was generated in the dump tank by the presence of the initial backpressure. This pressure pulse may have significantly affected the fuel flow. Simple calculations show that about one gram of finely-divided debris could produce such a pressure pulse by rapid transient heating of the gas in the dump tank. Although this makes a direct comparison of TRAN-5 with earlier experiments in the series more difficult, it probably indicates that the finely-divided debris at the front of the fuel slug is a fundamental property of the flow. It also indicates that the earlier TRAN Series I experiments are measuring realistic freezing phenomena which are not dominated by the low backpressure in the freezing channel.

1. PRESSURE TRANSDUCER DATA FROM TRAN-5

The ACRR power peaked at 328 ms, so $\Delta t \equiv t - 328$ ms. The pressure pulse was fully applied by $\Delta t = -30$ ms. Based on data from the helium reservoir (Figure 68) and dump tank (Figure 69) pressure transducers, gas flow into the dump tank began no later than $\Delta t = 120$ ms, and flow might have begun as early as $\Delta t = 30$ ms. Because of the very low pressures, radiation noise on the helium reservoir and above-solenoid-valve transducers was about twice as large as in TRAN-4. This made the absolute pressures recorded by these two transducers unreliable for about 100 ms after the ACRR pulse peak. Therefore the dump tank transducer was relied upon for interpreting the experiment in this time region. In addition, the above-solenoid-valve transducer signal became erratic at $\Delta t = 70$ ms, and went completely off scale in the negative direction at $\Delta t = 310$ ms (Figure 70). This is the typical behavior for severe transducer heating, and the radiographs later showed a large droplet of molten material deposited almost opposite the transducer face.

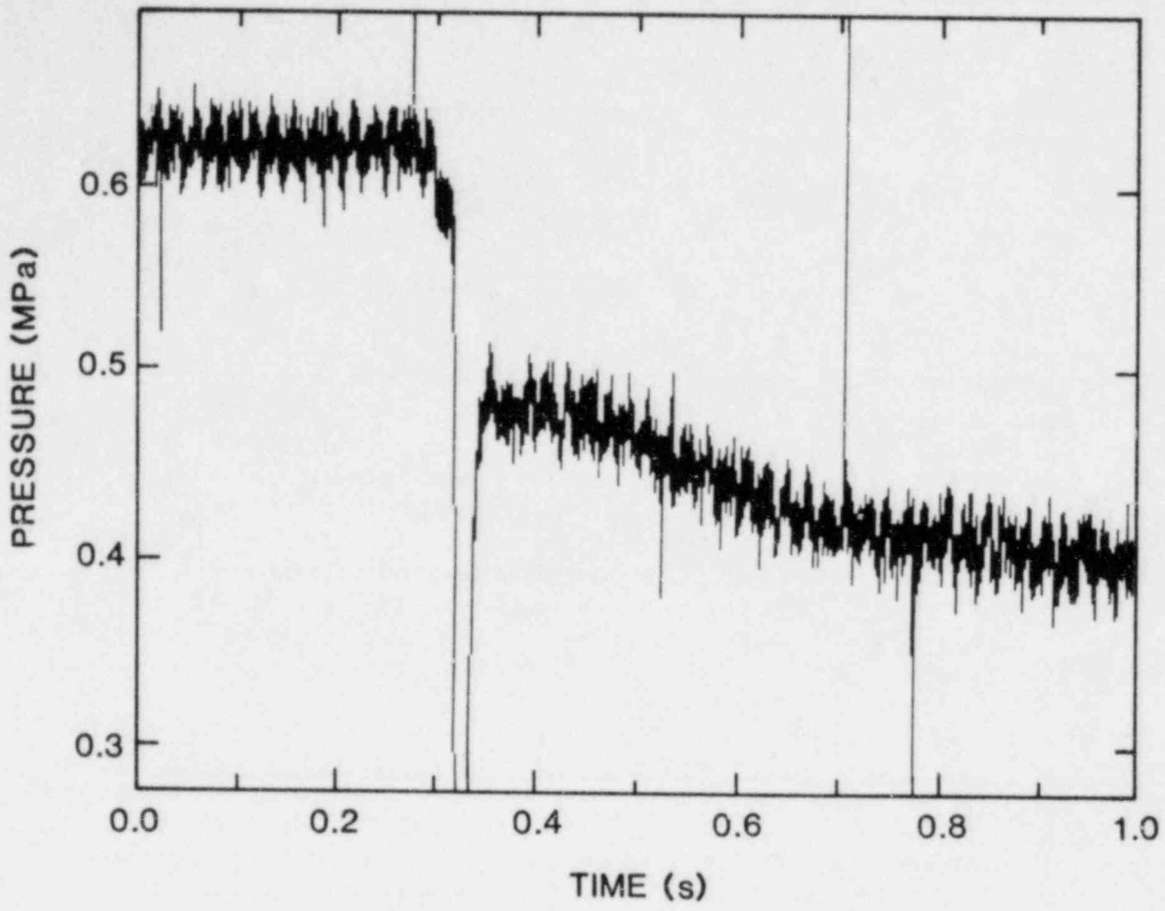

Figure 68 Short-term helium reservoir pressure in the TRAN-5 experiment.

The most striking change in the pressure behavior during TRAN-5 was the large transient pressure pulse observed at the dump tank (Figure 69). The pressure record began at the initial value of 0.2 MPa. There was no early negative transient as in all previous experiments, but instead the onset of a pressure increase at $\Delta t = -10 \pm 15$ ms. The 0.3-MPa-high pulse peaked at $\Delta t = 60$ ms, and decayed back to an absolute pressure of 0.34 MPa at $\Delta t = 400$ ms, after which a slow pressure rise similar to previous experiments brought the pressure to 0.5 MPa at $\Delta t = 7.7$ s. Because the pressure was applied well before the onset of radiation noise, the initial pressure signals of the helium reservoir and above-solenoid-valve transducers were used to calibrate the pressure changes.

Such a large but rapidly-decaying pressure pulse cannot be explained by a "puff" of gas passing through the freezing channel, because the gas would have to be extremely hot (and therefore at very high pressure), but not very massive. The rapid decay suggests heating of the gas already in the dump tank, perhaps by a mass of finely-divided fuel

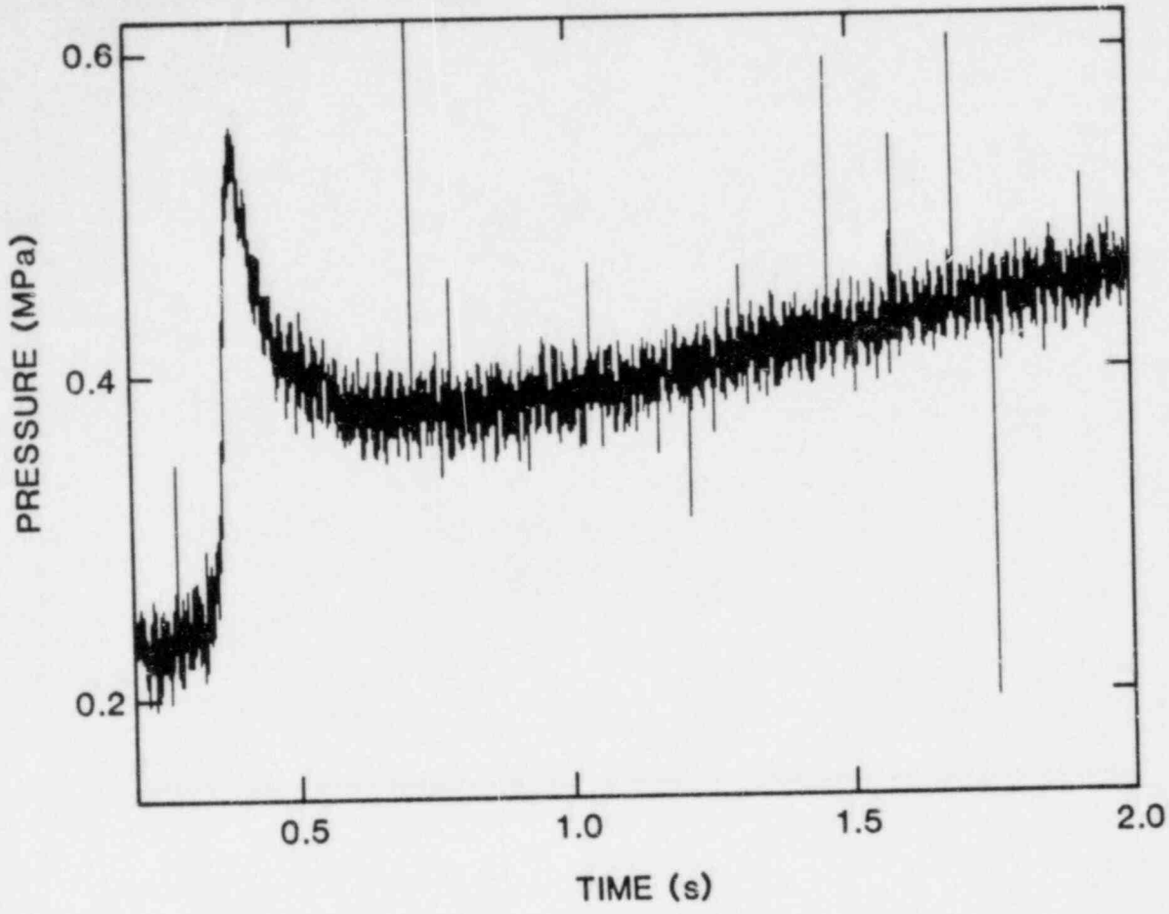

Figure 69 Short-term dump tank pressure in the TRAN-5 experiment.

and steel debris similar to that observed in TRAN-4. Although post-test analysis has not been performed, the gamma scans of TRAN-5 show the presence of fuel debris at the very top of the dump tank, in spite of the high background gas pressure.

Simple heat-capacity calculations show that the observed heating of the dump tank gas could be accomplished by cooling of one gram of fuel by a few hundred degrees. The heating would be facilitated by the fine scale of the debris, and spreading of the debris as it entered the dump tank would bring it into contact with much of the gas.

Because the absolute pressure in the dump tank was almost equal to the driving pressure applied below the molten fuel (for about 40 ms centered around Δt = 60 ms), the pressure pulse could have significantly affected the fuel flow up the freezing channel.

2. FUEL MOTION DETECTOR DATA FROM TRAN-5

No fuel motion detectors were installed on TRAN-5, in order to make room for additional thermocouples, and to save time in assembling and performing the experiment.

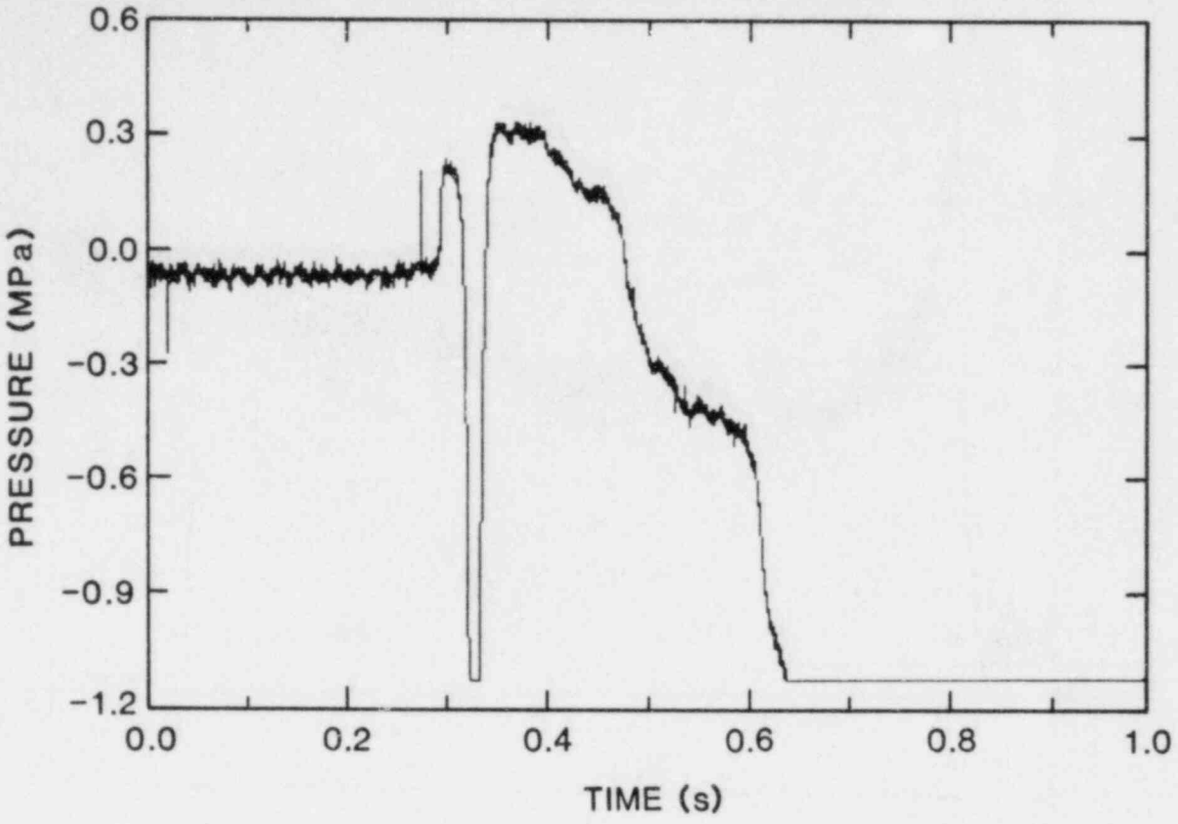

Figure 70 Short-term melting chamber pressure in the TRAN-5 experiment.

3. THERMOCOUPLE DATA FROM TRAN-5

The thermocouple data were consistent with flow of much of the fuel out of the fuel melting chamber, but penetration of the fuel for only a relatively short distance up the channel.

4. RADIOGRAPHY OF TRAN-5

The radiographs of TRAN-5 did not show the complex fuel crust shape observed in TRAN-4, and instead resembled TRAN-1 and TRAN-3. A fuel crust 46 ± 0.6 cm long was observed, with a relatively uniform thickness, which left the channel generally open. There was an increase in crust thickness over a few cm near the leading edge of the flow, and a fuel accumulation at the upper end of the crust, but this accumulation did not appear to block the channel. The fuel crust in the fuel melting chamber was very nonuniform in thickness, and may be composed in part of fuel droplets which have drained out of the freezing channel and the upper part of the melting chamber. A large droplet of fuel was observed in the pressure transducer housing just above the solenoid valve, more than 20 cm below the base of the fuel melting chamber. Small spheres of fuel were also observed in the exit port of the solenoid valve. This large amount of molten fuel below the

melting chamber, together with the pressure transducer traces, implies a large amount of late-time fuel drainage.

5. GAMMA SCANS OF TRAN-5

The gamma scan of TRAN-5 was one of the most complete made during the series. Figure 71 shows the axial dependence of the intensity of the 497.1 keV line of ^{103}Ru, with the implied final fuel distribution. A roughly uniform fuel crust 43.5 ± 0.4 cm long can be seen in the figure. A small amount of fuel was scattered along the rest of the freezing channel, with about 0.6 g of fuel in the dump tank. This included some against the cover plate at the very top of the dump tank. About 25 percent of the fuel was in the melting chamber, about 20 percent in the fuel crust in the freezing channel, and about 50 percent below the melting chamber.

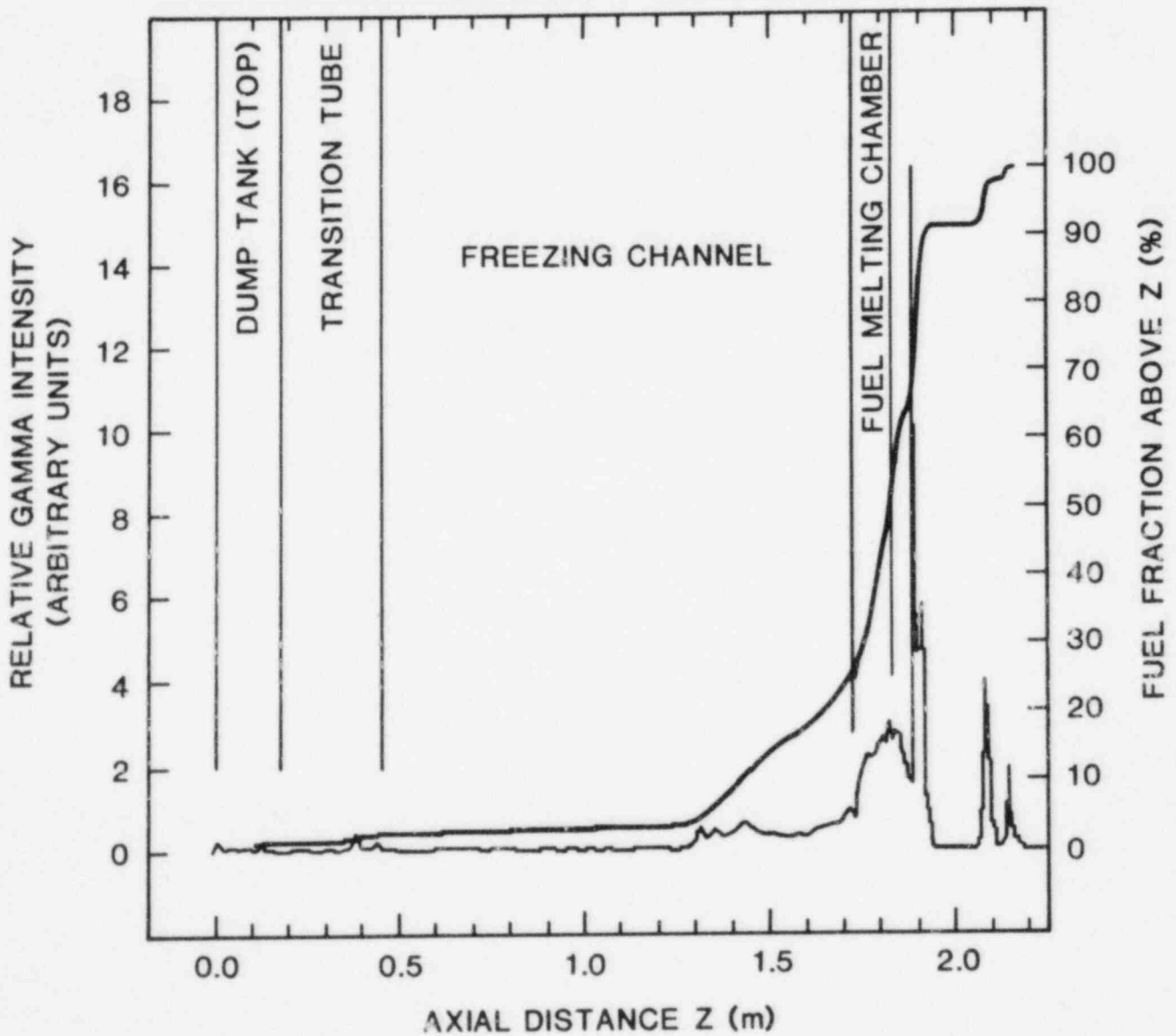

Figure 71 Gamma intensity and the normalized fuel distribution for the TRAN-5 experiment using the 497.1 keV line of ^{103}Ru.

6. EXAMINATION OF TRAN-5 IN HOT CELL FACILITY

TRAN-5 has not yet been examined in the HCF. If funding permits, the channel will be examined for steel melting and removal, the dump tank debris will be examined to see if the initial backpressure has affected its character, and the fuel in the melting chamber will be examined to see if it contains any steel which might have come from the freezing channel.

7. INITIAL FUEL AND STEEL CONDITIONS IN TRAN-5

Based on the fuel calorimetry experiments performed just before TRAN-3, the adiabatic initial fuel temperature was 3598 ± 150 K. The initial steel channel temperature averaged over ten points was 1148 ± 34 K, as shown in Figure 72.

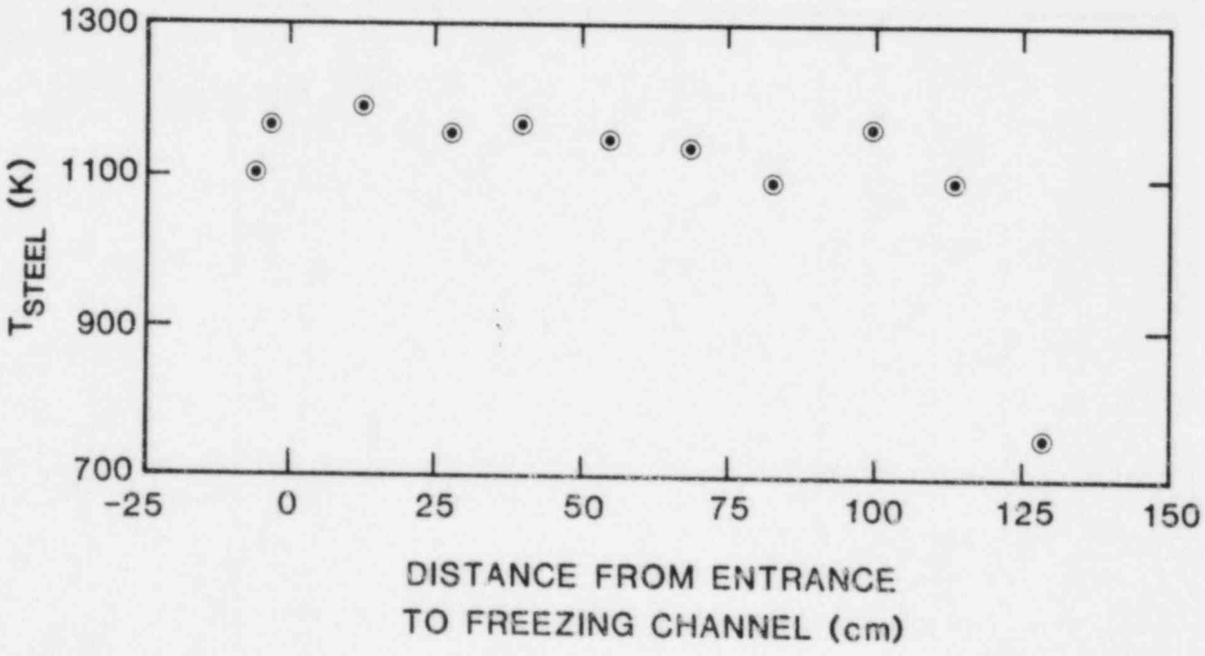

Figure 72 Initial temperature of the freezing channel of the TRAN-5 experiment.

APPENDIX H

FINITE-MASS CRUST GROWTH MODEL

A simple finite-mass crust growth model was developed to investigate the importance of finite-mass effects on the fuel freezing behavior. The model accounts for:

1) stable crust formation as in the conduction freezing model,

2) deposition of liquid film at the trailing edge of the finite-mass slug,

3) an overall energy balance in the bulk molten fuel as well as the effect of turbulent heat transfer from the possibly superheated bulk fuel to the crust (effect on growth constant λ), and

4) feedback from the decreasing mass of liquid fuel (due to crust growth and film deposition) on the liquid fuel slug velocity.

The model is basically an application of the principles of mass and energy conservation.

1. DERIVATION OF EQUATIONS FOR PENETRATION LENGTH

Consider a liquid slug of mass m_o in the channel at time $t = 0$ as shown in Figure 73. The channel walls move downward with a velocity u for $t > 0$. The mass in the liquid slug is continuously depleted by:

1) conduction freezing of UO_2 at the stainless steel wall that results in a stable crust adhered to the wall;

2) a liquid film of UO_2 from the back of the slug deposited in passing over the frozen UO_2 crust.

The governing equations for the conservation of mass, assuming conduction-freezing stable-crust growth coupled with liquid-film deposition, are given by:

$$\dot{m}_{out} = \left(D_o^2 - D_c^2\right)\left(\pi/4\right)u\rho_s + \left(D_c^2 - D_{fd}^2\right)\left(\pi/4\right)u\rho_l \qquad (H.1)$$

$$\delta_c = 2\lambda\left(\alpha_{f,l}\,\Delta z/u\right)^{1/2} \quad \left(\text{assumes } t^* \approx \Delta z/u\right) \qquad (H.2)$$

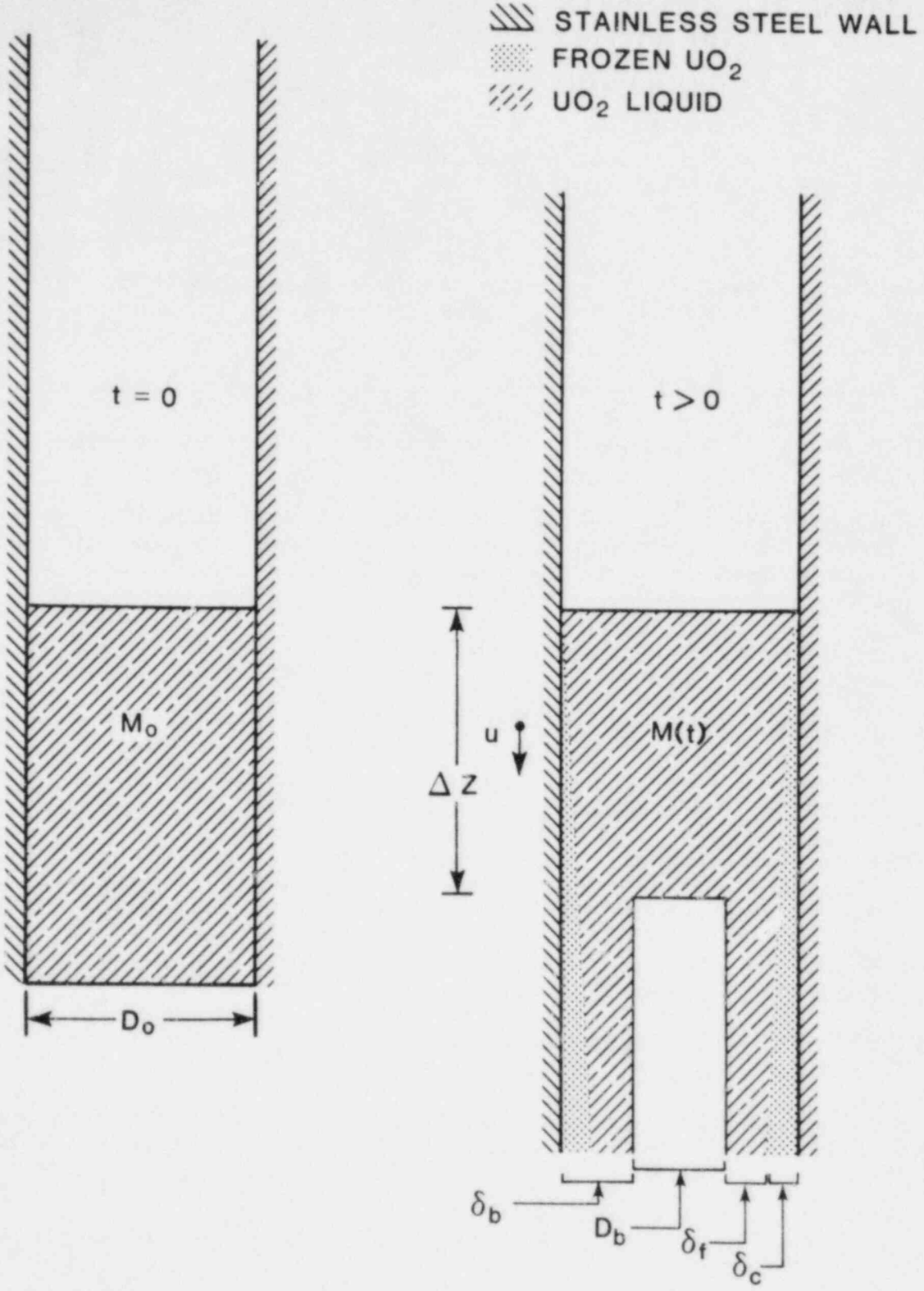

Figure 73 Features of the finite-mass crust growth model.

$$u^2 = \frac{\Delta P}{2\,(\Delta z/D)\,f\,\rho_l} \tag{H.3}$$

$$\pi\left[r_c^{\,2} - \left(r_c - \delta_f\right)^2\right] = 0.15\pi r_c^{\,2} \tag{H.4}$$

In these equations, D_c is the channel flow diameter at the trailing edge of the slug after the formation of a conduction-controlled frozen-UO_2 crust, δ_c is the UO_2 conduction crust thickness, D_{fd} is the channel flow diameter which results after liquid-film deposition over the crust, and δ_f is the liquid-film thickness. The final crust thickness at the back of the slug is then $\delta_b = \delta_f + \delta_c$ (Figure 73), and the open diameter is $D_b = D_{fd}$. Equation H.4 is an empirical relation for liquid film deposition derived in Reference 18. The equation states that the liquid volume fraction is 15% of the total flow volume available. To solve Eqs. H.1 - H.4 for final crust thickness, final crust length, and total flow time, all variables are first written as functions of mass alone.

The slug length, Δz, is given as:

$$\Delta z = \frac{m}{\rho_l \pi r_o^{\,2}} \tag{H.5}$$

(An implicit assumption in Eq. H.5 is that the overall slug length will not be significantly affected by neglecting the difference in density of liquid UO_2 in the slug and solid UO_2 in the crust. This assumption is valid as long as the cross-sectional mass is predominantly liquid.)

Subsequently, the velocity and crust thickness can be written as:

$$u^2 = \frac{\Delta P\,\pi D_o^{\,3}}{8mf} \tag{H.6}$$

and

$$\delta_c = 2\lambda\left[\frac{\alpha m}{\rho_l \pi r_o^{\,2}}\left(\frac{8mf}{\Delta P\,\pi D_o^{\,3}}\right)^{1/2}\right]^{1/2} \tag{H.7}$$

In Eq. H.1, the diameters can be written in terms of the radii to yield:

$$\dot{m}_{out} = \left(r_o^{\,2} - r_c^{\,2}\right)\pi u \rho_s + \left(r_c^{\,2} - r_{fd}^{\,2}\right)\pi u \rho_l \tag{H.8}$$

From Figure 73, the relationships

$$r_c = r_o - \delta_c \tag{H.9}$$

and

$$r_c = r_b + \delta_f \tag{H.10}$$

or

$$r_c = r_{fd} + \delta_f \tag{H.11}$$

are obtained, and substitution of Eq. H.9 in the first term of Eq. H.8, and Eq. H.11, solved for r_{fd}, into the second term yields:

$$\dot{m}_{out} = \left(2r_o\delta_c + \delta_c^2\right)\pi u\rho_s + \left(2r_c\delta_f - \delta_f^2\right)\pi u\rho_l \tag{H.12}$$

Rewriting the second term and comparing it to Eqs. H.4 and H.9 shows that:

$$\dot{m}_{out} = \left(2r_o\delta_c - \delta_c^2\right)\pi u\rho_s + 0.15\left(r_o - \delta_c\right)^2\pi u\rho_l \tag{H.13}$$

Let

$$G_1 = f\left(\Delta p\pi^3\rho_l^2 r_o^7\right)^{-1/2} \tag{H.14}$$

$$G_2 = 2\lambda\left(\alpha G_1\right)^{1/2} \tag{H.15}$$

$$G_3 = \left(\frac{\pi\Delta P r_o^3}{f}\right)^{1/2} \tag{H.16}$$

Then we have:

$$\delta_c = G_2 m^{3/4} \tag{H.17}$$

and

$$u = G_3 m^{-1/2} \tag{H.18}$$

Substitution of Eqs. H.17 and H.18 into Eq. H.13 gives the following expression for the rate of mass depletion from the liquid slug:

$$\dot{m}_{out} = \frac{a_1 m^{6/4} + a_2 m^{3/4} + a_3}{m^{1/2}} \tag{H.19}$$

where

$$a_1 = \left(0.15\rho_1 - \rho_s\right)G_2{}^2\pi G_3 \tag{H.20}$$

$$a_2 = \left(\rho_s - 0.15\rho_1\right)2r_o G_2\pi G_3 \tag{H.21}$$

$$a_3 = 0.15\rho_1 r_o{}^2\pi G_3 \tag{H.22}$$

The rate of change of mass in the slug is given as:

$$\left.\frac{dm}{dt}\right)_{slug} = -\dot{m}_{out} \tag{H.23}$$

Integrating both sides of Eq. H.23 yields an integral expression relating mass, m, in the slug to a time, t:

$$-\int_{m_o}^{m} \frac{dm}{\dot{m}_{out}} = t \tag{H.24}$$

Where $\dot{m}_{out}$ is given by Eq. H.19. The solution to Eq. H.24 depends on the sign of the term $(4a_1a_3 - a_2{}^2)$, which turns out to always be negative. If one makes the substitution of variables:

$$x = m^{3/4} \tag{H.25}$$

then the solution to Eq. H.24 is given by:

$$t = -\frac{4}{3}\left[\frac{\ln\left(a_1x^2 + a_2x + a_3\right)}{2a_1} + \frac{a_2}{a_1\left(a_2{}^2 - 4a_1a_3\right)^{1/2}} \tanh^{-1}\left(\frac{2a_1x + a_2}{\left(a_2{}^2 - 4a_1a_3\right)^{1/2}}\right)\right]_{x_o}^{x} \tag{H.26}$$

Equation H.26 can be evaluated for a given λ and m_o to yield the time t, at which a given mass, m, is left in the slug. Equation H.18 can be used to solve for the distance, z, travelled by the slug when it has reached a mass, m:

$$z = -G_3 \int_{m_o}^{m} \frac{dm}{a_1m^{6/4} + a_2m^{3/4} + a_3} \tag{H.27}$$

Equation H.27 must be solved numerically for a given m_o, m, λ, and ΔP. The liquid-film thickness, δ_f, can be written as:

$$\delta_f = 0.078\ (r_o - \delta_c) \tag{H.28}$$

so that combining Eqs. H.17 and H.28 yields the total UO_2 crust thickness behind the slug as a function of mass in the slug:

$$\delta_b = 0.078\ r_o + 0.922\ G_2 m^{3/4} \tag{H.29}$$

Thus, using Eqs. H.26, H.27, and H.29, one can solve for flow time, crust length, and total crust layer thickness as a function of mass in the slug.

2. SOLUTION FOR GROWTH CONSTANT WITH TURBULENT HEAT TRANSFER

An important parameter in equations H.26 - H.29 is the crust growth constant, λ. In the early conduction analysis of Epstein[10] it was determined that for UO_2/steel systems, a typical value for the growth constant is $\lambda = 0.8$. However, this solution for the growth constant is derived from a conduction heat transfer analysis at the solid/liquid UO_2 interface. Actually, the appropriate boundary condition is turbulent convective heat transfer (neglecting entrance region effects). The solution sets of Reference 10 can still be used to determine the growth constant λ by using an effective temperature, T', in the equations such that the calculated interfacial heat transfer is numerically equal to that of turbulent convective heat transfer.

For a conduction heat transfer analysis, the UO_2 solid/liquid interfacial boundary condition is given to be:

$$\kappa_s \left.\frac{dT}{dx}\right)_s = \kappa_l \left.\frac{dT}{dx}\right)_l + h\rho_l \frac{d\delta_c}{dt} \tag{H.30}$$

Equation H.30 balances the conduction through the liquid and the liberated heat of fusion upon solidification at the solid/liquid interface with the conduction through the crust. For convective heat transfer, however, the energy balance is actually:

$$\kappa_s \left.\frac{dT}{dx}\right)_s = h_c \left(T_b - T_{f,mp}\right) + h\rho_l \frac{d\delta_c}{dt} \tag{H.31}$$

One must therefore impose the condition that the liquid conduction term in Eq. H.30 is numerically equal to the convection term in Eq. H.31 by using an effective temperature slope in the liquid given by:

$$\kappa \left.\frac{dT}{dx}\right)_l \sim \kappa \frac{T' - T_{f,mp}}{r} = h_c \left(T_b - T_{f,mp}\right) \tag{H.32}$$

or

$$T' = \frac{h_c r}{\kappa}\left(T_b - T_{f,mp}\right) + T_{f,mp} \qquad (H.33)$$

where h_c is the turbulent heat transfer coefficient, and r is the channel radius.

The effective value of T' is then used as the bulk liquid temperature in the solutions of Reference 10 for λ.

Nomenclature

D channel diameter, cm

ΔP differential driving pressure, g - cm^3/s^2.

L channel length, cm

X_p penetration distance, cm

m_p mass penetration, g

t time, s

T temperature

C_p specific heat J/g-K

u variable velocity

f friction factor, ~0.007

h heat of fusion

h_c convective heat transfer coefficient

Δz slug length

t* flow time past a point on the wall

x variable substitution: $x = m^{3/4}$

Subscripts

s solid phase

l liquid phase

w wall

o initial conditions

f, UO_2 fuel or film

mp melting point

s, steel

c crust

fd film plus crust

Greek

ν kinematic viscosity, cm^2/s

κ conductivity, W/cm-K

λ crust growth constant

α thermal diffusivity cm^2/s

ρ density

δ crust thickness

REFERENCES

1. J. F. Jackson, M. G. Stevenson, J. F. Marchaterre, R. H. Sevy, R. Avery, and K. O. Ott, "Trends in LMFBR Hypothetical-Accident Analysis," pp. 1241-1264 in Proc. of the Fast Reactor Safety Meeting, April 2-4, 1974, Beverly Hills, CA, CONF-740401-P3, (1974).

2. G. A. Greene et al., "Assessment of the Thermal Hydraulic Technology of the Transition Phase of a Core-Disruptive Accident in a LMFBR," BNL-NUREG-27366, Brookhaven National Laboratory, Upton, NY, February, 1980.

3. D. C. Williams, et al., "LMFBR Accident Delineation Study: Phase I Final Report," Chs. IV.2 and IV.3 in NUREG/CR-1507, SAND80-1267, Sandia National Laboratories, Albuquerque, NM, 87185, Nov. 1980.

4. W. R. Bohl, "Some Recriticality Studies with SIMMER-II," Vol. III, pp. 1415-1424, in Proc. Int. Mtg. on Fast Reactor Safety Technology, August 19-23, 1979, Seattle, WA, American Nuclear Society (1979).

5. R. W. Ostensen, R. J. Henninger, and J. F. Jackson, "The Transition Phase in LMFBR Hypothetical Accidents," pp. 895-904, in Proc. Int. Mtg. Fast Reactor Safety and Related Physics, Chicago, IL, CONF-761001, U. S. Energy Research and Development Administration (1976).

6. See references in Section 1.2 of G. A. Greene, et al., "Two Phase Transient Solidification Dynamics of Flowing Fluids with Non-Condensible Vapors," BNL-NUREG-24486R, Brookhaven National Laboratory, Upton, NY 11973 (April, 1978).

7. R. W. Ostensen, et al., "Fuel Flow and Freezing in the Upper Subassembly Structure Following an LMFBR Disassembly," pp. 214-215 in Trans. Am. Nucl. Soc. 18, (1974).

8. B. W. Spencer, et al., "Results of Fuel Freezing Tests with Simulated CRBR-Type Fuel Pins", pp. 446-447 in Trans. Am. Nucl. Soc. 30, (1978).

9. G. Maurin and M. Amblard, "Approach of Molten Fuel Relocation Problem: Fuel Freezing," Vol. 2, pp. 1096-1106 in Proc. of ENS/ANS Int. Topical Meet. on Nuclear Power Reactor Safety, Brussels, Belgium, October 16-19, 1978.

10. M. Epstein et al., "Transient Solidification in Flow into a Rod Bundle," pp. 330-334 in J. Heat Transfer 102, (May, 1980).

11. R. W. Ostensen et al., ANL-RDP-18, Argonne National Laboratory (July 1973).

12. M. Epstein et al., "Transient Freezing of a Flowing Ceramic Fuel in a Steel Channel," pp. 310-323 in Nucl. Sci. and Engr. 61, (1976).

13. S. W. Eisenhawer, et al., "On the Physics of Fuel Streaming and Freezing in Fast Reactor Core Disruptive Accidents," SAND80-0484, Sandia National Laboratories, Albuquerque, NM 87185, August 1981.

14. Advanced Reactor Safety Research Quarterly Report: October - December 1981, SAND81-1529 (Vol 4), Sandia National Laboratories, Albuquerque, NM 87185.

15. N. K. Hayden, "An Analytic Model of Freezing Liquid Penetration in Tube Flow", Trans. Am. Nucl. Soc. 39:671, 1981.

16. J. V. Walker, et al., "The Design and Proposed Utilization of the Sandia Annular Core Research Reactor (ACRR)," Vol. V, pp. 2383-2393, in Proc. Int. Mtg. on Fast Reactor Safety Technology, August 19-23, 1979, Seattle, WA, American Nuclear Society (1979).

17. E. A. Bernard, D. J. Sasmor, W. J. Whitfield, and R. B. Stump, "Hot Cell Laboratory (HCL) Safety Analysis Report," Sandia National Laboratories, Albuquerque, NM 87185, December, 1979.

18. H. K. Fauske, W. D. Ford, and M. A. Grolmes, "Liquid Film Thickness for Slug Ejection," Trans. Am. Nucl. Soc. 13:646, 1970.

19. M. Pilch and P. K. Mast, "PLUGM: A Coupled Thermal-Hydraulic Computer Model for Freezing Melt Flow in a Channel," SAND82-1580, Sandia National Laboratories, Albuquerque, NM 87185, forthcoming.

20. J. F. Petersen, ed., "TAC2D: A General Purpose Two-Dimensional Heat Transfer Computer Code -User's Manual-," Sept. 1969, Gulf General Atomic Inc., P. O. Box 608, San Diego, CA 92112.

21. D. A. McArthur and W. E. Nelson, "Neutronics Calculations for Transition-Phase Fuel-Freezing Experiments in ACRR," Internal Memorandum, Sandia National Laboratories, Albuquerque, NM 87185, June, 1980.

22. S. A. Wright, P. J. McDaniel, and J. E. Powell, "The SPR-III 7-Pin In-Core Fuel Motion Detection Feasibility Experiments", Vol. V, pp. 2289-2301 in Proc. ENS/ANS Int'l. Mtg. on Fast Reactor Safety Technology, Seattle, Washington, August 19-23, 1979.

23. Belfab-Babcock and Wilcox, 305 Fentress Blvd., Daytona Beach, Florida, 32015.

24. C. M. Lederer and V. S. Shirley, Eds., TABLE OF ISOTOPES, 7th Ed., New York, John Wiley and Sons, Inc., 1978.

25. K. O. Reil, "ACRR Data Acquisition System," Sandia National Laboratories, Albuquerque, NM, 87185.

26. N. K. Hayden and D. A. McArthur, "Energy Coupling Factor Determination for Transition Phase Fuel-Freezing Experiments TRAN Series I," Report RS4450/82/34, Sandia National Laboratories, Albuquerque, NM 87185.

27. S. F. Duliere, S. J. Caldwell, E. Edge, and J. B. Duran, "Post-test Analysis of TRAN-4," Internal Memorandum, Sandia National Laboratories, Albuquerque, NM 87185, June, 1982.

DISTRIBUTION:

Division of Technical Information
and Document Control
NRC Distribution Contractor
U.S. Nuclear Regulatory Commission
15700 Crabbs Branch Way
Rockville, MD 20850
(250 copies for R7)

U.S. Nuclear Regulatory Commission (7)
Division of Accident Evaluation
Office of Nuclear Regulatory Research
Washington, DC 20555
Attn: D. F. Ross
O. E. Bassett
C. N. Kelber
G. Marino
R. T. Curtis
R. W. Wright
P. Wood

U.S. Nuclear Regulatory Commission
Office of Nuclear Reactor Research
Clinch River Breeder Reactor Program Office
Washington, DC 20555
Attn: C. Allen

U.S. Department of Energy
Office of Nuclear Safety Coordination
Washington, DC 20545
Attn: R. W. Barber

U.S. Department of Energy (2)
Albuquerque Operations Office
P. O. Box 5400
Albuquerque, NM 87185
Attn: J. R. Roeder, Director
Operational Safety Division
D. L. Krenz, Director
Energy Technologies Division
For: C. B. Quinn
R. N. Holton

Los Alamos National Laboratory
P. O. Box 1663
Los Alamos, NM 87145
Attn: C. R. Bell, Q-7

DISTRIBUTION -- Continued

Technology Management Center (3)
Argonne National Laboratory
Building 207
9700 S. Cass Avenue
Argonne, IL 60439
Attn: L. Baker
S. S. Borys
D. R. Ferguson

Brookhaven National Laboratory
Department of Nuclear Energy
Building 820
Upton, NY 11973
Attn: T. Ginsberg

Argonne National Laboratory (8)
9700 S. Cass Avenue
Argonne, IL 60439
Attn: L. W. Deitrich
C. Dickerman
A. E. Klickman
T. E. Kraft
J. M. Kramer
J. J. Sienicki
B. W. Spencer
D. P. Weber

University of Michigan
Nuclear Engineering Department
Ann Arbor, MI 48104

Dr. T. Theofanous
Purdue University
W. Larayette, IN 47906

Dr. M. Kazimi
Massachusetts Institute of Technology
Department of Nuclear Engineering
Cambridge, MA 02139

Dr. Carl A. Erdman
Nuclear Engineering Department
Texas A and M University
College Station, TX 77843

DISTRIBUTION -- Continued

General Electric Corporation (4)
310 DeGuigne Drive
Sunnyvale, CA 94086
Attn: S. M. Davies, Mgr., LSPB Project
T. I. Temme, Mgr., Probabilistic Risk Assessment
D. M. Switick, Mgr., Plant Safety
S. Rhow

Fauske and Associates, Inc.
16W070 West 83rd Street
Burr Ridge, IL 60521
Attn: Dr. Michael Grolmes

Fauske and Associates, Inc.
4950 Louise Avenue
Encino, CA 91316
Attn: Dr. Mike Epstein

Westinghouse HEDL (3)
P. O. Box 1970
MS W-221T (HE)
Richland, WA 99352
Attn: Alan Waltar
G. E. Culley
E. T. Weber

Projekt Schneller Brueter (8)
Kernforschungszentrum Karlsruhe GMBH
Postfach 3640
D75 Karlsruhe
West Germany
Attn: Dr. Kessler (2)
Dr. Heusener (2)
Dr. Froelich
Dr. Werle
Dr. Kuhn
Dr. Groetzbach
Dr. Ohnemus

DISTRIBUTION -- Continued

UKAEA Safety and Reliability Directorate (4)
Wigshaw Lane
Culcheth
Warrington WA3 4NE
Cheshire
England
Attn: Dr. J. Gittus, Director
Dr. M. J. Hayn
Mr. H. Teague
Dr. R. S. Peckover

AERE Harwell
Didcot
Oxfordshire OX11 ORA
England
Attn: Dr. J. R. Matthews,
Theoretical Physics Division

UKAEA (2)
Risley
Warrington WA3 6AT
Cheshire
England
Attn: Dr. B. Cowking, FRDD
Dr. D. Hicks, TRDD

Dr. F. Briscoe
Culham Laboratory
Culham
Abingdon
Oxfordshire OX14 X
England

Mr. C. P. Gratton
Division Head, SESD
Atomic Energy Establishment
Winfrith
Dorset DTZ 8DH
England

Mr. K. S. Norwood
Mail Stop B 12
Building 4500 N
Oak Ridge National Laboratory
P. O. Box X
Oak Ridge, TN 37830

DISTRIBUTION -- Continued

Joint Research Centre (2)
Ispra Establishment
21020 Ispra (Varese)
Italy
Attn: H. Holtbecker
P. Fasoli-Stella

Power Reactor and Nuclear Fuel
Development Corporation (PNC) (6)
Fast Breeder Reactor Development Project (FBR)
9-13, 1-Chome, Akasaka
Minato-Ku, Tokyo
Japan
Attn: Dr. A. Watanabe (3)
Dr. N. Tanaka
Dr. M. Saito
Dr. S. Kondo

Power Reactor and Nuclear Fuel (3)
Development Corporation (PNC)
Oarai Engineering Center
Oarai, Ibaraki-ken
Japan 311-13
Attn: Dr. K. Takahashi (3)

Centre d'Etudes Nucleaires de Cadarache (4)
Boite Postale No. 1
13115 St. Paul lez Durance
France
Attn: A. Meyer-Heine DERS/SIES
J. Cl. Melis DERS/SIES
M. Schwarz DERS/SIES
C. LeRigoleur DRNR/SYTC

1230 J. E. Powell
3141 C. M. Ostrander (5)
3151 W. L. Garner
3431 B. N. Yates
6255 D. O. Lee
6400 A. W. Snyder
6410 J. W. Hickman
6420 J. V. Walker
6420 M. Hasti
6420 M. Watkins
6421 T. R. Schmidt

DISTRIBUTION -- Continued

6421 J. T. Hitchcock
6422 D. A. Powers
6422 J. E. Gronager
6422 E. Randich
6423 P. S. Pickard (2)
6423 A. Furutani
6423 R. O. Gauntt
6423 D. A. McArthur (5)
6423 S. A. Wright
6425 W. J. Camp
6425 G. Kayser
6425 P. K. Mast (5)
6425 M. Pilch
6427 M. Berman
6440 D. A. Dahlgren
6442 W. A. von Riesemann
6449 K. D. Bergeron
6450 J. A. Reuscher
6451 T. F. Luera
6452 M. F. Aker
6453 W. J. Whitfield
6454 G. L. Cano
7100 C. D. Broyles
7550 F. W. Neilson (1)
Attn: O. J. Burchett, 7552
J. H. Gieske, 7552
8214 M. A. Pound

NRC FORM 335 (2.84) NRCM 1102 3201, 3202

U.S. NUCLEAR REGULATORY COMMISSION

BIBLIOGRAPHIC DATA SHEET

SEE INSTRUCTIONS ON THE REVERSE

1 REPORT NUMBER (Assigned by TIDC and Vol. No., if any)
NUREG/CR-3675
SAND81-1726

2 TITLE AND SUBTITLE
In-Core Fuel Freezing and Plugging Experiments: Preliminary Results of the Sandia TRAN Series I Experiments

3 LEAVE BLANK

4 DATE REPORT COMPLETED
MONTH: May YEAR: 1984

5 AUTHOR(S)
D. A. McArthur, N. K. Hayden, P. K. Mast

6 DATE REPORT ISSUED
MONTH: August YEAR: 1984

7 PERFORMING ORGANIZATION NAME AND MAILING ADDRESS (Include Zip Code)
Division 6423
Sandia National Laboratories
P. O. Box 5800
Albuquerque, NM 87185

8 PROJECT/TASK/WORK UNIT NUMBER

9 FIN OR GRANT NUMBER
A1016

10 SPONSORING ORGANIZATION NAME AND MAILING ADDRESS (Include Zip Code)
U. S. Nuclear Regulatory Commission
Office of Nuclear Regulatory Research
Division of Accident Evaluation
Washington, DC 20555

11a TYPE OF REPORT
Technical

b PERIOD COVERED (Inclusive dates)
10/80 - 12/83

12 SUPPLEMENTARY NOTES

13 ABSTRACT (200 words or less)

The freezing and plugging behavior of molten reactor materials (UO_2 and 316 SS) is of primary importance in analyzing hypothetical accident scenarios of the Liquid Metal Fast Breeder Reactor (LMFBR). However, the reactor materials melt and vaporize at such high temperatures that it is very idfficult to obtain data on the behavior of the pure materials in the laboratory. Because almost no data are available for the pure materials, several different theoretical models have been developed to predict freezing behavior. However, these models yield such a wide range of predictions that useful accident analyses are difficult to perform.

Described in this report is a new experimental apparatus (the "TRAN" apparatus) in which a pulsed nuclear reactor (the Sandia Annular Core Research Reactor) is used to melt the reactor materials rapidly. After the melt if formed, it is forced under moderate pressure into a "freezing" channel that has a geometry representative of the LMFBR fuel pin structure. The flow and freezing behavior of the pure reactor materials is then inferred from the final distribution of the frozen materials, as well as from the transient behavior of the driving pressure.

14 DOCUMENT ANALYSIS - a KEYWORDS/DESCRIPTORS
Liquid Metal Fast Breeder Reactor (LMFBR), Transition Phase, freezing and plugging, UO_2 data, loss-of-flow accidents, conduction freezing model, steel entrainment, blockage formation.

b IDENTIFIERS/OPEN-ENDED TERMS

15 AVAILABILITY STATEMENT

16 SECURITY CLASSIFICATION
(This page) UNC
(This report) UNC

17 NUMBER OF PAGES

18 PRICE

☆U.S. GOVERNMENT PRINTING OFFICE:1984—776-027/4366

120555078877 1 1AN1R7
US NRC
ADM-DIV OF TIDC
POLICY & PUB MGT BR-PDR NUREG
W-501
WASHINGTON DC 20555